NTNU

Norwegian University of
Science and Technology

# pH-dependence of chloride binding in ordinary Portland cement

Petter Hemstad

Chemical Engineering and Biotechnology
Submission date: March 2018
Supervisor: Kjell Wiik, IMA
Co-supervisor: Klaartje De Weerdt, KT
Alisa Machner, KT

Norwegian University of Science and Technology
Department of Materials Science and Engineering

# Preface

The work in this thesis was carried out between September 2017 and March 2018 in laboratories at the Department of Constructional Engineering, the Department of Materials Science and SINTEF. I am a 5$^{th}$ year student at NTNU studying materials science and have been employed as a research assistant for Alisa Machner and Klaartje De Weerdt since August 2016, working with analysis and preparation of cement paste samples. The interesting chemical properties and immense societal importance of concrete made me want to write a thesis related to concrete technology. How leaching and the lowered pH caused by leaching affects the chloride binding in cement is a topic that has yet to be fully explored. With my background in chemistry and experience working with cement research, it appeared to be a good opportunity to advance our understanding of the topic. Due to limited availability of materials and the limited time of a master thesis, the aim was to make a proof of concept for a method of studying the subject.

## Acknowledgements

First and foremost, I would like to thank my supervisors and employers Klaartje De Weerdt and Alisa Machner for their support, encouragement and helpful discussions, and for introducing me to the field of cement chemistry. Thank you to my supervisor Kjell Wiik for enabling this cross-institute project.

A warm thank you to Tone Anita Østnor and Anne-Kristin Mjøen at SINTEF for assistance with TGA, titration and pH-measurements, and for making me feel welcome in your laboratories. Acknowledgments are also due to Syverin Lierhagen for performing ICP-MS, Arild Monsøy for SEM sample polishing and Sergey Khromov for assisting me when the SEM occasionally broke down.

Thank you to all my friends, both back home and those I have been fortunate to meet during my studies in Trondheim. You have all made these last few years an absolute joy.

Finally, thank you to my family, and to my better half Frida. I cannot express my gratitude for all your unconditional love and support.

# Abstract

A new method for artificially leaching hydrated cement paste and studying how lowered pH in the pore solution affects chloride binding has been developed. Hydrated cement paste was exposed to a NaCl-solution before being acidified by adding small volumes of HCl in steps over several days, gradually lowering the pH. A pH-development curve was established, determining how the pH in the pore solution responded to increasing amounts of acid being added. The chloride binding of the cement paste as a function of the pH and free chloride concentration was then determined. For the range of pH from 12 to 13, decreasing pH increased chloride binding. At a pH of 11, the cement paste showed almost no chloride binding. The mechanisms of changes in chloride binding were investigated using TGA, XRD, SEM-EDS, ICP-MS and thermodynamic modelling. One of the main chloride binding phases, Friedel's salt, could not be detected with the applied techniques due to the cement paste being cured at 60 °C, therefore its influence could not be verified. Thermodynamic modelling does however confirm the possibility of Friedel's salt decomposing at pH 11. The increase in chloride binding from pH 13 to 12 is most likely related to the changes in the main hydrate phase C-S-H. The effect of pH on chloride binding should be accounted for in service life prediction models for concrete structures exposed to chlorides.

# Sammendrag

En ny metode for å studere hvordan pH i poreløsningen påvirker kloridbinding i hydrert sementpasta har blitt utviklet. Hydrert sement ble utsatt for en NaCl-løsning før HCl ble tilsatt i små doser over flere dager for gradvis å minke pH. Forholdet mellom mengden HCl og pH i poreløsningen ble bestemt. Deretter ble kloridbindingen i sementpastaen bestemt som en funksjon av pH i poreløsningen. For pH mellom 13 og 12 ga minking av pH en økning av kloridbinding, mens ved pH 11 ble sementpastaens evne til å binde klorider nesten fullstendig fjernet. Mekanismene som førte til endringer i kloridbinding ble undersøkt med TGA, XRD, SEM-EDS, ICP-MS og termodynamisk modellering. En av de viktigste kloridbindene fasene, Friedels salt, kunne ikke detekteres på grunn av at sementpastaen ble herdet på 60 °C. Den termodynamiske modellen forutser at Friedels salt dekomponerer ved pH 11, noe som delvis kan forklare den oberverte minkingen i kloridbinding. Økningen av kloridbinding fra pH 13 til 12 kan skyldes endringer i hovedhydratasjonsfasen C-S-H. Effekten pH har på kloridbinding i sement burde tas i betraktning i livstidsmodeller for armerte betongstrukturer utsatt for klorider.

# Abbreviations

| | |
|---|---|
| **BSE** | Backscatter electron imaging |
| **DEF** | Delayed ettringite formation |
| **EDS** | Energy dispersive spectroscopy |
| **GEMS** | Gibbs Energy Minimization Software for Geochemical Modelling |
| **ICP-MS** | Inductively coupled plasma mass spectroscopy |
| **LOI** | Loss on ignition |
| **OPC** | Ordinary Portland cement |
| **SEM** | Scanning electron microscopy |
| **TGA** | Thermogravimetric analysis |
| **XRD** | X-ray diffraction |
| **XRF** | X-ray fluorescence |

## Minerals and phases

The field of cement chemistry uses a shorthand notation when discussing common phases in cement. The notation is as follows:

| | | |
|---|---|---|
| C = CaO | S = $SiO_2$ | A = $Al_2O_3$ |
| F = $Fe_2O_3$ | H = $H_2O$ | \$ = $SO_3$ |

This table gives and overview of the phases relevant to the current study:

| **Name** | **Shorthand notation** | **General chemical formula** |
|---|---|---|
| Aluminate-ferrite-mono phases | AFm | $[Ca_2(Al,Fe)(OH)_6]\cdot X\cdot nH_2O$, X = 1 monovalent or ½ divalent anion |
| Aluminate-ferrite-tri phases | AFt | $[Ca_3(Al,Fe)(OH)_6\cdot 12H_2O]_2\cdot X_3\cdot nH_2O$, X = 1 monovalent or ½ divalent anion |
| Calcium aluminoferrite | $C_4AF$ | $4CaO\cdot Al_2O_3\cdot Fe_2O_3$ |
| Calcium-silicate-hydrate | C-S-H | $3CaO\cdot 2SiO_2\cdot 4H_2O$ |
| Dicalcium silicate | $C_2S$ | $2CaO\cdot SiO_2$ |
| Ettringite | $C_6A\$_3H_{31}$ | $3CaO\cdot Al_2O_3\cdot 3CaSO_4\cdot 32H_2O$ |
| Friedel's salt | $C_3AH_{10}\cdot CaCl_2$ | $3CaO\cdot Al_2O_3\cdot CaCl_2\cdot 10H_2O$ |
| Gypsum | $C\$H_2$ | $CaSO_4\cdot 2H_2O$ |
| Hydrotalcite | Htc | $Mg_6Al_2(OH)_{18}\cdot 3H_2O$ |
| Katoite | - | $Ca_6Al_7O_9(OH)_{15}$ |
| Kuzel's salt | $C_3AH_{11}\cdot ½CaCl_2\cdot ½CaSO_4$ | $3CaO\cdot Al_2O_3\cdot ½CaCl_2\cdot ½CaSO_4\cdot 11H_2O$ |
| Monocarbonate | $C_3AH_{11}\cdot CaCO_3$ | $3CaO\cdot Al_2O_3\cdot CaCO_3\cdot 11H_2O$ |
| Monosulphate | $C_4A\$H_{11}$ | $3CaO\cdot Al_2O_3\cdot CaSO_3\cdot 11H_2O$ |
| Natrolite | - | $Na_2O\cdot Al_2O_3\cdot 3SiO_2\cdot 2H_2O$ |
| Portlandite | CH | $Ca(OH)_2$ |
| Tobermorite | $C_5S_6H_5$ | $5CaO\cdot 6SiO_2\cdot 5H_2O$ |
| Tricalcium aluminate | $C_3A$ | $3CaO\cdot Al_2O_3$ |
| Tricalcium silicate | $C_3S$ | $3CaO\cdot SiO_2$ |

# Table of contents

Preface ..... i

Acknowledgements ..... i

Abstract ..... iii

Sammendrag ..... v

Abbreviations ..... vi

Minerals and phases ..... vii

1 Introduction ..... 1

1.1 Concrete ..... 1

1.2 Service life prediction ..... 2

1.3 Research goal ..... 2

2 Theory ..... 4

2.1 Current service life prediction models ..... 4

2.1.1 Effect of phase changes on chloride profiles ..... 5

2.2 Phases relevant to chloride binding ..... 6

2.2.1 Calcium-silicate-hydrates ..... 6

2.2.2 Portlandite ..... 7

2.2.3 Aluminate-ferrite hydrate phases ..... 8

2.3 Types of chloride binding ..... 9

2.3.1 Chemical binding ..... 9

2.3.2 Physical bonding ..... 10

2.4 Methods for analysing chloride content ..... 12

2.4.1 Profile grinding ..... 12

2.4.2 Exposure of hydrated cement pastes ..... 12

2.5 Factors influencing chloride binding ..... 13

2.5.1 Chloride concentration ..... 13

2.5.2 Associated cation ..... 15

2.5.3 Hydroxyl concentration (pH) ..... 15

2.5.4 Possible effect of pH on chloride profiles ..... 16

3 Experimental ..... 18

3.1 Experimental approach ..... 18
3.2 Chemicals ..... 18
3.2.1 Cement ..... 19
3.2.2 NaCl-solution ..... 20
3.3 Apparatus ..... 20
3.4 Sample preparation ..... 20
3.4.1 Mixing well-hydrated cement paste ..... 20
3.4.2 Chloride exposure ..... 21
3.5 Establishing the pH-development curve ..... 22
3.5.1 pH-measurements ..... 23
3.6 Chloride binding experiments ..... 23
3.6.1 Addition of HCl ..... 23
3.6.2 Chloride titration ..... 23
3.6.3 Chloride binding calculation ..... 24
3.6.4 Effect of centrifugation ..... 25
3.6.5 pH-measurements ..... 25
3.6.6 Weight measurements ..... 25
3.7 Analysis of phase assemblage ..... 26
3.7.1 Inductively coupled plasma mass spectroscopy ..... 26
3.7.2 Double solvent exchange ..... 26
3.7.3 Thermogravimetric analysis ..... 27
3.7.4 X-ray diffraction ..... 29
3.7.5 Scanning electron microscopy ..... 29
3.7.6 Thermodynamic model ..... 30
4 Results ..... 32
4.1 Thermodynamic model ..... 32
4.2 pH-development curve ..... 34
4.3 Chloride binding ..... 35
4.4 Phase assemblage ..... 37
4.4.1 ICP-MS ..... 37
4.4.2 TGA ..... 38
4.4.3 XRD ..... 41
4.4.4 SEM-EDS ..... 42

4.4.5 Suspension stability ..... 44
5 Discussion ..... 46
5.1 pH-development ..... 46
5.2 Chloride binding ..... 47
5.2.1 Effect of pH in pore solution ..... 47
5.2.2 Effect of free chloride concentration ..... 48
5.2.3 Effect of centrifugation ..... 49
5.2.4 Uncertainty of measurements ..... 49
5.3 Changes in phase assemblage caused by artificial leaching ..... 51
5.3.1 Sample preparation ..... 51
5.3.2 Portlandite ..... 52
5.3.3 C-S-H ..... 53
5.3.4 Aluminate-ferrite hydrate phases ..... 54
5.4 Mechanism of altered chloride binding ..... 55
5.5 Implications for service life prediction models ..... 56
5.6 Further work ..... 57
5.6.1 Repeating study with regular cement paste ..... 57
5.6.2 Improving determination of pH-development curve ..... 57
5.6.3 Sample preparation ..... 58
5.6.4 Chloride binding and pH ..... 59
6 Conclusion ..... 61
Bibliography ..... 62
Appendices ..... 67
Appendix A GEMS ..... 68
Appendix B Error calculations ..... 81
Appendix C BSE and EDS-images ..... 85
Appendix D EDS point scans ..... 93
Appendix E Developing the artificial leaching method ..... 103
Appendix F Weight measurements during acidification ..... 105

# 1 Introduction

## 1.1 Concrete

Concrete is the single most used building material in the world. Concrete is relatively cheap, can be cast in almost any desired shape, and has a relatively high compressive strength. To increase its ductility and take up tensile stress it is often contains a network of steel rebars (reinforcement). This composite material is called reinforced concrete [1].

Concrete consists of cement, water and aggregates of various sizes. Cement reacts with water to form the cement paste, binding the aggregates together and hardening. This is shown in Figure 1.1, which gives the approximate volumetric proportions of the different components in concrete. It also shows the difference between concrete, mortar and cement. Concrete always has a certain porosity. The porosity is partly filled with air and partly filled with water, which is then called pore solution.

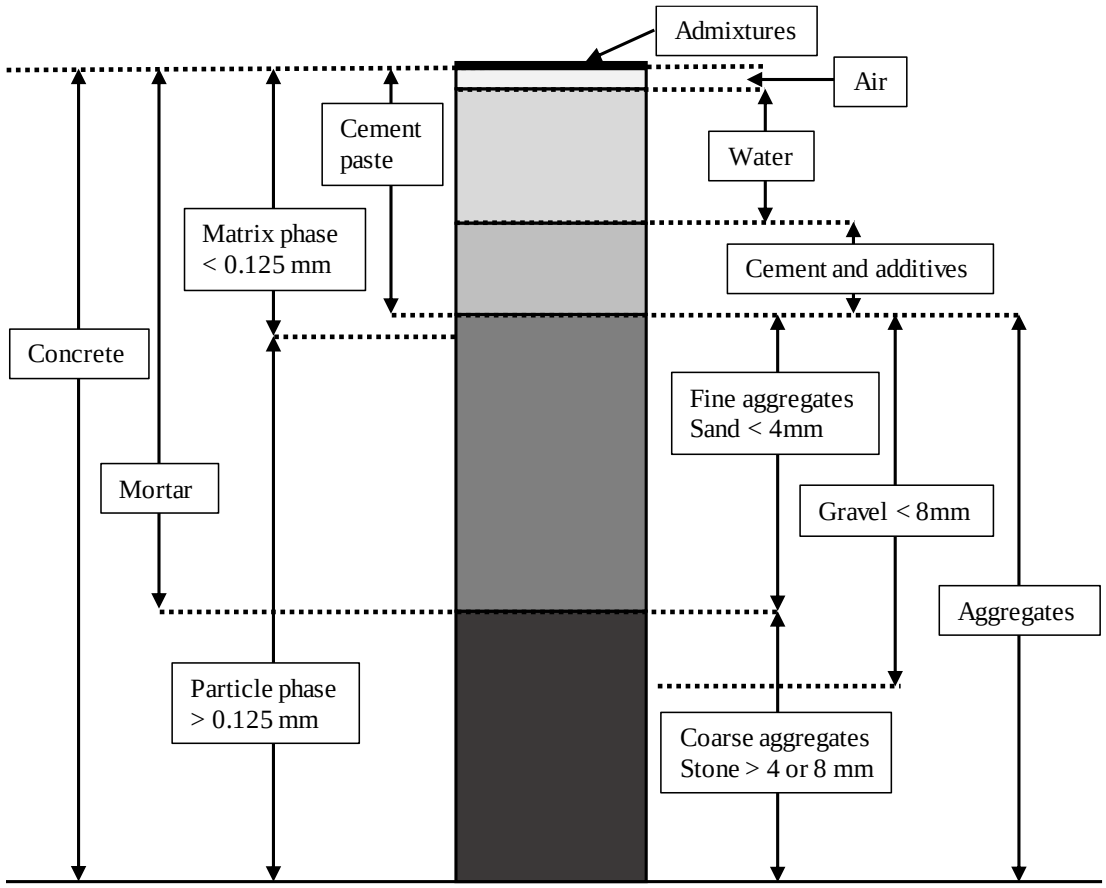


Figure 1.1: The composition of concrete given as approximate volumetric proportions. Adapted from Jakobsen [1].

## 1.2 Service life prediction

Reinforced concrete is a very durable construction material. However, its service life can be limited by certain deterioration mechanisms. One of the major deterioration mechanisms is chloride induced reinforcement corrosion [2]. Common external sources of chlorides are sea water and de-icing salts, making structures in marine environments and near roads particularly exposed. As chlorides diffuse into the concrete structure, the chloride concentration at the reinforcement will eventually increase. Above a critical chloride concentration, pitting corrosion of the reinforcement may be initiated which reduces the cross section of the reinforcement and thereby the load bearing capacity. This leads to cracking and spalling of the concrete cover because of the increased volume of the corrosion products [3]. The time until the critical concentration at the steel surface is reached is therefore commonly used as a limit state for the service life of a reinforced concrete structure [2].

Concrete structures are commonly designed with an intended service life. For large structures like bridges and dams it is often in the range of 100 years. Within that timeframe, the structure must maintain its safety and serviceability under the expected environmental exposure. Models for service life prediction are based on simplified descriptions of the major deterioration mechanisms [4–8]. The models are used to predict the service life based on given concrete properties such as water-to-cement-ratio (w/c), thickness of concrete cover around the reinforcement, and minimum cement content. They can also be used vice versa to determine required concrete properties to obtain a specified service life.

For service life prediction of chloride exposed reinforced concrete structures, the chloride ingress rate and chloride binding are two key factors. Ingress is the rate at which chlorides penetrate the concrete, while binding is adsorption and chemical binding of chlorides in the hydration products of cement. Ingress and binding of chlorides must therefore be fully understood if accurate models for service life prediction are to be developed.

## 1.3 Research goal

This thesis aims to develop a method of studying how the pH in the pore solution affects the chloride binding in cement. Such a method is required to explain and predict the ingress of chlorides in concrete structures exposed to sea water or de-icing salts. Previous studies have found that chloride binding increases for small decreases in the pH [9]. However, this was done by introducing chlorides in the mixing water, which will affect the microstructure of hydrated

cement [10]. Because of this effect, studies using admixed chlorides are not necessarily representative for external chloride ingress and binding in concrete. The focus of this thesis will therefore be to develop a method of studying chloride binding for hydrated cement pastes exposed to chlorides and lowered pH. The expected result is that slightly lowering pH of the pore solution will increase chloride binding, while large decreases in pH will reduce or completely remove the chloride binding.

The new method for determination of the bound chloride content is based on the method described by De Weerdt et al. [11]. Well-hydrated cement pastes of ordinary Portland cement (OPC) will be exposed to a NaCl-solution. HCl will then be added to lower pH without adding other types ions not already present in the system. First, a relationship between volumes of added acid and pH in the pore solution will be established. This relationship will be used to determine how much acid is required to reach specific pH-levels. The second part consists of acidifying five cement paste samples to targeted levels of pH and determine how the acidification affects the chloride binding. The effects of artificial leaching with HCl on the phase assemblage will then be studied, which will shed light on the mechanisms causing changes in chloride binding. Finally, the implications for service life models and further work will be discussed.

# 2 Theory

## 2.1 Current service life prediction models

Some current models for service life prediction adapt chloride content profiles from real structures to Fick's law [7,12]. The chloride profile describes how the chloride content of a structure varies with depth from the concrete surface. Fick's law is a mathematical model that describes diffusion caused by a concentration gradient [13]. Ions, such as chlorides dissolved in the pore solution, will always move from areas of high concentration to areas of lower concentration unless opposed by other forces. The flux of ions and therefore the change of concentration over time is related to a diffusion coefficient *D*. Equation 2-1 describes the law in one dimension. Several solutions of the law have been used to find diffusion coefficients for different concretes: Equation 2-2 describes a solution of the law with limited chloride supply [14], Equation 2-3 gives the error-function solution used for a constant supply of chlorides [15], and Equation 2-4 gives a numerical method of fitting a diffusion coefficient to the chloride profile [16].

$$\frac{\delta c}{\delta t} = D\frac{\delta^2 c}{\delta t} \tag{2-1}$$

$$c(x,t) = \frac{m_{Cl}}{\sqrt{\pi D t}} e^{-\frac{x^2}{4Dt}} \tag{2-2}$$

$$c(x,t) = C_s - (C_s - C_i)\,\mathrm{erf}\left(\frac{x}{\sqrt{4Dt}}\right) \tag{2-3}$$

$$c(x,t) = c(x,t-\Delta t) + D\frac{\Delta t}{(\Delta x^2)}\,[c(x-\Delta x, t-\Delta \mathrm{t}) + c(x+\Delta \mathrm{x}, \mathrm{t}-\Delta \mathrm{t}) - 2(\mathrm{c}(x,t-\Delta \mathrm{t}))] \tag{2-4}$$

Here $c$ is the total chloride content at a depth $x$ and time $t$ in the concrete, $D$ is the diffusion coefficient, $m_{Cl}$ is the total mass of diffusing chloride, $C_s$ is the surface concentration of chloride and $C_i$ is the total background chloride content.

Figure 2.1 shows the chloride profile of a mortar exposed to a finite amount of chlorides, a fitting of the profile to Equation 2-2 and a numerical simulation of the profile with Equation

2-4. The data fits Fick's law in the deeper sections yet deviates significantly in the outer sections. Similar chloride profiles have also been reported elsewhere [17,18]. Newer studies have tried to refine the equations [6], but any solution based on Fick's law cannot account for the observed deviation. As a result, current methods ignore the outer sections and use only the parts of the chloride profile that fits the mathematical model. These solutions are only approximations, thus the diffusion coefficient is called "apparent" [6].

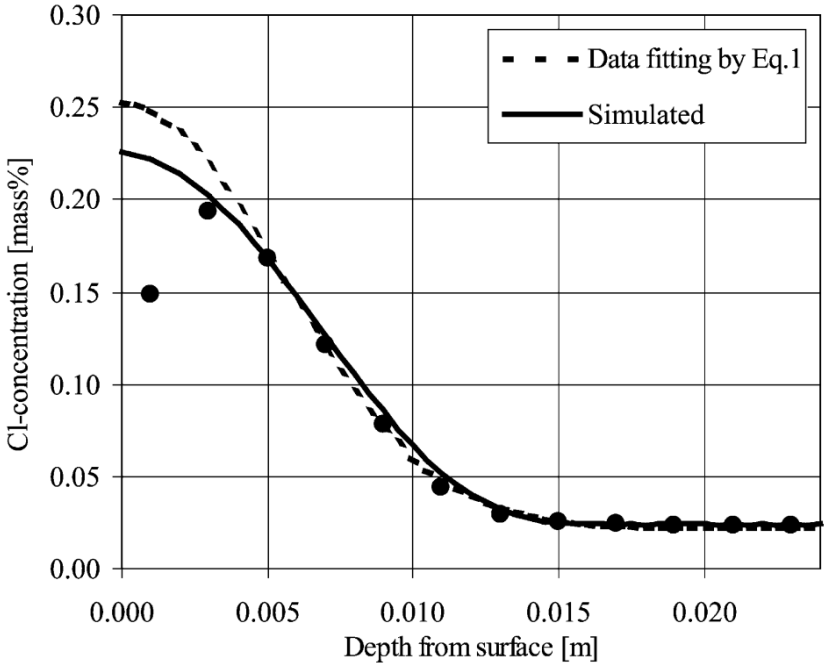


Figure 2.1: Illustration of the deviation of chloride profiles in concrete from Fick's law. Dots are experimental results, the solid line is a numerical simulation of the profile (Equation 2-4) using $D = 5.5\times10^{-12}$ m$^2$ /s, while the dashed line is a fitting of the data to Equation 2-2 with $D = 2.7\times10^{-12}$ m$^2$ /s. Concrete structures exposed to external chlorides show lower chloride content near the surface than a couple of centimetres deeper. From Nielsen and Geiker [5].

### 2.1.1 Effect of phase changes on chloride profiles

Phase changes in the cement paste might be an explanation for why the chloride profiles for concrete structures deviate from Fick's law. When concrete is exposed to sea water there are several phase changes that occur with varying depths of penetration [18]. Due to high $Ca(OH)_2$ and alkali metal content the pore solution of hydrated cement is highly alkaline, with a pH close to 13 [19]. Constant exposure to sea water of near neutral pH will reduce the pH of the pore solution. The phase assemblage in the cement paste will change both because the pH is lowered,

and because of ingress of ions from the sea water. In this study the combination of changes in the phase assemblage and lowering of the pH in the pore solution is referred to as leaching.

The phase changes caused by leaching could change the chloride binding of the cement paste, which might explain why the chloride profiles deviate from Fick's law near the exposed surface. Which phase changes are caused by lowered pH and ion ingress should be investigated separately to improve our understanding of the phenomenon. There are currently no methods for studying how changing the pH of the pore solution in hydrated cement affects its chloride binding. There is therefore a need to develop such a method that enables the study of not only how the chloride binding changes with changing pH, but also what is causing the changes in binding. The mechanisms are very likely to be related to the main chloride binding hydrate phases: The aluminate-ferrite hydrates and the calcium-silicate-hydrates (C-S-H).

## 2.2 Phases relevant to chloride binding

To discuss the chloride binding of hydrated cement it is important to understand some of the main cement hydration phases [19]. Figure 2.4 shows the approximate volumes of the different phases in hydrated cement paste.

### 2.2.1 Calcium-silicate-hydrates

C-S-H is the main cement hydration phase. The approximate formula is $3CaO{\cdot}2SiO_2{\cdot}4H_2O$, though the exact composition varies depending on several factors including the cement composition, w/c-ratio, and the curing temperature [19]. It is common to discuss the composition of C-S-H in terms of the atomic calcium to silicon ratio (Ca/Si or inversely Si/Ca) of the phases, which can be determined by energy dispersive spectroscopy (EDS) [20] or Si NMR [21].

C-S-H is mainly an amorphous gel, which provides most of the strength to the cement [1,19]. It has a layered structure that is similar to the mineral tobermorite ($Ca_5Si_6O_{16}(OH)_2{\cdot}4H_2O$, Figure 2.2 [22]) but with shorter and more disorganized layers [23]. Each layer is formed by calcium ions with attached silicate ions and hydroxyl groups, with interlayer calcium ions and water [19]. Each third silicate in tobermorite points towards the interlayer and bridges neighbouring silicate ions that are attached to the calcium oxide layers. The transition from the tobermorite-structure (Ca/Si = 0.83) to the C-S-H-structure (Ca/Si typically 1.6-2.0 in cement pastes [19]) can be explained by the combination of three defect mechanisms: Removal of bridging $SiO_4^{4-}$-tetrahedra, replacement of two $H^+$ from hydroxide with calcium, and increased

calcium content in the interlayer. These three defects will be randomly combined and distributed in the C-S-H, resulting in no long range order and an amorphous structure [24].

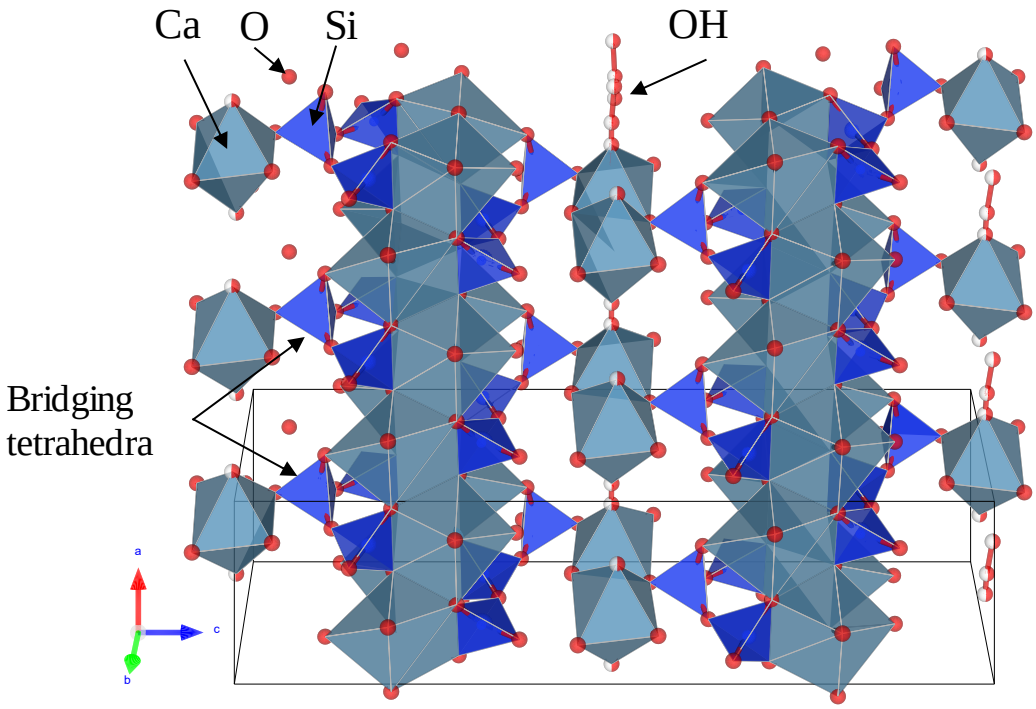


Figure 2.2: Crystal structure of tobermorite, which is similar to C-S-H but with more organized layers and a lower Ca/Si-ratio. Adapted from Bonaccorsi et al. [22] using Vesta [25].

### 2.2.2 Portlandite

Portlandite, denoted CH in cement chemistry shorthand, is the second most abundant hydration product in cement [1]. Figure 2.3 shows the structure of portlandite, which can be considered as stacked sheets of $Ca(OH)_6$ octahedra held together by hydrogen bonds [26,27].

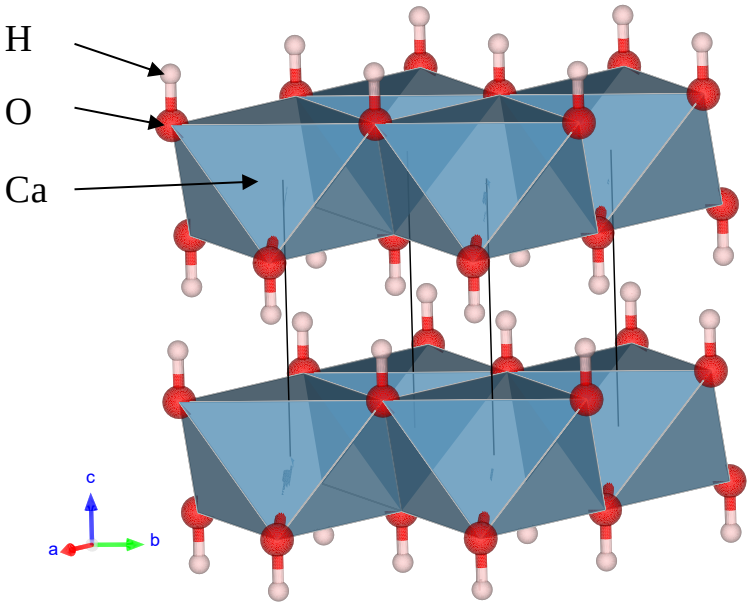


Figure 2.3: The crystal structure of portlandite. It has a layered structure, consisting of stacked $Ca(OH)_6$-octahedra held together by hydrogen bonds. Adapted from Henderson and Gutowsky [26] using Vesta [25].

### 2.2.3 Aluminate-ferrite hydrate phases

The aluminate-ferrite hydrate phases are hydrated calcium oxide phases with solid solutions of alumina and ferrite. They are divided in two subgroups: Aluminate-ferrite-mono hydrate (AFm) and aluminate-ferrite-tri hydrate (AFt). The AFm-phases have similar structures to CH, where 1/3 of the $Ca^{2+}$-ions are replaced with $Al^{3+}$ or $Fe^{3+}$-ions [19,28]. This leads to a change in crystal lattice parameters and positive charging of the layers. The structure incorporates water and anions in the interlayer to compensate for the charge. A general formula for AFm-phases is $[Ca_2(Al,Fe)(OH)_6]\cdot X\cdot nH_2O$, where X is a monovalent anion like $OH^-$ or half a divalent anion like $SO_4^{2-}$ [28]. Individual phases are often named after the anion it contains, for instance monosulphate ($3CaO\cdot Al_2O_3\cdot CaSO_3 \cdot 11H_2O$) and monocarbonate ($3CaO\cdot Al_2O_3\cdot CaCO_3 \cdot 11H_2O$). AFt-phases have a general formula of $[Ca_3(Al,Fe)(OH)_6\cdot 12H_2O]_2\cdot X_3\cdot nH_2O$, where X is a monovalent or ½ divalent anion.

The curing temperature greatly affects the stability of the aluminate-ferrite hydrate phases. When cement pastes are cured at elevated temperatures near 60 °C, the main AFt-phase ettringite ($3CaO\cdot Al_2O_3\cdot 3CaSO_4 \cdot 32H_2O$) is destabilized. AFm-phases will then be favoured instead [29]. When pastes cured at elevated temperatures are later kept at 20 °C, parts of the

AFm-phases will transform to AFt after a few months. This process is known as delayed ettringite formation (DEF) [30].

## 2.3 Types of chloride binding

Some hydrates in concrete can bind chlorides from the pore solution. The chlorides can be bound chemically or physically. The chloride content is commonly given as wt% of concrete mass or as grams chloride bound per gram cement (g/g cement). Figure 2.4 shows the typical composition of a hydrated OPC-paste and how chlorides from sea water exposure are distributed in the paste [31]. Most of the chlorides in a concrete are bound, either chemically or physically.

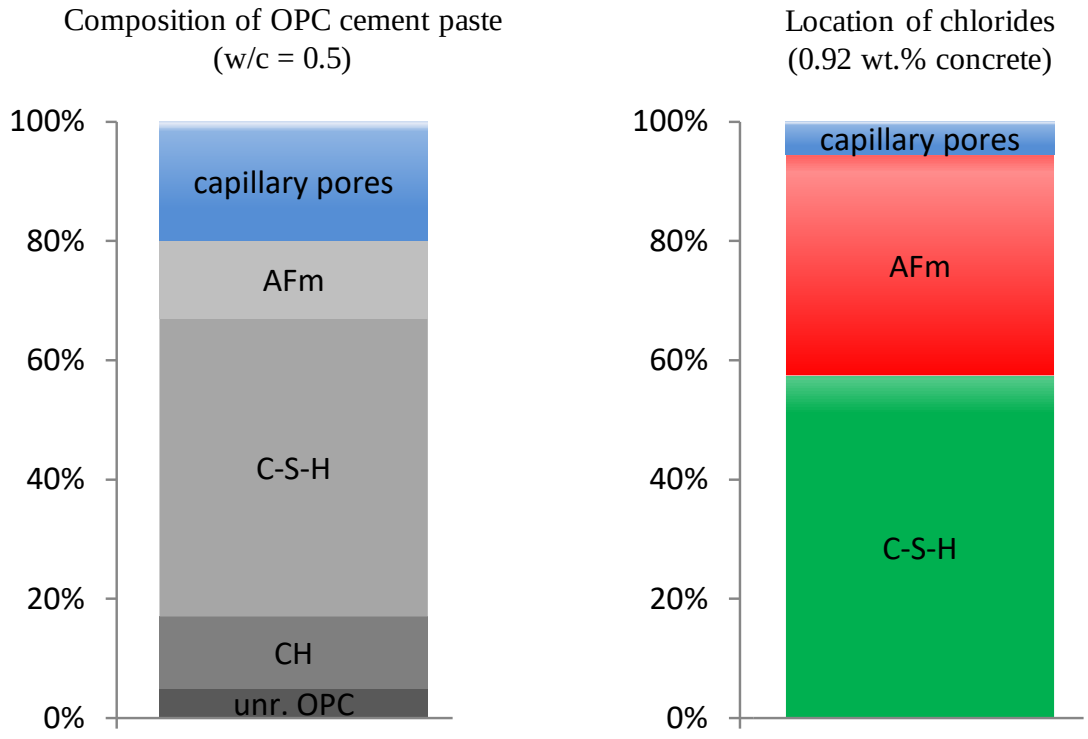


Figure 2.4: Typical composition of hydrated cement pastes and distribution of chlorides. The majority of chlorides are either bound chemically in AFm-phases or physically by C-S-H. Adapted from a lecture by De Weerdt et al. [31].

### 2.3.1 Chemical binding

Chemically bound chlorides are those that take part in a chemical reaction and are incorporated in the crystal structure of a solid phase. A large portion of the chemically bound chlorides will be incorporated in chloride-containing AFm phases such as Friedel's salt

($3CaO{\cdot}Al_2O_3{\cdot}CaCl_2 \bullet 10H_2O$) [19], or at high sulphate activity Kuzel's salt ($3CaO{\cdot}Al_2O_3{\cdot}½CaCl_2{\cdot}½CaSO_4 \cdot 11H_2O$) [32–34]. In hydrated cement pastes exposed to chlorides, Friedel's salt forms as chlorides react with unhydrated tricalcium aluminate ($3CaO{\cdot}Al_2O_3$ or $C_3A$) [19,35–37], or by anion exchange of other AFm-phases [34,37].

The stability of Friedel's salt appears to be related to pH. Roberts [35] studied the decomposition of Friedel's salt when it is exposed to various solutions. Alkaline solutions saturated with $Ca(OH)_2$ lead to higher dissolution than water. Increasing the pH of the solution by adding NaOH or KOH also increased dissolution. Other studies show that carbonation of concrete leads to reduced pH in the pore solution and increases the solubility of Friedel's salt [37].

### 2.3.2 Physical bonding

Physically bound chlorides refer to the chlorides that are adsorbed on the C-S-H phases. The mechanisms and degree of adsorption are still topics of discussion [12]. Adsorption on a charged surface is described by the electrical double layer theory [36]. Figure 2.5 presents a schematic drawing of how ions in solution will adsorb on a charged surface.

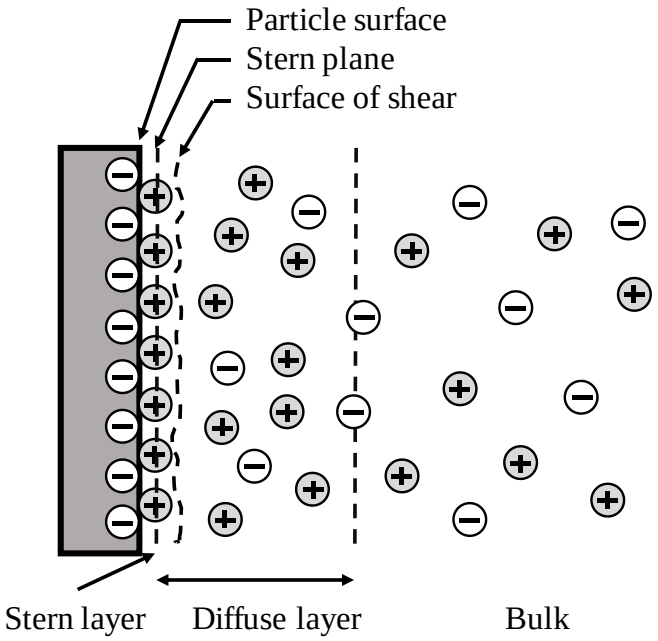


Figure 2.5: Illustration of the distribution of ions near the surface of a charged particle submerged in liquid. Counter-ions of the opposite charge to the particle will adsorb on the surface. Adapted from Hiemenz and Rajagopalan [36].

Pure C-S-H has a negative surface charge at low calcium concentrations (< 2 mM), while at higher concentrations the calcium ions adsorb on the surface and shield the negative charge. When the calcium concentration approaches lime saturation (22 mM) which might occur upon exposure to $CaCl_2$, the adsorbed calcium leads to an apparent reversal of the surface charge [38,39]. Anions like $OH^-$ and $Cl^-$ will then accumulate in the diffuse layer, but not adsorb directly on the hydrate surface [40]. Speaking of chloride binding or chloride adsorption by C-S-H is therefore not strictly correct, but the term will be used in this study for the sake of simplicity.

Plusquellec [41] discussed a cause for the common misconception that C-S-H directly adsorbs chloride. When C-S-H is filtrated before analysis, anions will adsorb on the surface along with the cations to preserve charge neutrality of the solids. Analysis of chloride-exposed C-S-H that has been filtrated will therefore appear as if chlorides adsorb on the surface while in suspension, although it is only an effect of the experimental procedure. Figure 2.6 shows an illustration of this concept.

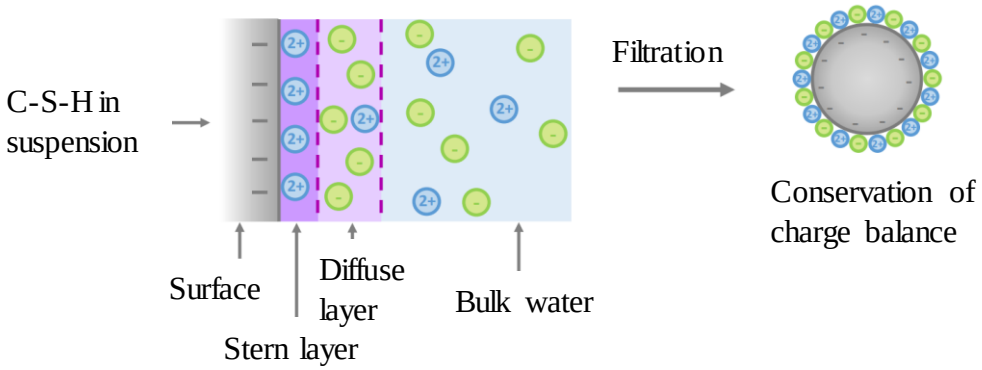


Figure 2.6: Illustration of how filtration affects the observed chloride binding by C-S-H. When the C-S-H is in suspension, only cations (mainly $Ca^{2+}$) are adsorbed on the surface. Upon filtration, anions will also adsorb to preserve the neutral charge of the solid phase. Analysing the C-S-H after filtration will give the incorrect impression that chlorides adsorb directly on the surface rather than accumulate in the diffuse layer. Adapted from Plusquellec [41].

## 2.4 Methods for analysing chloride content

### 2.4.1 Profile grinding

A common method of studying chloride content in concrete is profile grinding, which gives a chloride content gradient as a function of depth in the concrete [12]. It is used to analyse existing concrete structures exposed to chlorides. There are different ways of conducting a profile grinding experiment, one such is described in De Weerdt et al. 2016 [42]: A core is drilled and extracted from the structure while collecting the powder in separate batches for different depths. The ground powders are then dissolved in $HNO_3$. The solutions are then filtrated, and the chloride content is determined by potentiometric titration. The result is the chloride profile, which is the acid soluble chloride content in the concrete as a function of depth. This includes the chlorides in pore solution, and those bound chemically and physically. These profiles are used in current models for service life prediction as described in Section 2.1.

### 2.4.2 Exposure of hydrated cement pastes

With profile grinding it is difficult to distinguish the chlorides in pore solution from those bound by hydration phases. With the exposure-method it is possible to study only the chloride binding of the cement hydrates. The method is described by De Weerdt et al. [11,43]: A well-hydrated cement paste is prepared by curing cement paste, crushing it and adding additional water. The well-hydrated paste is then exposed to a chloride salt solution of known concentration. It is assumed that after some time the exposure solution and the cement paste in the sample will be in equilibrium, so that studying the exposure solution is equivalent to studying the pore solution. The chloride concentration of the exposure solution is then measured by potentiometric titration. The remaining amount of chlorides in solution is subtracted from the initial amount to find the chloride binding of the cement hydrates. Knowing the amount of chlorides added and the total volume of water, the amount of bound chloride per gram cement paste can be calculated. It is common to give the chloride binding in terms of the hydrated cement weight, that is the weight of the cement paste subtracted free water that is not chemically bound in hydrate phases.

Plusquellec [41] showed that centrifuging a sample of chloride-exposed C-S-H before chloride titration has an impact on the measured chloride binding. A larger chloride concentration was measured in the solution of a centrifuged sample compared to a non-centrifuged sample, leading to an apparent lower binding after centrifuging. Higher rotational speeds gave a further increase in chloride concentration measured. Therefore, results from centrifuged and non-centrifuged

samples cannot be compared directly, neither can samples centrifuged at different speeds. Since hydrated cement pastes have a large amount of C-S-H, it is likely that the same effect of centrifugation applies to chloride exposed cement pastes. This has however yet to be verified experimentally.

## 2.5 Factors influencing chloride binding

### 2.5.1 Chloride concentration

The chloride binding isotherm is the relationship between chloride binding by the cement paste and the free chloride concentration in the pore solution. Since the composition and abundance of chloride binding phases varies between different cementitious systems, the binding isotherms will be unique to a system [33]. Figure 2.7 shows an example of chloride binding isotherms for hydrated OPC-pastes exposed to chloride solutions [11].

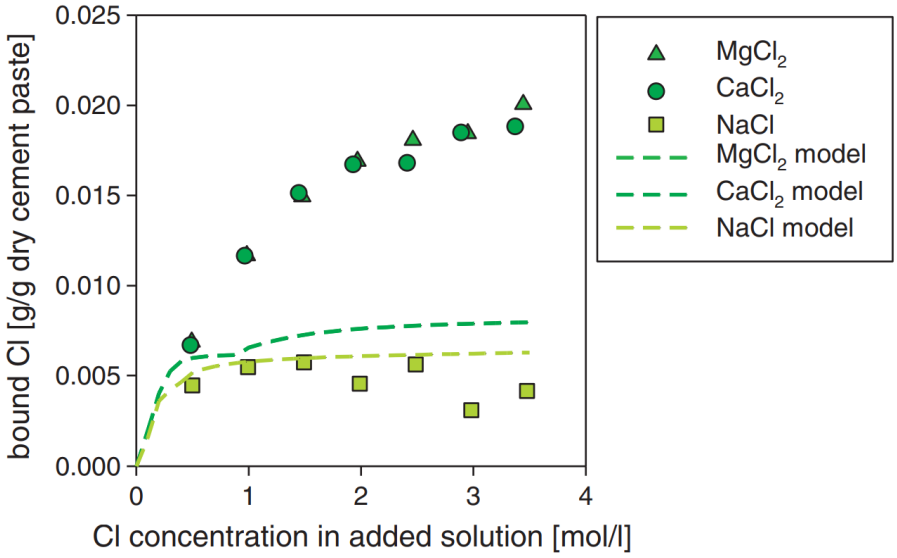


Figure 2.7: Chloride binding isotherms for hydrated cement pastes exposed to solutions of NaCl, $CaCl_2$ and $MgCl_2$. The dashed lines are the expected chloride bindings as predicted by a thermodynamic model. From De Weerdt et al. 2015 [11]. The large deviation in chloride binding for $CaCl_2$ and $MgCl_2$ compared to the model is likely caused by chloride binding of C-S-H, which the model does not account for.

Tuuti [44] studied binding isotherms at chloride concentrations below 0.8 M, and found a linear correlation. Later studies, for instance by Tang and Nilsson [45], showed that Langmuir/Freundlich-isotherms gave a better fit for experimental data with free chloride

concentrations from 0.01 M to 1 M. Equation 2-5 gives the Langmuir-isotherm,

$$C_b = a\, C_f/(1 + b\, C_f) \quad \text{2-5}$$

where $C_b$ is the amount of bound chloride, $C_f$ is the free chloride concentration, $a$ and $b$ are constants unique to the system. It is close to linear for low values of $C_f$ but flattens out and approaches a constant value as $C_f$ increases. The Freundlich-isotherm is described by Equation 2-6,

$$C_b = \alpha\, C_f^{\beta} \quad \text{2-6}$$

where α and β are constants unique to the system. It can have a higher slope than the Langmuir-isotherm, meaning it predicts a larger binding for high values of $C_f$ [33]. Figure 2.7 shows the chloride binding isotherms reported by De Weerdt et al. [11] for hydrated OPC paste exposed to NaCl, $CaCl_2$ and $MgCl_2$, with free chloride concentrations ranging from around 0.2 M to 1.6 M. The binding isotherm for NaCl remained almost constant in the chloride concentration range that was tested. This suggests that the binding capacity was reached before a free concentration of 0.2 M. In this case, a Langmuir-isotherm could be used to describe the chloride binding, since the binding reaches a plateau. For $CaCl_2$ and $MgCl_2$, the binding increased in a manner better described by the Freundlich-isotherm. The binding still appears to be increasing after the highest value for free chloride concentration that was included in the study. The authors suggested that binding by C-S-H was the main cause for the increased chloride binding of the samples exposed to $CaCl_2$ or $MgCl_2$. Their thermodynamic model could not account for binding by C-S-H, thus it predicted lower binding only caused by the formation of Friedel's or Kuzel's salt.

Machner et al. [46] investigated the chloride binding of a similar OPC cured at different temperatures, and using similar methods as De Weerdt et al. [11]. The chloride binding of equal samples exposed to NaCl and $CaCl_2$ increased with increasing free chloride concentrations below 0.9 M. Above 0.9 M the binding isotherm for NaCl reached a plateau regardless of curing temperature, where the binding only increased slightly for increases in free chloride concentration. The chloride binding isotherm for $CaCl_2$ however continued to increase rapidly

for the tested range of free chloride concentration. Figure 2.8 shows the reported values for the cement paste cured at 60 °C and a fitting of the NaCl-data to a Langmuir isotherm and the $CaCl_2$-data.

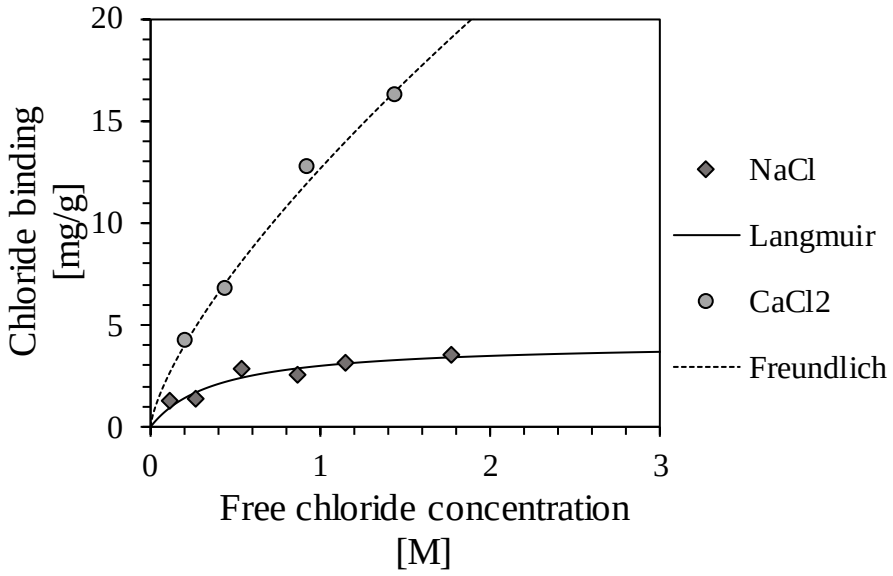


Figure 2.8: Reported values for chloride binding of a hydrated OPC-paste cured at 60 °C and exposed to NaCl and $CaCl_2$ of varying concentration, from Machner et al. [46]. A fitting of the NaCl-data to a Langmuir isotherm and the $CaCl_2$-data to a Freundlich isotherm using the least squares method is also included.

### 2.5.2 Associated cation

Sea water contains a variety of cations associated with chloride salts. Three common salts are NaCl, $CaCl_2$ and $MgCl_2$. Studies conducted on the effect of the associated cation have shown an increased chloride binding in cement pastes exposed to $CaCl_2$ and $MgCl_2$ compared to NaCl [9,11,33,47–49]. The difference between the chloride binding of the various salts increases with chloride concentration. De Weerdt et al. [11] found that at a free chloride concentration of approx. 1.5 M, hydrated pastes exposed to NaCl bound approximately 0.005 g chloride per g cement paste, while exposure to $CaCl_2$ lead to a binding of 0.020 g/g (Figure 2.7).

### 2.5.3 Hydroxyl concentration (pH)

In addition to changing the phase assemblage of the cement, the chloride salts may influence the pH of the pore solution. This effect is negligible for NaCl, but $CaCl_2$ and $MgCl_2$ cause a significant drop in pH. De Weerdt et al. [11] reported a decrease in the pH of the pore solution

of a hydrated OPC-paste from 13.2 to 12.2 after exposure to 0.75 M $CaCl_2$-solution, which also lead to an increase in chloride binding from 7 to 20 mg/g cement. Other studies have also observed simultaneous lowering of pH and increased chloride binding [9,33,46–49].

Tritthart [9] studied the chloride binding in hydrated cements where chlorides were introduced in the mixing water. For the same amount of chlorides added, the binding only changed when the pH of the mixing water was different. In each case, lower pH was associated with higher binding. Tritthart suggested that $CaCl_2$ and $MgCl_2$ cause a drop in pH due to precipitation of hydroxides [9]. Since the pore solution in concrete is saturated with $Ca^{2+}$, additional calcium added by salts will precipitate as $Ca(OH)_2$ and thus reduce the hydroxide concentration by the reaction given in Equation 2-7. $MgCl_2$ reacts with $Ca(OH)_2$ to precipitate as $Mg(OH)_2$, as shown in Equation 2-8.

$$Ca_{aq}^{2+} + 2OH_{aq}^{-} \rightleftarrows Ca(OH)_{2,solid} \quad 2\text{-}7$$

$$MgCl_{2,aq} + Ca(OH)_{2,solid} \rightleftarrows Mg(OH)_{2,solid} + CaCl_{2,aq} \quad 2\text{-}8$$

De Weerdt et al. [11] found a linear relationship between chloride binding and pH, independent of associated cation. The increased chloride binding in samples exposed to $CaCl_2$ and $MgCl_2$ compared to NaCl might therefore be due to the reduction in pH [9,11]. It is likely not a side effect, but rather the cause of increased chloride binding.

Changing pH influences both the chemical and physical bonding of chloride. Roberts [35] indicated that lowering the pH would slightly increase the stability of Friedel's salt, thus increasing the chemical chloride binding of the cement. Lowering the pH too far would however decrease its stability and lead to reduced binding [37,47].

Since $OH^-$ and $Cl^-$ both accumulate in the diffuse layer around C-S-H, they can be considered as competitively adsorbing ions. Reducing pH would reduce the competition from $OH^-$, thereby increasing the apparent adsorption of $Cl^-$ in the diffuse layer [9].

### 2.5.4 Possible effect of pH on chloride profiles

The effects of pH on chloride binding can possibly explain why chloride profiles from concrete structures deviate from Fick's law. The acid soluble chloride content increases with increased chloride binding. As Figure 2.4 shows, the majority of chlorides in a cement paste are either

chemically bound in AFm-phases or in the diffuse layer around C-S-H. Figure 2.9 shows the same chloride profile as Figure 2.1 with zones indicating the effect of lowered pH. In zone A the chloride content is lower than Fick's law predicts. This might be due to the large drop in pH caused by long term exposure to water of neutral pH, leading to the decomposition of C-S-H and AFm-phases and therefore severely reduced chloride binding. The chloride content will then be low, even though the pore solution might contain more chlorides than deeper in the structure. Zone B is where the drop in pH is small enough to not destroy any of the chloride binding hydrates and simultaneously sufficiently large to cause increased binding. In zone C the sea water exposure has not yet lead to considerable leaching, thereby not effecting the chloride binding. In this zone the chloride content will therefore follow regular diffusion as described by Fick's law.

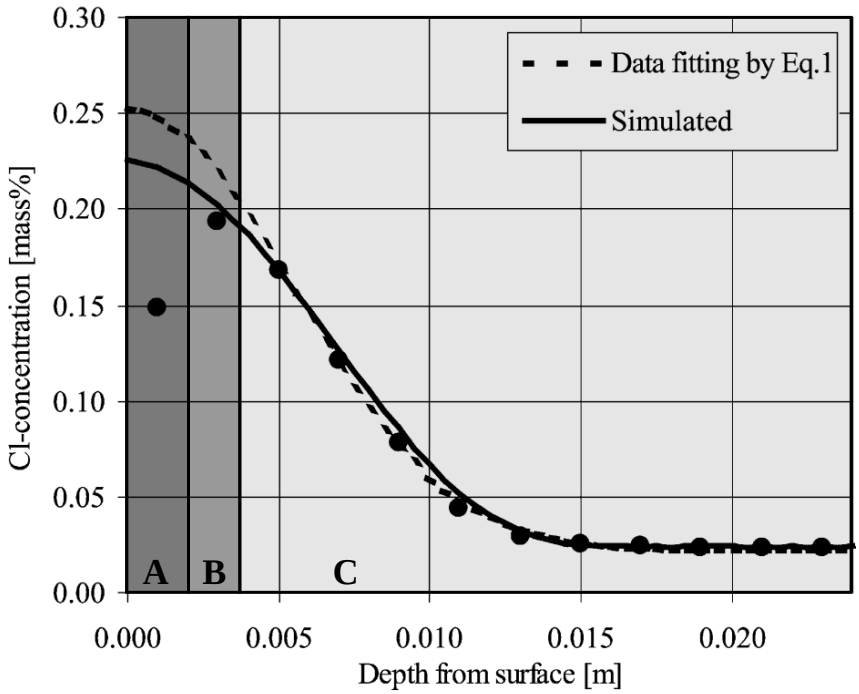


Figure 2.9: The chloride profile and data fittings from Nielsen and Geiker 2003 [5] as in Figure 2.1. The different zones where chloride binding might be influenced by pH is indicated: In zone A, harsh leaching leads to a large decrease in pH and therefore lower chloride binding. Zone B is where a small drop in pH increases the chloride binding, leading to a maximum in the chloride profile. Zone C is not yet affected by leaching, which makes the chloride binding independent of concrete depth. Chlorides will then diffuse predictably according to Fick's law.

# 3 Experimental

In this chapter the experimental setup of the study is described. First an overview of the experimental approach is presented, then an overview of the chemicals and apparatuses used are given. The procedures are divided into four sections, the first of which is sample preparation, detailing the mixing and chloride exposure of the well-hydrated cement paste. The second section details how the pH-development curve was established. The third section describes the chloride binding experiments, and the final section details the phase assemblage study.

## 3.1 Experimental approach

This section gives a short overview of all the experimental work carried out in the current study.

Well-hydrated OPC paste was exposed to NaCl, then the pH was lowered by adding HCl in small steps. The process of lowering pH of the pore solution by acidifying the exposure solution of a hydrated cement paste will from here on be referred to as "artificial leaching". To one of the samples acid was added until the whole sample tube was filled. The pH was measured after each addition, resulting in a pH-development curve showing the relationship between volume of added acid and pH of the exposure solution. The pH-development curve was used to determine what amount of acid was to be added to the other samples. For these samples, the chloride concentration and pH were measured after all steps of acid addition were completed. The measured chloride concentration of the exposure solution was used to calculate the amount of bound chlorides, which was then plotted as a function of pH in the pore solution. The slow but still ongoing hydration of the well-hydrated cement paste of each of the samples was stopped with double solvent exchange, before they were analysed with thermogravimetric analysis (TGA), X-ray diffraction (XRD) and SEM-EDS (scanning electron microscopy with energy dispersive spectroscopy). Concentrations of elements in solution were studied with inductively coupled plasma mass spectrometry (ICP-MS).

## 3.2 Chemicals

Table 3.1 gives the chemicals and materials used in the project.

Table 3.1: Overview of materials and manufacturers. Oxide composition of OPC is provided in Table 3.2.

| Material | Purity | Manufacturer |
|---|---|---|
| OPC | ≥ 99.8 % | Norcem |
| NaCl | ≥ 99.7 % | Merck |
| 4 M HCl | ≥ 99.7 % | VWR |
| Isopropyl alcohol | ≥ 99.7 % | VWR |
| Petroleum ether | ≥ 99.0 % | Merck |
| 65 % $HNO_3$ | ≥ 99.7 % | Merck |
| Polyvinyl alcohol | ≥ 98.0 % | Merck |

### 3.2.1 Cement

The OPC was produced by Norcem AS. Table 3.2 presents the oxide composition of the clinker, provided by Norcem.

Table 3.2: Oxide composition of the OPC clinker as determined by X-ray fluorescence (XRF). Results provided by Norcem AS. LOI stands for "loss on ignition" at 1050 °C.

| Composition | Weight percent [%] |
|---|---|
| LOI | 1.07 |
| $SiO_2$ | 19.91 |
| $Al_2O_3$ | 5.15 |
| $TiO_2$ | 0.28 |
| MnO | 0.06 |
| $Fe_2O_3$ | 3.42 |
| CaO | 62.73 |
| MgO | 2.34 |
| $K_2O$ | 1.09 |
| $Na_2O$ | 0.48 |
| $SO_3$ | 3.16 |
| $P_2O_5$ | 0.11 |
| Sum | 99.80 |

### 3.2.2 NaCl-solution

A 1.5 M NaCl-solution was manually prepared by dissolving 116.881 ± 0.001 g NaCl in 1 l ultra-pure $H_2O$. The concentration was verified with titration to be 1.50 ± 0.01 M.

## 3.3 Apparatus

Table 3.3 gives an overview of the analytical apparatuses used in the study.

Table 3.3: Overview of apparatuses used for analysis in the current study.

| **Method** | **Apparatus** | **Manufacturer** |
|---|---|---|
| Chloride titration | Titrando 905 | Metrohm |
| pH-measurements | 6.0255.100 Profitrode | Metrohm |
| Centrifuge | Heraeus Megafuge 8 | Thermo Fisher |
| TGA | DSC 3 | Mettler Toledo |
| XRD | D8 Focus | Bruker |
| SEM | S-3400N | Hitachi |
| EDS | X-Max 80 $mm^2$ | Oxford Instruments |
| ICP-MS | 8800 Triple Quadrupole | Agilent |

## 3.4 Sample preparation

### 3.4.1 Mixing well-hydrated cement paste

In the current study the cement paste that was used had a high degree of hydration and a significant amount of free water which was not chemically bound in hydrate phases. What is referred to as "well-hydrated cement paste" in the following sections is a moist sand-like paste, which can be thought of as a combination of free water and cement paste. The cement paste can again be divided into hydrates and dry binder (the dry cement powder before hydration). TGA was used to determine the weight percentages of free water, hydrates and dry binder, see Section 3.7.3.

The well-hydrated OPC was provided by Alisa Machner and was originally prepared for her PhD project in 2016 [50]. The paste was mixed in batches of 540 g, using 360 g OPC and 180 g deionized water (w/c = 0.5) in a Braun MR 5550CA high-shear mixer. The mixing procedure was blending for 30 seconds, letting the mixture rest for 5 minutes, before blending for another

60 seconds. After mixing, the paste was poured into 125 ml bottles, which were sealed with lids and parafilm. The bottles were then stored in water baths up to their bottleneck at 60 °C. To maximize hydration, the samples were ground and rehydrated after 3 months curing. They were crushed in a jaw crusher and sieved through a 1 mm sieve. Remaining particles were crushed further in a rotating disc mill until they also passed the sieve. After crushing, the samples were put in 1 l polypropylene bottles with additional 30 wt% of water. The bottles were then sealed with lids and parafilm and stored for another 4 months at 60 °C. After this final curing, the bottles containing the well-hydrated cement pastes were stored at 20 °C for one year before chloride exposure, which was also performed at 20 °C.

### 3.4.2 Chloride exposure

Table 3.4 gives a summary of the chloride exposure for the six samples in the current study. All samples have the same cement binder composition and were exposed to NaCl solution of the same concentration (1.5 M). The sample names indicate the solid composition (100 % well-hydrated OPC paste) and the total volume of acid added. They were prepared by weighing 15 ± 0.01 g of the well-hydrated cement paste into 50 ml centrifuge tubes and adding 20 ml of a 1.5 M NaCl exposure solution to them. The tubes were then closed with screw-on lids and parafilm, and thoroughly shaken to mix the liquid and the solid. They were then left for two weeks at 20 °C to reach equilibrium, while being shaken once per week to ensure full exposure. After these two weeks the pore solution in the paste and the exposure solution are assumed to have the same composition. Samples OPC-0 through OPC-17 were intended to be used for chloride binding and pH-measurements, while sample OPC-22.5Max was used to establish the pH-development curve. Sample OPC-0C was used as a centrifugation-test.

Table 3.4: Summary of experimental setup, showing amounts of well hydrated OPC-paste, NaCl exposure solution and 4 M HCl what was ideally added to each sample. Exact values were determined by weighing the samples before and after any substanses were added.

| **Sample name** | **OPC [g]** | **1.5 M NaCl [ml]** | **Total volume 4 M HCl [ml]** |
|---|---|---|---|
| OPC-0C (Centrifugation) | 15 ± 0.01 | 20 | - |
| OPC-0 (Reference) | 15 ± 0.01 | 20 | - |
| OPC-0.5 | 15 ± 0.01 | 20 | 0.5 |
| OPC-2.5 | 15 ± 0.01 | 20 | 2.5 |
| OPC-5 | 15 ± 0.01 | 20 | 5 |
| OPC-17 | 15 ± 0.01 | 20 | 17 |
| OPC-22.5Max (pH development) | 15 ± 0.01 | 20 | 22.5 |

## 3.5 Establishing the pH-development curve

The first part of the experiments was establishing the relationship between the volume of added acid and the resulting pH of the pore solution, here referred to as the pH-development curve.

HCl was chosen to acidify the samples to avoid adding new ions to the system. With a concentration of 4 M it was also strong enough to be able to lower the pH of the exposure solution efficiently. Other acids such as $HNO_3$, $H_2SO_4$, $H_3PO_4$ and HF were considered. $HNO_3$, $H_2SO_4$ and $H_3PO_4$ were dropped because the effect the anions might have on the phase assemblage of the cement paste, in particular the AFm-phases which incorporates anions [51]. HF could have been used to avoid the increase in chloride concentrations caused by adding HCl, but the dangers of using HF would have outweighed the potential benefits.

Sample OPC-22.5Max was used to establish the pH-development curve. 4 M HCl was added in steps until the sample tube was filled. The acid was first added in 10 steps of 0.25 ml, then 4 steps of 0.5 ml, 2 steps of 1 ml, then 8 steps of 2 ml which filled the sample tube. The final volume of acid was 22.5 ml. The pH of the sample was measured 10-15 minutes and 1-3 days after each addition (“instant pH” and “pH at EQ” respectively in Figure 4.4).

### 3.5.1 pH-measurements

Before measuring the pH, the sample was centrifuged at 4000 rpm for 2 minutes and 30 seconds. This was necessary due to the low amount of clear supernatant. To avoid measuring directly in the sample tube, 2 ml of the supernatant was pipetted into 15 ml centrifuge tubes, in which the pH was measured. After each measurement the remaining supernatant was poured back into the sample. The electrode was calibrated each day before the measurements using buffer solutions of pH 7, 10 and 13.

## 3.6 Chloride binding experiments

After establishing the pH-development curve, five samples were prepared using the same methods but with different final acid volumes (see Table 3.4). The chloride binding of these samples was then determined.

### 3.6.1 Addition of HCl

No acid was added to sample OPC-0, which served as a reference sample. To the other samples, different amounts of 4 M HCl were added in the same steps as for the pH-development sample to reach total volumes of 0.5, 2.5, 5 and 17 ml, as shown in Table 3.4. After each addition, the samples were shaken and left to rest. Acid was added each workday, leading to a minimum resting time of 1 day and a maximum of 3 days. The samples were weighed before and after each acid addition. These weight measurements and the calculated amount of HCl added is presented in Appendix F.

After having the full amount of acid added, the samples were stored at 20 °C for two weeks. They were all shaken once per week. To ensure separation of liquid and solids, the samples were transported from the 20 °C storage room to the laboratory at least one day prior to analysis.

### 3.6.2 Chloride titration

Table 3.5 gives a summary of the chloride titration measurements.

Table 3.5: Overview of the amount of liquid that was extracted from each sample for the chloride titration experiments.

| Sample | Method 1 # of measurements | Method 1 Volume [ml] | Method 2 # of measurements | Method 2 Volume [ml] |
|---|---|---|---|---|
| OPC-0C (Centrifugation) | - | - | 6 | 1 |
| OPC-0 (Reference) | 4 | 0.2 | - | - |
| OPC-0.5 | 4 | 0.2 | - | - |
| OPC-2.5 | - | - | 6 | 1 |
| OPC-5 | - | - | 6 | 0.75 |
| OPC-17 | - | - | 6 | 0.5 |
| OPC-22.5Max (pH-trial) | - | - | - | - |

Sample OPC-0 was measured two weeks after exposure to the NaCl solution. All other samples were analysed two weeks after their full amounts of acid had been added. Two different variations of the same method were used. For Method 1, used for sample OPC-0 and OPC-0.5, 0.2 ml of the liquid phase was extracted for analysis. The chloride concentration was measured using 0.1 M $AgNO_3$ and a 5 ml burette. The extracted liquid was pipetted into measurement beakers with 1 ml 1:10 65 % $HNO_3$ and 2.5 ml 2 g/l polyvinyl alcohol. To this mixture approximately 20 ml of deionized water was added before titration. The exact same procedure was used for sample OPC-0.5 and later again for sample OPC-0, but then by extracting 3 times 0.2 ml to get more data points.

Method 2 was adopted for the remaining samples to reduce the error caused by deviations in extracted volume. Method 2 used a 20 ml burette and a larger sample volume of 0.5-1 ml. All the other measurement parameters were equal to the Method 1. Samples OPC-2.5, OPC-5 and OPC-17 were analysed with the second method.

### 3.6.3 Chloride binding calculation

The amount of bound chloride was determined by calculating the total amounts of chloride added to the sample and subtracting the amount in solution. The amount of bound chloride is then divided by the amount of cement paste without free water in the sample. Equation 3-1 describes the calculation of chloride binding.

$$C_b = \frac{Cl_{tot} - Cl_{sol}}{m_{paste}}$$

$$= \frac{Mm_{Cl^-} \cdot [V_{NaCl} \cdot C_{NaCl} + V_{HCl} \cdot C_{HCl} - (V_{NaCl} + V_{H_2O,\text{paste}} + V_{HCl}) \cdot C_{Cl^-}]}{m_{paste}} \quad \text{3-1}$$

Here $C_b$ is the amount of bound chlorides in g chlorides per g cement paste, $Cl_{tot}$ and $Cl_{sol}$ are the total amounts of added chloride and the remaining chlorides in solution respectively, both in grams. $m_{paste}$ is the mass of cement paste (without free water) initially put into the sample (determined by drying paste at 40 °C for 10 hours, see Section 3.7.3), $Mm_{Cl}$- is the molar mass of the chloride ion, $V_{NaCl}$ and $C_{NaCl}$ are the volume and concentration of the exposure solution. $V_{HCl}$ and $C_{HCl}$ are the volume and concentration of the HCl added to the sample. $V_{H2O,\ paste}$ is the volume of water in the cement paste, which is found by TGA of the wet cement paste. $V_{HCl}$ is the added volume of acid and $C_{Cl}$- is the measured chloride concentration.

### 3.6.4 Effect of centrifugation

The chloride concentration of OPC-0C (Centrifugation) was measured using Method 2. First, three measurements were taken before centrifugation. After centrifugation at 2400 rpm for 2 minutes and 30 seconds, three more measurements were made. The pH of sample OPC-0C was assumed to be the same as sample OPC-0.

### 3.6.5 pH-measurements

Measurements of pH in the chloride binding samples was performed in the exact same way as for the pH-development sample, as described in Section 3.5.1. The pH was always measured after the chloride titration experiments were concluded, to avoid affecting the determination of the chloride binding.

### 3.6.6 Weight measurements

To keep track of evaporation losses, losses during measurements, and amount of added acid, the weights of the filled sample tubes were closely monitored between the different steps of the experiments. A Mettler PE 160 balance was used for weighing, which has an accuracy of ± 1 mg. Sample OPC-22.5Max, the pH-development sample, was weighed before and after each pH-measurement and acid addition. The 15 ml tubes used for pH-measurements were also weighed before use, with liquid inside the tube and after the liquid was poured back into the sample. The other samples were weighed before and after acid addition, chloride titration and

pH-measurement. Weight measurements for the acid additions to the chloride binding samples are provided in Appendix F.

## 3.7 Analysis of phase assemblage

After concluding measurements of pH and chloride binding, the exposure solution and the solid phases were studies using ICP-MS, TGA, XRD and SEM-EDS.

### 3.7.1 Inductively coupled plasma mass spectroscopy

The concentrations of elements in the liquid phase was analysed using ICP-MS. After centrifuging the samples, 5 ml of the supernatant was extracted into 15 ml centrifuge tubes. To acidify and dilute the samples, 150 µl of the extracted supernatant was pipetted into new 15 ml centrifuge tubes together with 104 µl 65 % $HNO_3$. This mixture was then diluted to 15 ml using ultra-pure $H_2O$, which meant a 100 times dilution of the sample and a resulting $HNO_3$-concentration of 0.1 M. These diluted samples were then submitted for analysis at the ICP-HR-MS-lab at NTNU.

To verify the validity of the ICP-MS results, a charge balance between $Ca^{2+}$, $K^+$, $Na^+$, $Cl^-$ and $OH^-$ was used to calculate a rough estimate for the pH. This estimated pH was then compared to the pH measured with the potentiometric measurements. Equation 3-2 gives the calculation for expected pH, where *[A]* is the concentration of ion *A* in M divided by 1 M. An alternative and more accurate method could have been to calculate the expected pH using GEMS.

$$pH_{ICP-MS} = 14 + \log_{10}[OH^-] = 14 + \log_{10}(2 \cdot [Ca^{2+}] + [Na^+] + [K^+] - [Cl^-]) \qquad 3\text{-}2$$

### 3.7.2 Double solvent exchange

To analyse the solid fraction of the samples, 3-4 spatulas of the solids were extracted. The hydration was stopped, and the water removed by double solvent exchange. The well-hydrated, moist unexposed cement paste was also put through the same process (referred to as "OPC-No Cl" to indicate that the paste had not been exposed to chlorides). Approximately 3-5 g of the wet solids were placed in 125 ml plastic bottles with 100 ml isopropyl alcohol. The bottles were shaken for 30 seconds before resting for 5 minutes. After resting the liquid was decanted and another 100 ml isopropyl alcohol was added. The bottles were again shaken for 30 seconds and left to rest for 5 minutes, before the contents were poured into a vacuum

filtration unit. The isopropyl alcohol was filtrated off, and 20 ml petroleum ether was added. The ether and solids were stirred with a glass rod for 30 seconds before resting for 5 minutes. The contents were then filtrated until dry and stored in a vacuum desiccator (at 0.8 bar) for at least one day before roughly half was ground to pass a 63 µm sieve. The ground solids were used in TGA and XRD, while the unground solids were used for SEM-EDS.

### 3.7.3 Thermogravimetric analysis

TGA was used to determine the free water content in the well-hydrated cement paste before chloride exposure, and to investigate the phase assemblage before and after chloride exposure. For all the TGA analyses, approximately 150 mg of the solids were placed in 600 µl alumina crucibles.

To determine the free water content of the cement paste, non-solvent exchanged well-hydrated paste was dried at 40 °C until the weight was constant (after 10 hours) while purging with $N_2$ at 50 ml/min. The weight loss was normalized to the initial sample mass, giving the free water content of the well-hydrated cement paste.

The samples that had been solvent exchanged and ground were heated from 40 to 900 °C with a heating rate of 10 °C/min while purging with $N_2$ at 50 ml/min. The resulting weight loss curves were used to determine changes in phase assemblage by comparing peaks in the derivative of the weight-temperature curve. Most important were the peaks for portlandite (T ≈ 460 °C) and Friedel's salt (T ≈ 140 °C and between 250-400 °C).

The CH-content of the samples was determined by integrating the portlandite-peak in the derivative TGA-curves (the peaks in Figure 4.7 near 450 °C). Equation 3-3 describes the calculations used to determine the CH-content relative to the initial sample mass ($w_{40}$), which is denoted as $CH_{\%}$. It was calculated by multiplying the mass loss of the CH-peak ($w_{400}$-$w_{500}$) with the molar mass ratio of $Ca(OH)_2$ to $H_2O$ ($Mm_{Ca(OH)_2}/Mm_{H_2O}$) and dividing by the initial mass of the sample placed in the TGA ($w_{40}$) [52].

$$CH_{\%} = \frac{w_{400} - w_{500}}{w_{40}} \cdot \frac{Mm_{Ca(OH)_2}}{Mm_{H_2O}} = \frac{w_{400} - w_{500}}{w_{40}} \cdot \frac{74\ g/mol}{18\ g/mol} \qquad 3\text{-}3$$

The TGA only reveals the relative weight percentages of the decomposing phases. Since the cement pastes were exposed to acid, some phases were dissolving, which meant that the relative

weight percentages of the non-dissolving phases increased relatively. Figure 3.1 shows this concept. The CH-content in the different samples could therefore not be directly compared without normalization to a common basis.

The following calculations assume that while portlandite was present in the system it was the only phase that dissolved. This means that the weight loss percentage between 40 and 400 °C (before the portlandite peak, denoted $w_{40}$-$w_{400}$) should be constant regardless of acid exposure, as none of the other hydrates are assumed to be affected by the acid addition. The only difference in $w_{40}$-$w_{400}$ between sample OPC-0 and the samples exposed to acid should therefore be due to the dissolution of portlandite increasing the relative weight percentage of the remaining hydrates.

The wt% of CH for each of the samples, $CH_{\%}$, was first normalized to the weight percentage of dry binder in sample OPC-0, which is the weight percentage at 550 °C denoted $w^0_{550}$. To compensate for the change in relative weight percentages caused by acid exposure, the wt% of CH normalized to $w^0_{550}$ was multiplied with an adjustment factor. This factor was equal to the ratio between mass loss between 40 and 400 °C for sample OPC-0 ($w^0_{40}$-$w^0_{400}$) and the mass loss for the investigated sample ($w_{40}$-$w_{400}$). These calculations are described in Equation 3-4. The final normalized portlandite content is denoted $CH^N_{\%}$ and is equal to the wt% of CH in each of the samples, normalized to the dry binder weight in sample OPC-0 and corrected for dissolution. Values for $CH^N_{\%}$ for the samples in the current study are presented in Table 4.4 and included in Figure 4.4 (denoted as *CH-content* for simplicity).

$$CH^N_{\%} = \frac{CH_{\%}}{w^0_{550}} \cdot \frac{w^0_{40} - w^0_{400}}{w_{40} - w_{400}} \qquad 3\text{-}4$$

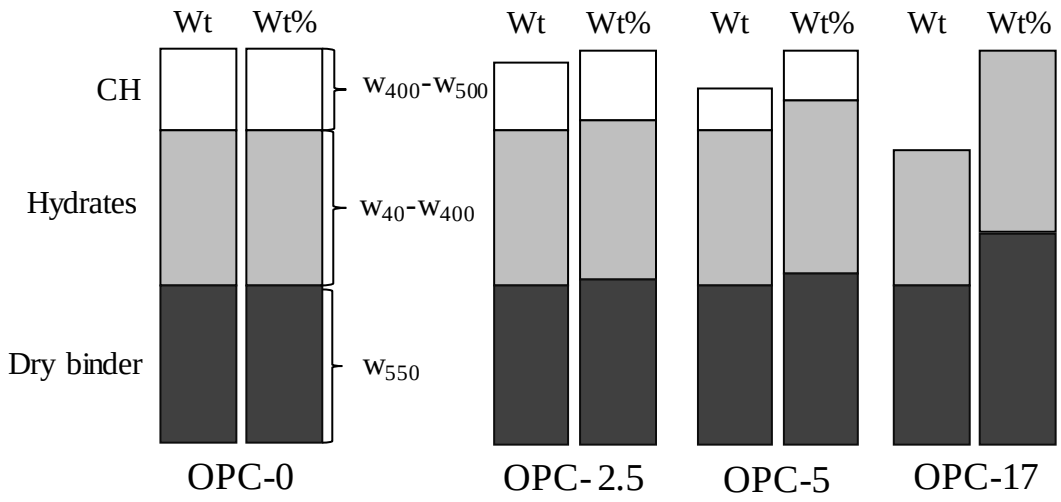


Figure 3.1: Illustration of how acid exposure changes the phase assemblage of the cement paste. The two bars per sample indicate how the total mass of the solid phases (Wt) and their relative weight percentages (Wt%) change upon acid addition. This illustration assumes that while there is portlandite present, it is the only phase that dissolves as acid is added. Thus, the amount of dry binder and other hydrates should not change. As portlandite dissolves, the weight fraction of portlandite ($w_{400}$-$w_{500}$) decreases, which causes the weight fraction of other hydrate phases ($w_{40}$-$w_{400}$) and dry binder ($w_{500}$) observed by TGA to increase. The CH-content can therefore not be directly normalized to the dry binder weight as is commonly done to compare CH-content from different hydrated cements [52]. The calculations in the current study therefore normalize the CH-content to the dry binder weight of sample OPC-0, where no portlandite has been dissolved, and adjust for the change in weight fractions by multiplying with a common basis. Here the ratio of hydrate phase weight loss for sample OPC-0 to the sample currently being studied was used (see Equation 3-4). For sample OPC-17 where all portlandite is dissolved, other hydrates have dissolved as well. There is however no need to use this normalization method for OPC-17 or OPC-22.5Max, as the content is zero regardless of normalization.

### 3.7.4 X-ray diffraction

The dried and ground powders were analysed using XRD to confirm phase changes. Approximately 0.5 g of the powders were placed in 27 mm diameter sample holders. They were analysed in a Bruker AXS D8 Focus with a Lynxeye detector, operating at 40 kV and 40 mA with a CuKα radiation source (wavelength 1.54 Å). The slit was set to 0.2 mm, scanning from 5-55° 2θ.

### 3.7.5 Scanning electron microscopy

Parts of the non-ground dried powders were impregnated with epoxy and polished for use in SEM-EDS. The impregnation and polishing were carried out by the polishing laboratory at the Department of Geology and Mineral Resources Engineering at NTNU. Before analysis the surfaces were coated with carbon in a Cressington 208 Carbon Coater to prevent charging. BSE

and EDS-maps of all samples were captured, in addition to 100 EDS point-scans of the cement paste matrix per sample. EDS was carried out at 10 mm working distance using 15 kV accelerating voltage and 70 µA probe current.

An estimate of the Ca/Si-ratio for all the samples was made using the EDS point scan data. In the plots of Al/Si-ratio (Appendix D.I), the right-most edge of the C-S-H point cloud gives the approximate composition of the pure C-S-H phase [20].

### 3.7.6 Thermodynamic model

A simulation of the system was run in the Gibbs Energy Minimization Software for Geochemical Modelling (GEMS, http://gems.web.psi.ch [53,54]). With GEMS, a prediction was made for the composition and phases for the sample setup in the current study at equilibrium. Details on how to set up the model in the software are provided in Appendix A.

The model uses the 15 g wet hydrated cement paste as a basis. The cement pastes prepared in the laboratory were mixed with a w/c-ratio of 0.5, meaning the original paste had 2/3 of the weight as cement and 1/3 as water. After an additional 30 wt% water was added, the wt% of cement in the well-hydrated paste was $2/3 \cdot 1/1.3$, whilst the wt% of water was $1 - (2/3 \cdot 1/1.3)$. In the model the amount of cement clinker is therefore set to be $(15 \cdot 2/3 \cdot 1/1.3)$ g, and the amount of water to be 15 g – $(15 \cdot 2/3 \cdot 1/1.3)$ g.

The GEMS software assumes full reaction of the input materials. The only way to account for unreactive phases is therefore to calculate the composition of the input material if the unreactive phases were removed. For this model it was assumed that $TiO_2$, MnO and $P_2O_5$ and calcium aluminoferrite ($4CaO{\cdot}Al_2O_3{\cdot}Fe_2O_3$ or $C_4AF$) were inert. The reaction degree of MgO was assumed to be 30 % due to the high curing temperature of the cement paste, which has been shown to cause the formation of hydrotalcite ($Mg_6Al_2(OH)_{18} \cdot 3H_2O$) [55].

The amounts of $TiO_2$, MnO, $P_2O_5$ and MgO in the cement clinker were known from the XRF results (see Table 3.2), so they were first subtracted from the composition. The remaining oxide composition was normalized to 100 %, before determining the amount of $C_4AF$.

The amount of $C_4AF$ was calculated using Bogues calculations for cement clinker composition, described in Equation 3-5 [56]. The calculations assumed that $Fe_2O_3$ is only present as $C_4AF$, and that the total atomic ratio of $Al_2O_3$ to $Fe_2O_3$ is larger than 0.64, which is required for there to be sufficient $Al_2O_3$ to form $C_4AF$ with all $Fe_2O_3$. This was the case for the cement clinker used in the current study. The wt% of $C_4AF$ in the clinker was then calculated to be equal to

the molar mass ratio of $C_4AF$ to $Fe_2O_3$, multiplied with the wt% of $Fe_2O_3$. Using the amount of $C_4AF$, the wt% of unreactive $Al_2O_3$ ($Al_2O_{3,\ unreacted}$) and $Fe_2O_3$ ($Fe_2O_{3,\ unreacted}$) was calculated using Equation 3-6 and 3-7 respectively. It should be noted that Equation 3-7 necessarily becomes a reformulation of Equation 3-5 because all iron was assumed to be in $C_4AF$. Since all $C_4AF$ was removed, all $Fe_2O_3$ was removed as well.

$$C_4AF\ (wt\%) = \frac{Mm_{C_4AF}}{Mm_{F_2O_3}} \cdot F_2O_3\ (wt\%) = 3.0432 \cdot F_2O_3\ (wt\%) \qquad 3\text{-}5$$

$$Al_2O_{3,unreacted} = \frac{Mm_{Al_2O_3}}{Mm_{C_4AF}} \cdot C_4AF\ (wt\%) = 0.596 \cdot Al_2O_3\ (wt\%) \qquad 3\text{-}6$$

$$Fe_2O_{3,unreacted} = \frac{Mm_{Fe_2O_3}}{Mm_{C_4AF}} \cdot C_4AF\ (wt\%) = \frac{C_4AF\ (wt\%)}{3.0432} = Fe_2O_3\ (wt\%) \qquad 3\text{-}7$$

All $Al_2O_3$ and $Fe_2O_3$ in $C_4AF$ was subtracted from the normalized cement composition before the result was normalized again to 100 g cement. With the resulting oxide composition, the number of moles of each element was calculated, which was used as input for the GEMS-model. The input values are provided in Appendix A.I.

The chloride binding predicted by the model was calculated using Equation 3-8. $C_b$ is the amount of bound chlorides in g chloride per g cement paste without free water, $n_{Fs}$ is the molar amount of Friedel's salt, $Mm_{Cl}$- is the molar mass of the chloride ion and $m_{paste}$ is the mass of cement paste without free water (set to 70 % of the well-hydrated paste in the model, i.e. $0.7 \cdot 15$ g based on drying of the real well-hydrated paste using TGA, as described in Section 4.4.2). Note that the CH-content and bound chlorides are not normalized to the same parts of the cement paste, The CH-content is normalized to the amount of dry binder, which does not include hydrates, whereas the chloride binding is normalized to the cement paste including hydrate phases, only subtracting free water.

$$C_b = 2 \cdot n_{Fs} \cdot Mm_{Cl^-} \cdot \frac{1}{m_{paste}} \qquad 3\text{-}8$$

# 4 Results

## 4.1 Thermodynamic model

Figure 4.1 shows the volume of the phases in the samples as a function of the amount of HCl added, as predicted by the GEMS-model. The y-axis is cut off to focus on the solid phases, thus only a small part of the volume of exposure and pore solution is shown. The model predicted that the amount of portlandite drops linearly with increasing acid addition, and that it is completely dissolved at 21 ml of acid. The C-S-H begun dissolving when more than 21 ml acid was added.

The volume of AFt-phases remained stable until 33 ml of acid was added, after which the volume decreased steadily and was fully removed at 36 ml acid. Hydrotalcite ($Mg_6Al_2(OH)_{18} \cdot 3H_2O$) maintained the same volume from 0-36 ml acid. At high volumes of acid and low pH, the model predicted the formation of natrolite ($Na_2O{\cdot}Al_2O_3{\cdot}3SiO_2 \cdot 2H_2O$), gypsum ($CaSO_4 \cdot 2H_2O$) and M-S-H (magnesium-silicate-hydrate). These acid volumes are however beyond the scope of the current study.

The amount of Friedel's salt remained near constant in the range of 0–28 ml acid, before it starts dissolving until nothing is left at 32 ml acid. Friedel's salt is the only phase that binds chlorides in the thermodynamic model, thus the model also predicts constant chloride binding in the range of 0-28 ml acid. Figure 4.3 presents the calculated chloride binding of the model, found using Equation 3-8.

Figure 4.2 shows the concentration of different elements in the exposure and pore solution of the samples as a function of the amount of added acid, as predicted by GEMS. Also included is the predicted hydroxyl concentration, which drops as acid is added. The pH from the model is plotted in Figure 4.4. The concentrations of Ca, Cl, Mg and Si increase, whilst those for Na and K drop for the entire modelled range of acid. The concentrations of S and Al initially decrease as acid is added. The concentration of S flats out, remaining constant while AFt is stable, before increasing after AFt dissolves. The concentration of Al starts to increase after 20 ml acid is added, then starts to decrease after 30 ml.

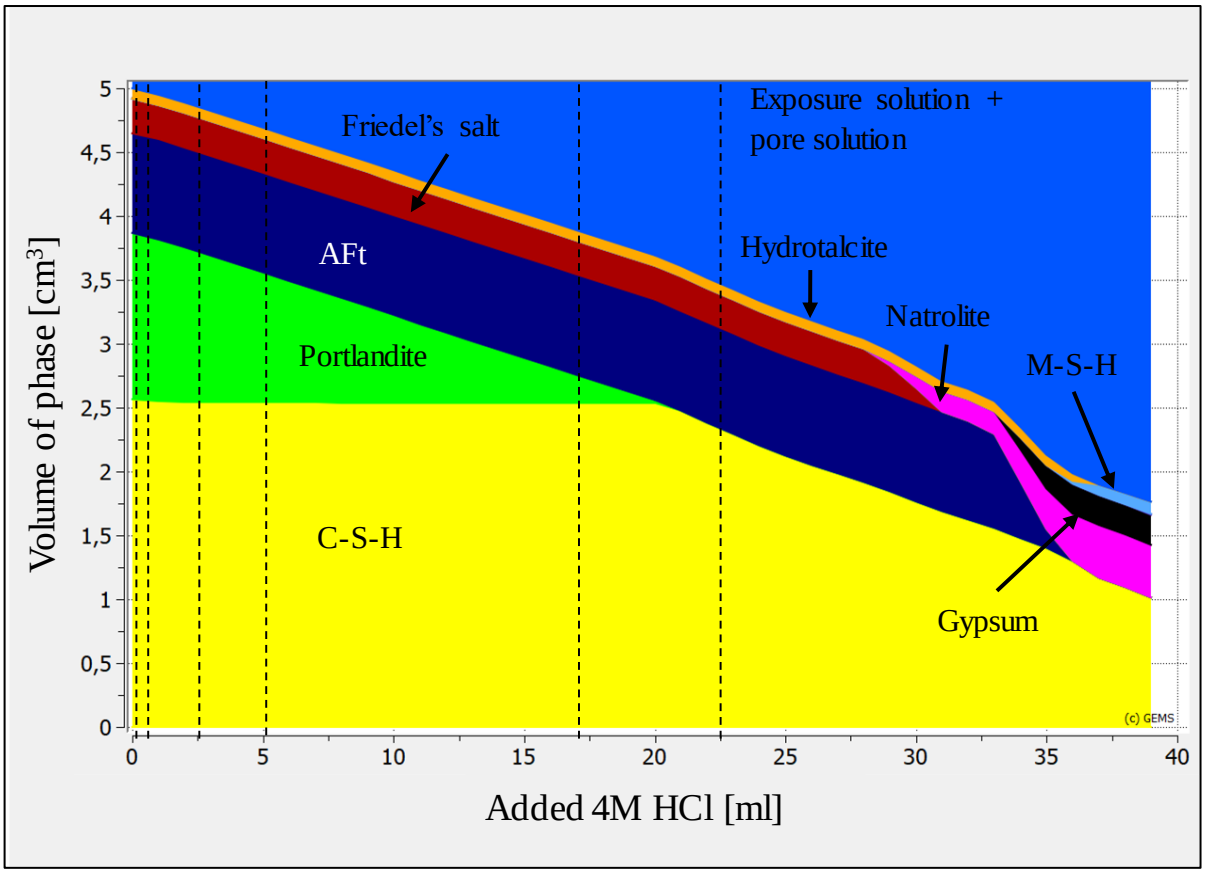


Figure 4.1: GEMS-model of phase assemblage in the samples when exposed to increasing amounts of 4 M HCl. The dashed lines indicate the acid volumes added to the samples in the current study.

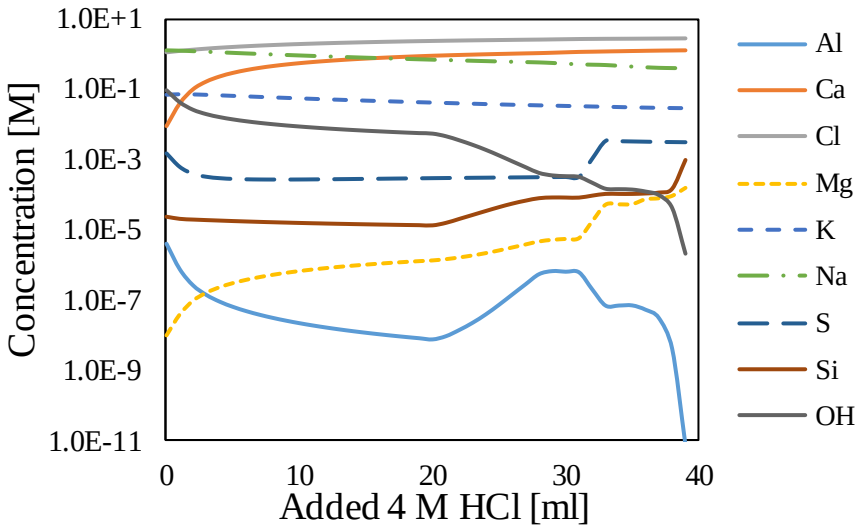


Figure 4.2: GEMS-model of the liquid phase (exposure solution) of the samples in the current study. The y-axis is in a logarithmic scale with base 10.

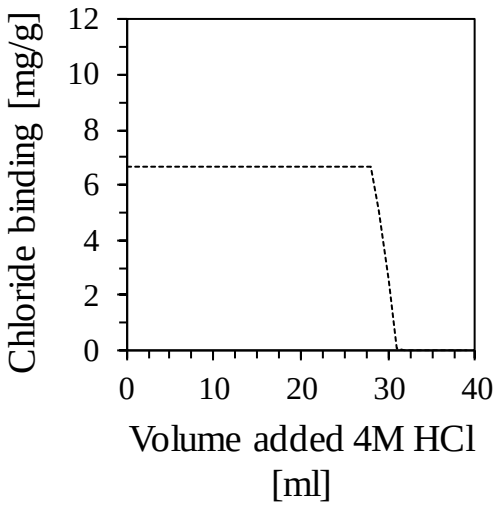


Figure 4.3: The chloride binding of 15 g well hydrated cement paste as predicted by the thermodynamic GEMS model. The chloride binding is based on the amount of Friedel's salt, which remained constant in the range of 0-28 ml acid added. The amount of bound chlorides (Equation 3-8) was divided by the mass of cement paste without free water, which in the model was equal to $0.7 \cdot 15$ g (see Section 3.7.6 and Appendix A).

## 4.2 pH-development curve

Figure 4.4 shows the measured pH-development curve determined by acidifying sample OPC-22.5Max until the sample tube was filled. The pH-values were measured both directly after adding acid (Instant pH) and 1-3 days after (pH at EQ). Also included is the pH and CH-content as predicted by the thermodynamic model, and the CH-content of the samples that were studied with TGA (all except OPC-0C). The CH-content decreased with increasing acid additions, both for the samples and in the model. The model predicted a considerably higher CH-content than was observed in the samples.

The pH decreased continuously with increasing amounts of HCl. However, it did not turn neutral or acidic despite adding large volumes of acid. For small additions, the difference between pH at equilibrium and directly after adding were close to zero. The difference increased in later additions, likely because of larger amounts added per step and lower buffer capacity due to lower CH-content.

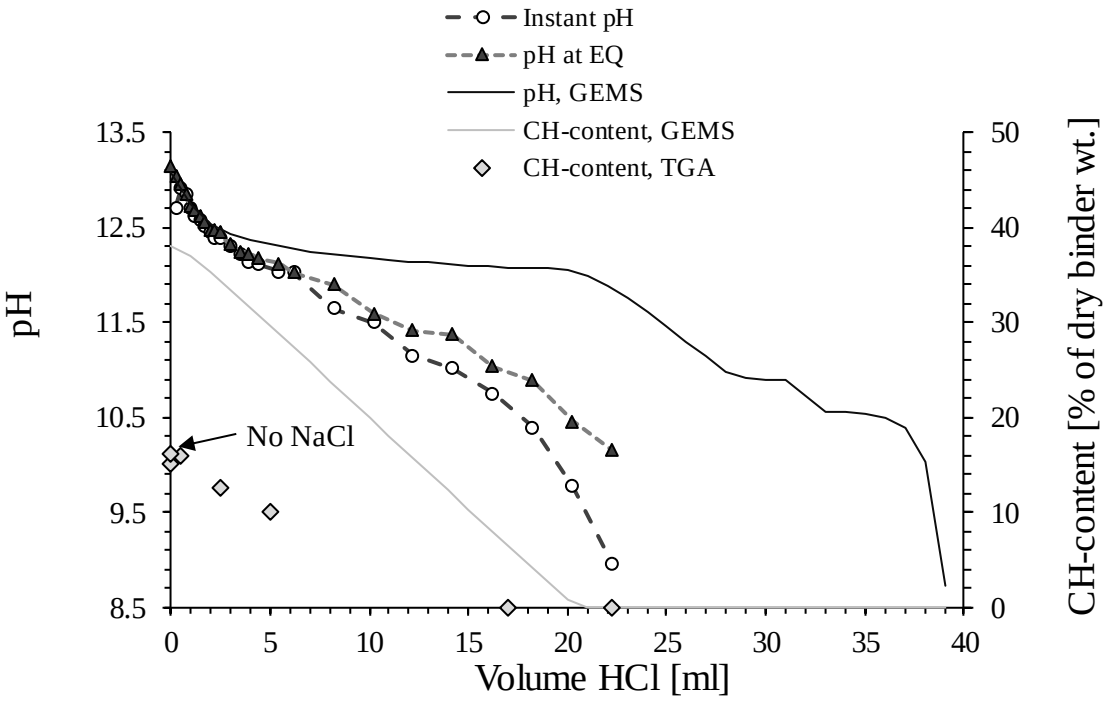


Figure 4.4: pH of sample OPC-22.5Max (the pH-development sample) as a function of added 4 M HCl, compared to the results of the GEMS-model showing expected pH. The lines for "Instant pH" and "pH at EQ" are from measurements of sample OPC-22.5Max directly after and 1-3 days after adding acid respectively. The portlandite-content as determined by TGA, normalized to the amount of dry binder in sample OPC-0 is also included ("CH-content, TGA" in the figure, see Section 3.7.3 for details and Table 4.4 for values), along with the CH-content as predicted by the GEMS-model. The "Dry binder wt." on the secondary axis refers to the weight of dry binder in the sample before acid addition. For the samples that is the weight of sample OPC-0 at 550 °C, for the GEMS-model it is the amount of OPC put into the model (15 · 2/3 · 1/1.3, see Section 3.7.6).

## 4.3 Chloride binding

Table 4.1 presents the measurements of pH and the determined average chloride concentrations of the exposure solution in the samples. Average chloride binding in mg chloride per g cement paste without free water is also included. The measured pH-values lie closely to those of the pH-development curve for the same acid volumes. The uncertainty of pH-measurements was estimated to be ± 0.1, while the errors in chloride concentration and binding are calculated using a Gaussian error propagation (detailed in Appendix B).

Table 4.1: Overview of pH, average chloride concentrations and average chloride binding for the samples in the current study. The chloride binding is given in mg chloride bound per g cement paste without free water. The amount of cement paste without free water per sample was determined by drying the well-hydrated cement paste in the TGA, as described in Section 3.7.3. The error for determining the pH is estimated to be ± 0.1, while error for chloride concentration and binding is calculated with Gaussian error propagation (see Appendix B for details on error calculation).

| **Sample** | **pH** | **Average [$Cl^-$] [M]** | **Average chloride binding [mg/g]** |
|---|---|---|---|
| OPC-0 | 13.2 ± 0.1 | 1.15 ± 0.01 | 6.3 ± 0.9 |
| OPC-0.5 | 13.0 ± 0.1 | 1.19 ± 0.01 | 7.4 ± 1.2 |
| OPC-2.5 | 12.5 ± 0.1 | 1.39 ± 0.01 | 8.7 ± 0.8 |
| OPC-5 | 12.2 ± 0.1 | 1.59 ± 0.02 | 10.3 ± 0.9 |
| OPC-17 | 11.0 ± 0.1 | 2.37 ± 0.03 | 0.3 ± 2 |

Figure 4.5 shows the calculated amount of bound chlorides for the samples as a function of the pH in the liquid phase (subfigure A) and the free chloride concentration (subfigure B). The arrow indicates the direction of increased acid additions. Adding acid lead to lowered pH and increased free chloride concentration.

Below 5 ml of added acid there was a clear trend of increasing chloride binding with increasing free chloride concentration and decreasing pH. The sample exposed to 17 ml acid showed close to no chloride binding. This indicated that after adding a certain amount of acid, the binding phases were dissolved or in some other way prevented from binding chlorides.

The centrifugation-test of sample OPC-0C resulted in chloride binding values of 2.6 ± 0.2 mg/g before and after centrifugation.

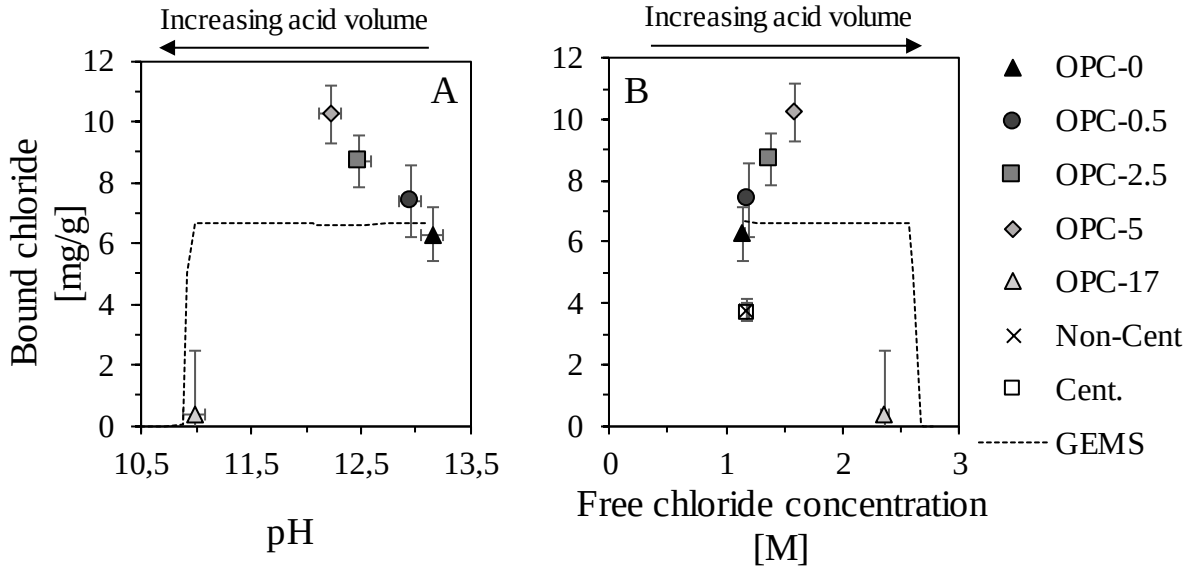


Figure 4.5: Average values for chloride binding of the samples as a function of the pH (A) and the free chloride concentration (B) in the exposure solution of the samples, from Table 4.1. The chloride binding is given as mg bound chloride per g cement paste without free water. All data points have errors calculated with Gaussian error propagation for the y-axis. The pH-values have an estimated ± 0.1 error, whilst the free chloride concentration values are also calculated with Gaussian error propagation (see Appendix B).

## 4.4 Phase assemblage

### 4.4.1 ICP-MS

Table 4.2 shows the concentration of elements in the liquid phase of the samples as determined by ICP-MS. There was a clear trend of increased concentration for Ca and Cl with increasing acid addition, whilst the concentrations of K and Na decreased. The concentration of S decreased for 5 ml or less of added acid, then increased for 17 ml and decreased for 22.5 ml acid. There were no clear trends for Fe, Al and Si. Some of the measured concentrations were negative, indicating that the concentrations were below the detection limit of the instrument or that there were errors in the preparation of the samples for the ICP-MS.

These results are not reliable, as can be seen by the estimated pH of the solution calculated using a charge balance (Equation 3-2, described in Section 3.7.1). Table 4.3 shows the steps in the calculation and the resulting pH and $OH^-$concentration. For all samples except OPC-17, the calculated concentration of $OH^-$ was negative, meaning the pH could not be calculated. For sample OPC-17 the pH was calculated to be 12.0, which is higher than the measured 11.0 ± 0.1.

Table 4.2: Results from the ICP-MS measurements of the samples in the current study. The reported values are adjusted for the dilution and acidification during the sample preparation (described in Section 3.7.1). The values for pH are from the measurements performed before ICP-MS. Some values are below zero (highlighted in grey), indicating that the concentration was below the detection limit or that the results are unreliable.

| Sample | pH | Al [M] | Ca [M] | Cl [M] | Fe [M] | K [M] | Na [M] | S [M] | Si [M] |
|---|---|---|---|---|---|---|---|---|---|
| OPC-0 | 13.2 | 5.9E-6 | 6.4E-3 | 1.1E+0 | -2.1E-7 | 7.6E-2 | 5.6E-1 | 3.9E-3 | -5.1E-5 |
| OPC-0.5 | 13.0 | 2.9E-6 | 9.0E-3 | 1.1E+0 | -2.3E-7 | 6.8E-2 | 3.8E-1 | 2.2E-3 | -4.7E-5 |
| OPC-2.5 | 12.5 | 2.0E-6 | 1.1E-1 | 1.3E+0 | -1.7E-7 | 6.8E-2 | 4.2E-1 | 3.1E-4 | 8.6E-5 |
| OPC-5 | 12.2 | 4.4E-5 | 2.7E-1 | 1.4E+0 | 1.8E-5 | 5.9E-2 | 2.2E-1 | 2.3E-4 | 1.3E-4 |
| OPC-17 | 11.0 | -9.1E-8 | 1.1E+0 | 2.3E+0 | 1.1E-7 | 4.4E-2 | 2.4E-2 | 7.2E-3 | 1.1E-4 |
| OPC-22.5Max | 10.2 | 1.1E-6 | 1.3E+0 | 2.5E+0 | -1.0E-7 | 3.8E-2 | -1.0E-1 | 3.9E-3 | 4.5E-4 |

Table 4.3: Charge balance of the ICP-MS results presented in Table 4.2. The concentration of $OH^-$ is calculated using a charge balance between $Ca^{2+}$, $Na^+$, $K^+$, $Cl^-$ and $OH^-$, using Equation 3-2.

| Sample | 2·Ca+Na+K [M] | Cl [M] | $OH^-$ [M] | Charge balance pH |
|---|---|---|---|---|
| OPC-0 | 6.4E-1 | 1.1E+0 | -4.4E-1 | - |
| OPC-0.5 | 4.6E-1 | 1.1E+0 | -6.0E-1 | - |
| OPC-2.5 | 7.1E-1 | 1.3E+0 | -5.4E-1 | - |
| OPC-5 | 8.1E-1 | 1.4E+0 | -5.7E-1 | - |
| OPC-17 | 2.3E+0 | 2.3E+0 | 1.1E-2 | 12.0 |
| OPC-22.5Max | 2.5E+0 | 2.5E+0 | -7.8E-2 | - |

### 4.4.2 TGA

After drying the non-solvent exchanged well-hydrated cement paste not exposed to chlorides at 40 °C for 10 hours, it lost 30.5 ± 0.2 % of its mass. This percentage was used as the amount of free water in the well-hydrated cement paste in the chloride exposed samples. This means that of the 15 g well-hydrated cement paste in each sample tube there was 4.58 g of free water and 10.42 g cement paste.

Figure 4.6-A present the TGA-curves (TG-curves) for all the chloride exposed samples and for the well hydrated OPC paste that has not been exposed to any chloride solutions (OPC-No Cl).

Figure 4.6-B shows the time-derivative of the TGA-curves in Figure 4.6-A (DTG-curves). Figure 4.7 shows a selected region of the DTG curves in the temperature region of 300-520 °C. The portlandite peak in Figure 4.7 near 450 °C showed a clear decrease in the CH weight loss peak with increasing acid addition. Since portlandite dissolved, the weight loss peaks of all other non-dissolving phases increased. Table 4.4 gives the calculated CH-content of the samples in the current study, normalized to the dry binder weight of sample OPC-0 and adjusted for dissolution (as described in Section 3.7.3). It shows that the CH-content corrected for dissolution also drops with increasing acid additions, in agreement with the qualitative observations from the DTG curves.

The peaks near 350 °C are from the decomposition of AFm, most likely Friedel's salt [52]. The peaks changed upon chloride exposure of the paste, shifting from one peak to two. After 17 ml of acid exposure the peak shape changed back to one peak, which was shifted to higher temperature compared to the original peak.

There was a clear shift in the DTG-curve of the non-chloride exposed hydrated paste, OPC-No Cl. Its peaks were similar in shape to those of sample OPC-0 (except for the Friedel's salt peaks), but the peaks were shifted approximately 20 °C higher than for the chloride exposed samples. The samples had similar sample sizes, but the difference might have been caused by varying coarseness.

Table 4.4: Calculated CH-content of the samples in the current study, normalized to the wt% of dry binder in sample OPC-0 (see Section 3.7.3 for details). The CH-content of the hydrated cement paste before chloride exposure is also included (No NaCl). Standard deviations were calculated with Gaussian error propagation

| **Sample** | **CH-content [wt% of dry binder]** |
|---|---|
| OPC-No Cl | 15.8 ± 0.2 |
| OPC-0 | 15.1 ± 0.2 |
| OPC-0.5 | 15.9 ± 0.2 |
| OPC-2.5 | 12.6 ± 0.2 |
| OPC-5 | 9.9 ± 0.2 |
| OPC-17 | - |
| OPC-22.5Max | - |

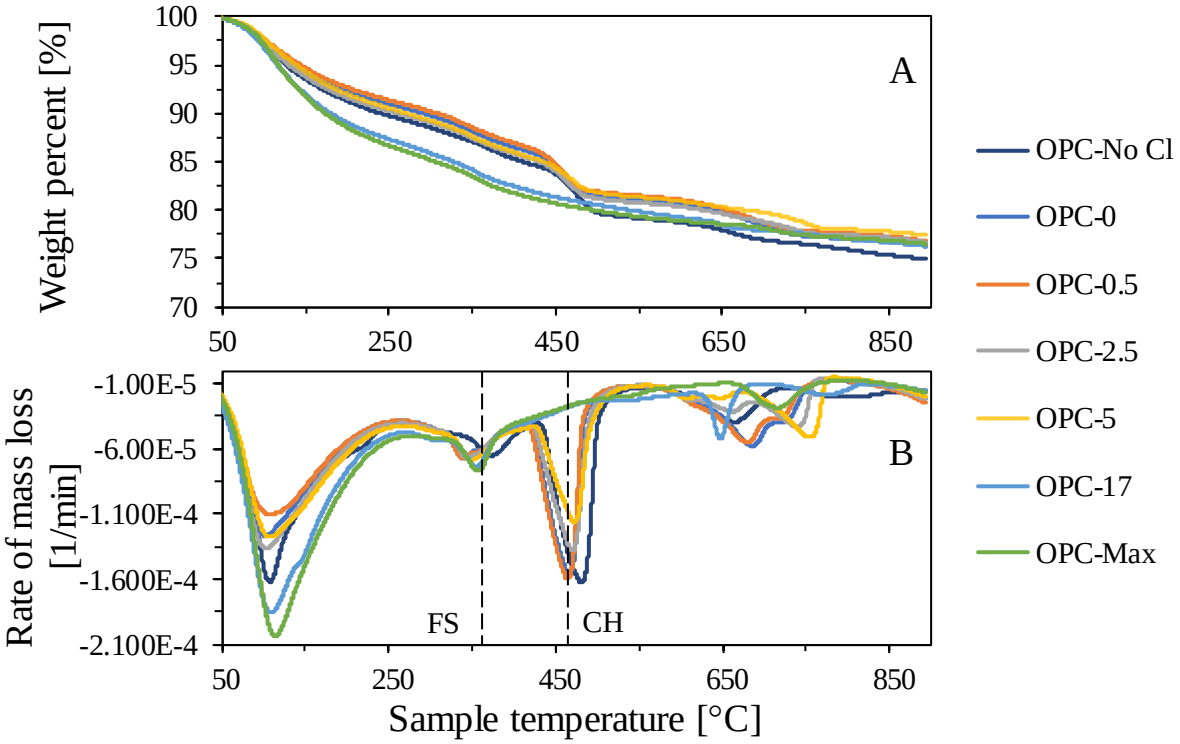


Figure 4.6: Weight loss curves (TG) of all samples from 40 to 900 °C (A) and the derivative (DTG) of the weight loss curves (B), as determined by TGA. Results from paste not exposed to chlorides (OPC-No Cl) is also included. Peaks for Friedel's salt (FS) and portlandite (CS) are highlighted.

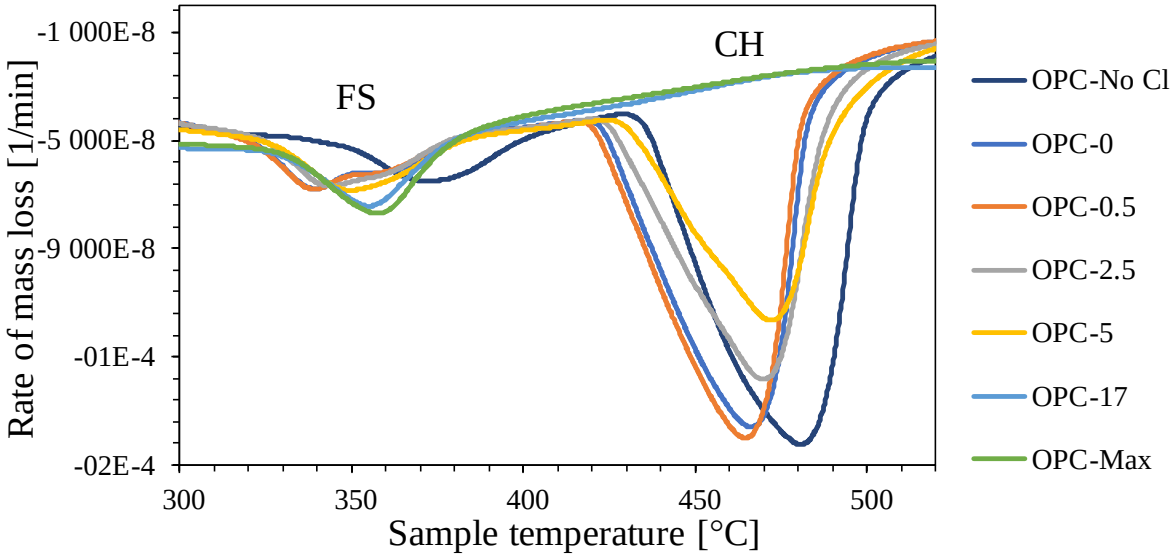


Figure 4.7: Close up of the temperature-region from 300-520 °C of the DTG curves in Figure 4.6-B. The change in shape of the peak near 350 °C indicates changes in the AFm-phases, likely the formation of Friedel's salt (FS) as chlorides were introduced to the cement pastes. The peak near 450 °C is from the decomposition of portlandite (CH). Increasing additions of acid lead to lower amounts of portlandite.

### 4.4.3 XRD

Figure 4.8 shows the full spectra (5-55° 2θ) of all samples in the current study, including that from the cement paste not exposed to chlorides (OPC-No Cl). Reflection angles for ettringite (Ett), Friedel's salt (FS), portlandite and NaCl are indicated. No other phases were conclusively detected by XRD, though some reflections indicated the presence of katoite ($Ca_3Al_2O_6 \cdot 6H_2O$, reflections at 17.54, 20.28 and 28.83° 2θ).

Figure 4.9 shows selected ranges of the XRD-spectra, from 8.5 to 12 and 31 to 35° 2θ. A strong reflection for ettringite was observed in all samples, except for OPC-0.5. There was no clear observable reflection peak for Friedel's salt at 11.19° 2θ, which indicates that the phase is either absent or has low crystallinity. The portlandite content appears to decrease with increasing additions of acid, in concurrence with the results from TGA. Strong reflection for NaCl was observed for all chloride-exposed samples.

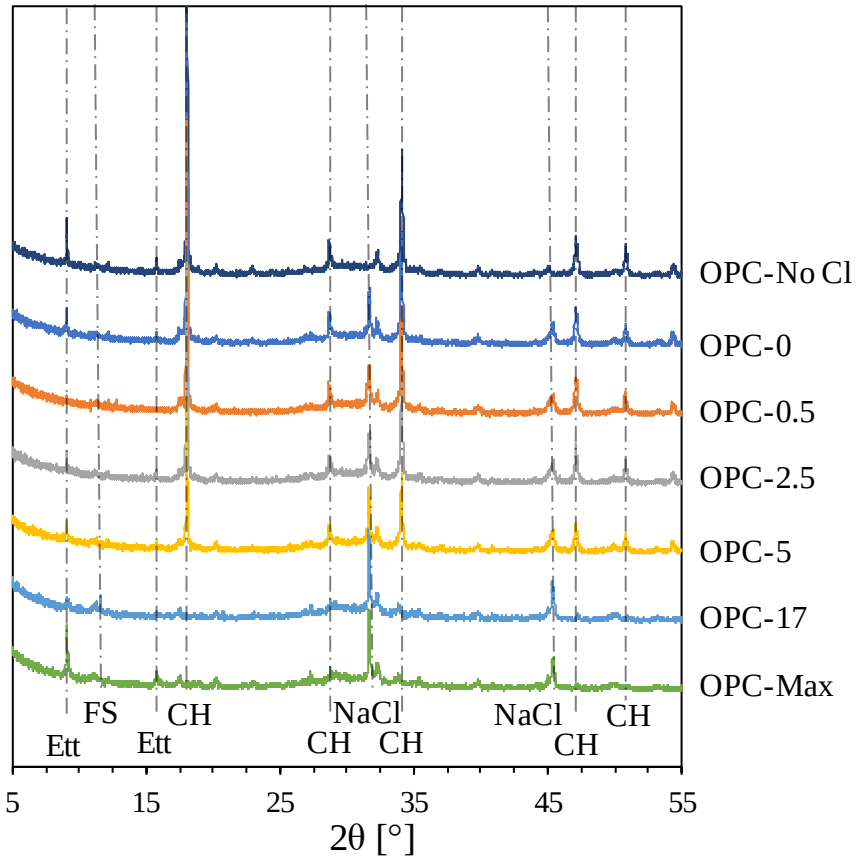


Figure 4.8: Full XRD-spectra of the range 2θ from 5 to 55 with indicators of diffraction angles for ettringite (Ett), Friedel's salt (FS), portlandite (CH) and NaCl. Lack of distinct diffraction for Friedel's salt indicates low crystallinity or an absence of the phase.

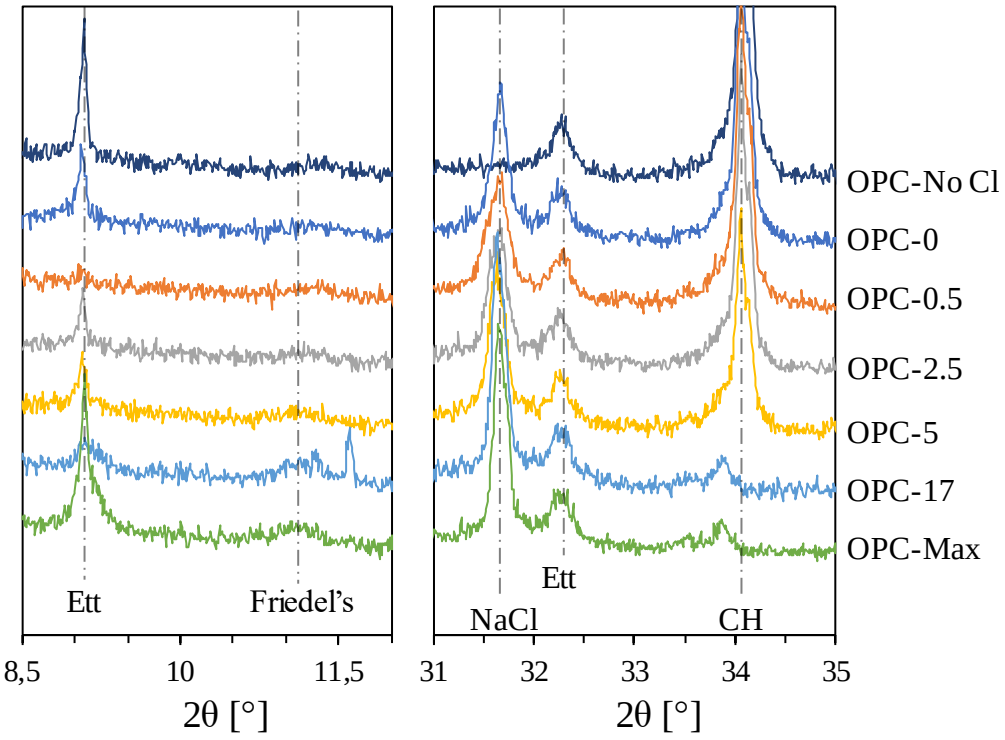


Figure 4.9: XRD-spectra of the range 2θ from 8.5 to 12 (left) and from 31 to 35 (right) with indicators of diffraction angles for ettringite (Ett), Friedel's salt, NaCl and CH. Lack of distinct diffraction for Friedel's salt indicates low crystallinity or an absence of the phase. The lack of ettringite reflection for OPC-0.5 and the peak for OPC-17 near 11.7 are likely caused by errors in the scan or inhomogeneity of the solids. The portlandite content decreases with increasing amounts of HCl, in agreement with the TGA-results. NaCl likely crystalizes during solvent exchange. The reflection at 33.9° 2θ might indicate the presence of katoite.

### 4.4.4 SEM-EDS

Backscatter electron (BSE) images and accompanying EDS-maps are presented in Appendix C. Point-scans of all samples are given in Appendix D. More maps were taken, but only a selected set is included in the appendices. Figure 4.10 shows a BSE overview of how the samples appeared in the SEM: Cement particles of various sizes (grey) randomly scattered in the epoxy (black). The polished samples were homogeneous, so the included BSE and EDS-maps are representative of the samples.

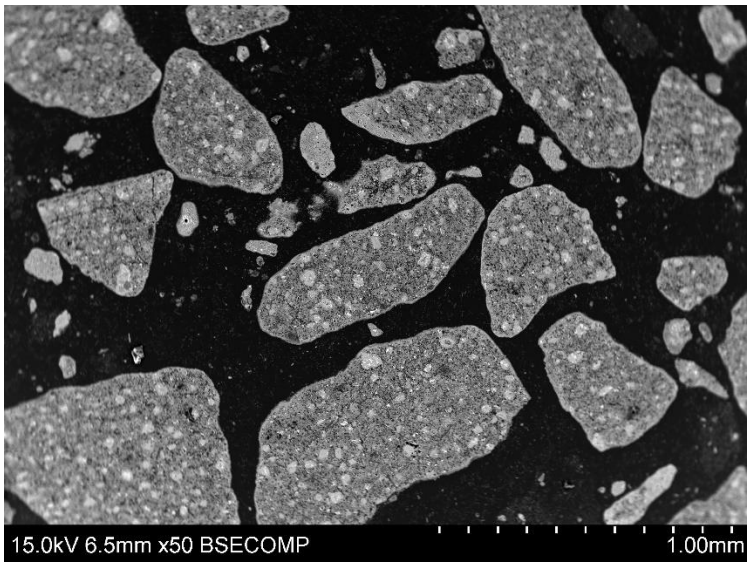


Figure 4.10: Overview BSE-picture of OPC-17 taken at 50 times magnification. All samples had a similar look with cement particles of varying sizes (grey) spread out randomly in the epoxy (black). The samples appeared to be homogeneous, showing no difference in average particle size between different areas.

The EDS-maps of the cement particles showed no clear indications of distinct AFm or AFt-phases, which should be regions enriched in Al, Ca, O, and S or Cl. Only the maps gathered from a region in the epoxy (Appendix C.VIII) showed some distinct AFm/AFt-areas. EDS point scans showed that the aluminium-rich phases were mostly $C_4AF$. Analyses of the matrix showed some indication of AFm-phases mixed in with the C-S-H. The AFm-phases showed little trend towards monosulphate, Friedel's salt or Kuzel's salt, and were therefore most likely monocarbonate.

Figure 4.11 shows the observed Ca/Si-ratios of C-S-H from all the samples, compared to the Ca/Si-ratio of the non-chloride exposed cement paste and the prediction from the thermodynamic model. For the samples the Ca/Si-ratio increases with increasing acid additions from 0 to 5 ml acid, from ca. 1.48 to 1.59. At 17 ml acid the ratio drops back down to 1.54, while at 22.5 ml the ratio drops down to 1.25. The thermodynamic model slightly overestimates the ratio, and the observed decrease for sample OPC-17 and OPC-22.5Max occurs at larger acid volumes in the model. It does show the same slight increase in the Ca/Si-ratio for acid additions smaller than 5 ml.

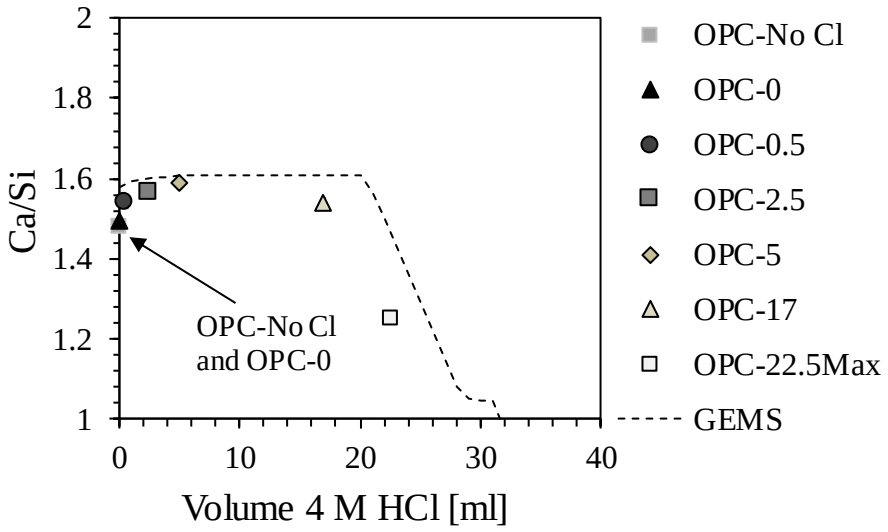


Figure 4.11: The molar Ca/Si-ratio of C-S-H from all the samples in the current study as determined by EDS, plotted as a function of the volume of acid added to the sample. The ratio for cement paste which was not exposed to NaCl or HCl (No NaCl) and the ratio of the C-S-H from the thermodynamic model (GEMS) are also included.

### 4.4.5 Suspension stability

Figure 4.12 shows all the samples in the current study after having been left undisturbed for one week. Sample OPC-0 and OPC-0.5 and OPC-2.5 were relatively stable suspensions of cement paste in water, where the height of the paste inside the tube was nearly constant over time. There were three distinguishable regions: A foamy layer atop the clear supernatant with the cement paste suspension below. The suspension was a mixture of light and dark grey cement paste.

When more than 5 ml of acid was added to a sample there was a clear visible change in the cement paste. The dark grey cement particles sedimented to the bottom of the sample tube, while the light grey particles accumulated just atop the dark grey sediment. Samples OPC-17 and OPC-22.5Max sedimented rapidly within minutes of shaking, while OPC-5 sedimented over the course of a day.

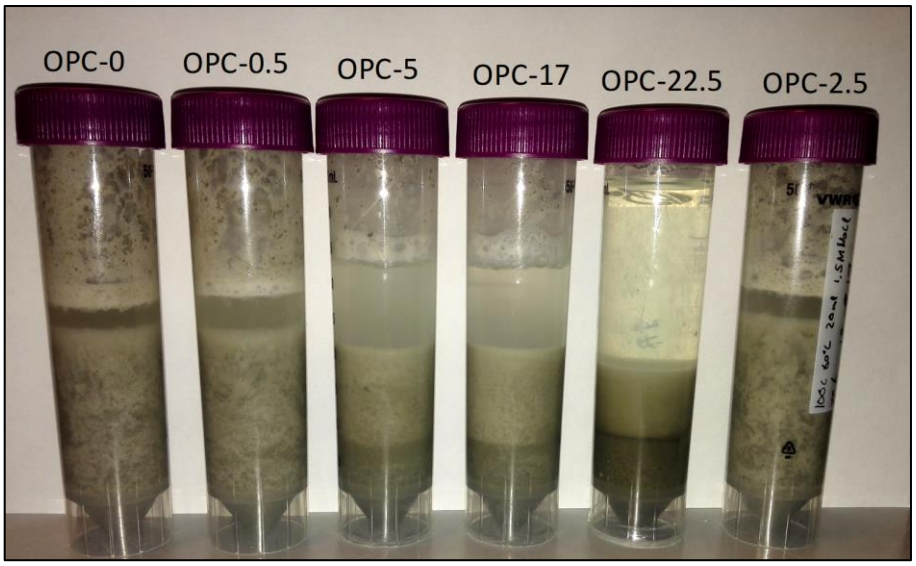


Figure 4.12: Picture of all the samples used in the current study (except OPC-0C), showing the visual change in phases occurring when acid is added. The picture was taken after chloride titration, which is why there is only a small amount of supernatant left in the samples.

# 5 Discussion

## 5.1 pH-development

The first step towards studying the pH-dependency of chloride binding was to determine if the pH could be lowered by addition of HCl, and how much the pH changed as acid was added. The result is a pH-development curve, which can be used to tailor the acid additions to reach specific levels of pH in the chloride binding experiments. The usefulness of this curve can be seen in how close the pH-values for the chloride binding samples lie to the pH-development curve. It should be noted that the pH-development curve is unique for each cement paste. The curve will vary depending on the buffer capacity and alkalinity of the paste.

Figure 4.4 shows the pH-development curve obtained experimentally and as predicted by the thermodynamic model. The pH in the liquid phase dropped continuously as more acid was added to the hydrated paste, as expected. Simple models only accounting for the liquid phase (as described in Appendix E and in Figure E.2) are not able to predict the development of the pH. This is due to the large buffering capacity of the cement paste, mostly due to the high portlandite content. The thermodynamic GEMS-model, which accounts for the solids, provided more accurate predictions of pH for low additions of acid (as can be seen in Figure 4.4). The model does however overestimate the pH. This might be due to the model not having accurate data for the reaction products of OPC in lower pH-ranges, or due to an overestimation of the portlandite content. The model used in the current study was not able to accurately predict the pH-development, but it is still possible that accurate thermodynamic models can be made.

The procedure used to determine the pH-development curve in the current study was carefully developed to limit local dissolution of solids other than portlandite upon acid addition. Adding the acid in small steps of 0.25 ml with at least one day between additions was done to that end. Centrifuging the samples and adding the acid to the high pH supernatant decreased the likelihood of direct contact between the acid and the solids. Figure 4.4 shows that there was hardly any difference in pH directly after adding acid and one day later when less than 7 ml acid was added in steps of 0.25 ml. This indicates that for these small additions the system rapidly reaches equilibrium. The risk of locally dissolving phases other than portlandite is therefore low. To reduce the time required to establish the pH-development curve, the acid dosage could be increased to 1 ml or several additions could be performed each day.

The uncertainty of the pH-measurements was estimated to be ± 0.1. The pH electrode was calibrated using buffer solutions with pH 7, 10 and 13 prior to each day of measurement. To determine the repeatability of the measurements, triplicates of the sample should have been prepared. However, this was not possible in the current study due to lack of materials.

A more exact evaluation of the error could have been made by measuring solutions of known pH. Finding highly accurate values was not a main concern of the current study, as the goal was to make a proof of concept for lowering the pH of the pore solution of hydrated cement paste using acid. All pH-measurements were performed using the same buffer-solutions for calibration, so the change in pH after each acid addition is accurate even if the exact values are uncertain.

## 5.2 Chloride binding

Based on the pH-development curve, HCl-dosages required to reach pH-levels of 13.2, 13.0, 12.5, 12.2 and 11.0 could be determined. One sample was prepared for each of these pH values. Once the samples had reached equilibrium between the acidified exposure solution and the pore solution of the cement paste, the amount of bound chlorides was determined, and the pH was measured.

### 5.2.1 Effect of pH in pore solution

Figure 4.5-A shows the amount of bound chlorides as a function of pH in the pore solution. There is an almost linear increase in chloride binding of the samples as the pH decreases from 13.2 to 12.2. When the pH drops down to 11.0, the cement paste loses its binding capacity.

Lowered pH in pore solution has previously been observed to be associated with increased chloride binding [9,11,33,47–49]. However, no previous studies have systematically studied how pH affects chloride binding for chlorides introduced after hydration. A previously unreported result is that after reaching a sufficiently low pH, the chloride binding drops to almost zero. Due to the limited availability of cement paste and therefore the number of samples, the exact point at which the chloride binding decreases is unknown. If it continues to increase until it rapidly drops to zero or gradually starts to decline remains to be investigated.

### 5.2.2 Effect of free chloride concentration

Figure 5.1 combines the chloride binding results from the current study (Table 4.1 and Figure 4.4-B) with the chloride binding isotherms determined by Machner et al. [46] on similar samples. In the case of NaCl the binding isotherm reaches a plateau at free chloride concentrations above 1 M, where the binding only increases slightly with increased free chloride concentration [11,46]. This means that increasing the chloride concentration above 1 M should not contribute to increased chloride binding. However, upon addition of HCl the chloride binding increases more rapidly than could be explained by the increase in free chloride concentration. The reason for this is most likely changes in the phase assemblage caused by the lowered pH.

The chloride binding with HCl develops more like a $CaCl_2$ binding isotherm like that from De Weerdt et al. [11] (Figure 2.7) or Machner et al. [46] (Figure 2.8) , rather than a NaCl isotherm. $CaCl_2$ has a similar effect on the system as HCl, as previously noted by Tritthart [9]. Both $CaCl_2$ and HCl lower the pH and increase the calcium concentration, the former by supplying additional Ca and the latter by dissolving portlandite.

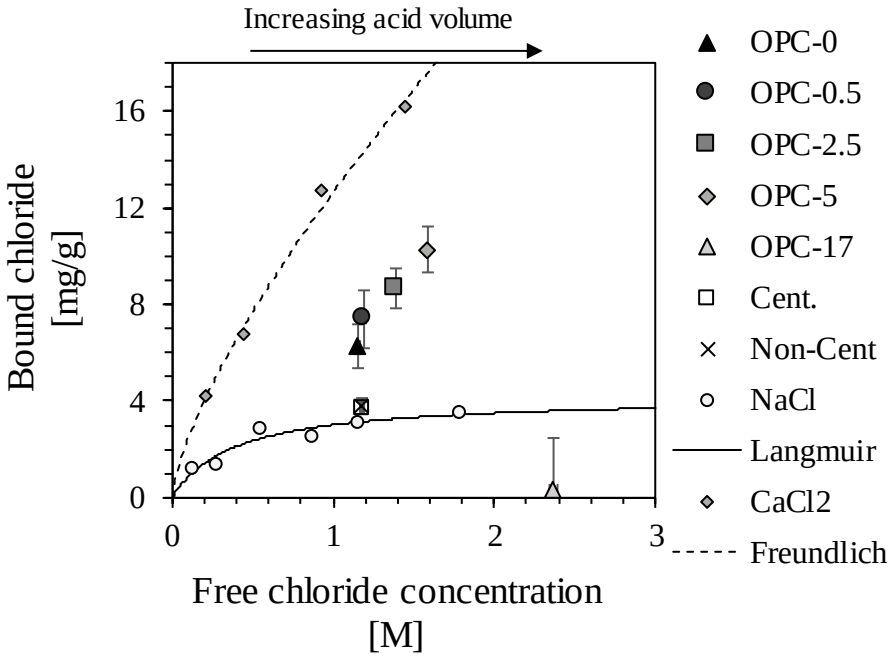


Figure 5.1: Results of chloride binding experiments in the current study, from Table 4.1. The results from Machner et al. [46] studying the same cement paste exposed to NaCl and $CaCl_2$ with corresponding Langmuir and Freundlich binding isotherms (both from Figure 2.8) are also included. "Non-cent" and "Cent." are the values for sample OPC-0C, studying the effect of centrifugation on chloride binding. Increased free chloride concentration is not sufficient to explain the increased binding observed in this study, nor the reduced binding when the pH drops to 11. The difference between the isotherm and the reference sample (0 ml HCl) is likely due to the reference sample not being centrifuged [41]. The results from OPC-0C indicate that centrifugation has no effect, thus there is currently no explanation for the different chloride binding of OPC-0 and OPC-0C.

### 5.2.3 Effect of centrifugation

As discussed in Section 2.4.2, centrifuging the samples before chloride titration affects the measured concentration and therefore the calculated chloride binding [41]. In Figure 5.1 the results from the centrifugation test sample OPC-0C (Cent. and Non-cent) lie very close to each other and to the value reported by Machner et al. [46], who centrifuged the samples before chloride titration. This indicates that centrifugation had little effect on the chloride binding in the current study. However, more samples would have to be tested to confirm this. The reason for the difference in chloride binding between OPC-0 and OPC-0C cannot currently be explained.

### 5.2.4 Uncertainty of measurements

The amount of bound chlorides is calculated using the total amount of added chlorides, the titrated free chloride concentration, the volume of free water and the mass of solids in the

sample (as described in Section 3.6.3). When calculating the chloride binding, the errors in each of these factors propagate. Error propagation calculation, detailed in Appendix B, showed that the uncertainty of a single chloride binding value could range from 1.4 to 3.6 mg/g (Table 4.1). The most important sources of uncertainty originate from the extracted sample volume for chloride titration the total volume of HCl added.

The extracted sample volume for chloride titration affects the determination of the free chloride concentration. The extracted volume is limited by the amount of liquid available in the sample and by the volume of the burette. When using a 5 ml burette, the extracted sample volume had to be around 0.2 ml (meaning a maximum measurable chloride concentration of 2.5 M with a $AgNO_3$-titrant concentration of 0.1 M) to stay within the burettes volume when titrating the sample. Any missing or extra droplets caused by mistakes during pipetting would then have a considerable impact on the calculated chloride binding. For sample OPC-0, an error of ± 0.02 ml (a small droplet) of extracted solution would be ± 10 % of the extracted volume, leading to a change of ± 6 mg/g in chloride binding. Since the chloride binding of the sample was calculated to be 4.3 mg/g, this is equal to an error of almost 150 % caused by a single droplet. For sample OPC-5, the same deviation of ± 0.02 ml solution would only be 27 % of the extracted volume, and lead to a change of ± 3 mg/g in chloride binding. This is only an error of approximately 40 % of the calculated binding of 7.1 mg/g. Switching to the 20 ml burette thus increasing the extracted volume to approximately 1 ml was therefore a significant improvement upon the titration method. The importance of precise pipetting is still quite evident.

The second large source of uncertainty for the calculation of bound chlorides is the volume of HCl added to the sample. The volume of HCl affects both the total amount of chloride in the sample and the total volume of solution. The error becomes more important as the number of acidification-steps increases. Since the acid is added in steps, each with the same uncertainty, the uncertainty of the total volume is the error of one addition multiplied with the square root of the number of additions. Weighing the sample before and after each addition of acid makes detection of pipetting-errors possible. The actual amount of HCl added can then be calculated using the density and concentration provided by the manufacturer.

## 5.3 Changes in phase assemblage caused by artificial leaching

To explain the increased chloride binding observed upon HCl addition the phase assemblage of the exposed cement pastes was investigated. First, the potential errors introduced by the sample preparation are discussed, followed by a description of the changes to the major phases.

### 5.3.1 Sample preparation

When interpreting the results from the phase assemblage study, potential errors caused by the sample preparation of the solids should be kept in mind. The solids sampled for analysis might not fully represent the composition of the entire sample. High acid additions caused the samples to separate (see Figure 4.12 for a picture and description of the samples), and only about 3-5 g of solids were extracted from each sample. For future studies, the entire sample should be extracted to avoid possible inhomogeneous extraction.

The current sample preparation methods were not able to fully remove the exposure solution from the solids. After the extraction the samples are treated with a double solvent exchange procedure (Section 3.7.2), aiming to remove the excess exposure solution from the solids. However, XRD and SEM-EDS showed the presence of NaCl crystals precipitated from the exposure solution in the samples. This shows that there is a need to improve the sample preparation step. One possible solution could be rinsing with purified water to extract the exposure solution before the solvent exchange procedure [57,58].

Direct comparison of the amount of a given phase present in the artificially leached samples is complicated due to the reduction in the mass of the sample upon HCl addition, as can be seen in the thermodynamic model (Figure 4.1). TGA gives the relative weight percentages of different phases in the cement paste, but these will change upon leaching. The method that was employed in the current study (detailed in Section 3.7.3) relies on the assumption that no other hydrate phases dissolve while portlandite is still present in the sample, an assumption that could not be verified with the current setup. Another solution could be to normalize the phases using for example the $Fe_2O_3$-content determined with X-ray fluorescence (XRF) of the pastes after solvent exchange [55]. Due to time limitations this was not done in the current study. However, as a decrease in the sample weight due to the dissolution of portlandite causes a relative increase of other weight loss peaks, the results can still be evaluated semi-quantitatively for weight loss peaks that decrease with increasing amounts of acid added (such as the portlandite-peak).

### 5.3.2 Portlandite

As Figure 4.4 shows, the portlandite content of the cement paste drops steadily with increasing HCl addition. XRD (Figure 4-10), EDS (can be seen in the EDS-maps in Appendix C, and from the point scans in Appendix D) and TGA confirm that portlandite is present at lower acid volumes and disappears after 17 ml of acid is added.

The experimental results and the thermodynamic model appear to agree on an almost linear relationship between volume of acid added and the amount of CH that dissolves. The model does however greatly overestimate the amount of portlandite. This is likely a large contributor to the difference in the experimental and modelled pH-development, as the model will overestimate the buffer capacity of the cement paste. Two factors that influenced this are the reaction degree of the cement in the model and the removal of $C_4AF$ and other minor phases. Removing these phases meant a relative increase in the main clinker phases $3CaO{\cdot}SiO_2$ ($C_3S$), $2CaO{\cdot}SiO_2$ ($C_2S$) and $3CaO{\cdot}Al_2O_3$ ($C_3A$). $C_3S$ and $C_2S$ react during hydration to form C-S-H and portlandite [19], and an increase in their relative weight percentages would increase the resulting portlandite content. The model calculates the expected phase composition at full hydration, which also increases the portlandite content compared to the real paste. To reduce the reactivity of the OPC, the model input could have replaced all $C_4AF$ with unreactive OPC rather than normalizing the remaining composition without $C_4AF$ to 100 %. However, the reported version of the model had chloride binding which fit well with the experimental data, which was more important for the current study than the exact amount of portlandite.

Another possible explanation for the overestimation of portlandite could lie in how the model simulates C-S-H. If the model had predicted a Ca/Si-ratio much lower than that observed by EDS, it would likely have compensated by increasing the portlandite content. However, as can be seen in Figure 4.11 and Figure 5.2, the Ca/Si-ratio in the model lies very close to the experimental data for acid volumes equal to or less than 5 ml. Therefore, the C-S-H-simulation is probably not the reason for the model's overestimation of portlandite content.

The values for the CH-content, both from TGA and GEMS, deviate from previously reported values. Typical CH-content as determined by TGA lies in the range of 15-25 % of the dry binder mass [19]. The non-chloride exposed paste has a CH-content of 15.8 ± 0.2 %, which is low although within the expected range. The chloride exposed samples have lower CH-contents due to the lowering of pH and increase of free water volume, both factors leading to higher solubility of portlandite. As for the GEMS-model, the predicted content is as large as 38 % before acid

exposure. The CH content is too large to be sufficiently explained by the factors discussed previously.

### 5.3.3 C-S-H

C-S-H is, as mentioned in Section 2.2.1, an amorphous phase with variable composition and is therefore difficult to quantify. SEM-EDS does however enable investigation of changes in the elemental ratios of the phase.

According to the thermodynamic model (Figure 4.1) C-S-H remains stable while there is portlandite in the cement paste. The model expects the portlandite to be fully dissolved after 21 ml acid has been added, after which the C-S-H will start to decompose. Figure 4.11 shows that there are changes in the C-S-H even though its volume remains constant. The EDS data and the model both show that the Ca/Si-ratio of the C-S-H increases slightly for small volumes of acid added.

Considering that the model overestimates the amount of portlandite, it is more informative to consider at what pH the model predicts decomposition and changes in C-S-H, rather than at what volumes of acid. Figure 5.2 shows the Ca/Si-ratio of the C-S-H as determined by EDS, and the predicted Ca/Si-ratio and volume of C-S-H in the GEMS model. According to the model the decomposition of C-S-H starts at a pH of 12.5, at which point the Ca/Si-ratio also rapidly declines as the pH decreases. This indicates that for sample OPC-17 and OPC-22.5Max, it is possible that decomposition of the C-S-H has occurred. The decomposition or large change in Ca/Si-ratio might be the reason for the visual changes in the samples (as described in Section 4.4.5), where the solids began to separate into different regions after approximately 5 ml of acid was added. It is possible that the changes to the C-S-H affected the electric charge of the phase, leading to changed zeta potential and destabilization of the suspension [36]. Zeta potential measurements were not conducted for the current study but could be included in further work to illuminate the cause for the change in suspension stability.

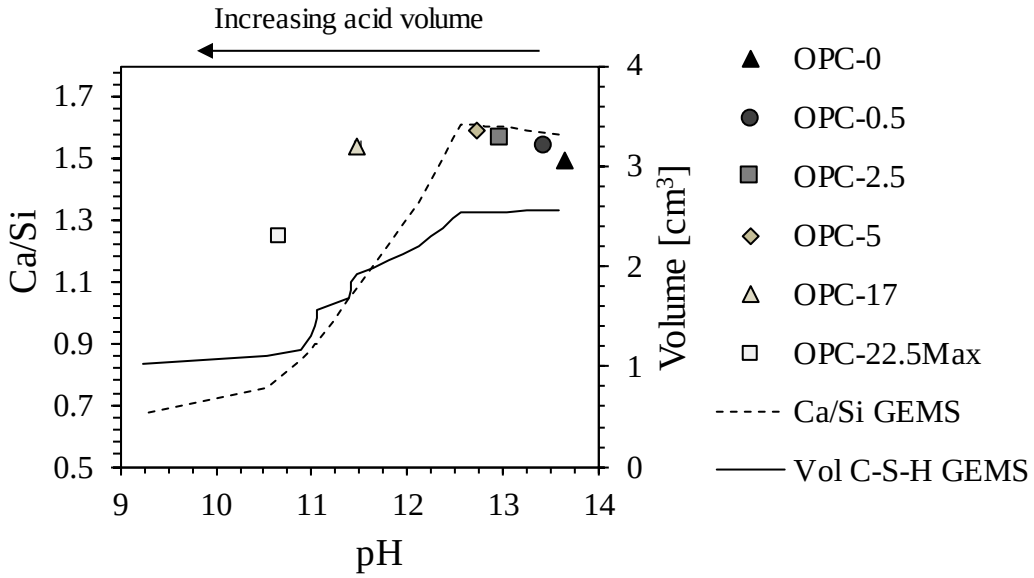


Figure 5.2: Atomic Ca/Si-ratios of C-S-H from the samples in the current study and as predicted by GEMS, both as a function of the pH in the pore- and exposure solution. Also included om the secondary axis is the volume of C-S-H as predicted by GEMS. The model predicts that C-S-H starts to decompose when the pH drops below 12.5, accompanied by a decline in the Ca/Si-ratio of the phase.

The results from the EDS should be carefully interpreted. The changes in the C-S-H composition caused by sample preparation for SEM-EDS might have caused an artificial increase in the calcium content due to precipitation from the exposure solution. However, similar trends of changed Ca/Si-ratio have been observed by De Weerdt and Justnes [59] who showed that in cement paste leached by sea water, C-S-H was decalcified from a Ca/Si-ratio of 1.8 down to 1.

### 5.3.4 Aluminate-ferrite hydrate phases

The thermodynamic model predicts the presence of Friedel's salt in the chloride containing samples, but above 28 ml of acid addition Friedel's salt would start to decompose. Neither the presence nor the decomposition could be verified by XRD as no characteristic reflection peaks for Friedel's salt were observed in any of the XRD spectra (Figure 4.9). There is a slight rise in the spectra near $2\theta = 11.19°$, which might indicate that the phase is present but has low crystallinity.

The absence of typical diffraction peaks for crystalline AFm phases such as Friedel's salt ($3CaO{\cdot}Al_2O_3{\cdot}CaCl2 \cdot 10H2O$, 11.19° 2θ), monocarbonate ($3CaO{\cdot}Al_2O_3{\cdot}CaCO_3 \cdot 11H_2O$, 11.7° 2θ) or monosulphate ($3CaO{\cdot}Al_2O_3{\cdot}CaSO_3{\bullet}11H_2O$, 10.3° 2θ) in the XRD-spectra is most likely

related to the peculiar curing regime of the cement paste. The paste was cured for 7 months at 60 °C, before being stored at 20 °C for over a year. Ettringite is not stable at 60 °C but lowering of the curing temperature will have caused delayed ettringite formation, transforming parts of the AFm-phases to ettringite [30]. The occurrence of delayed ettringite formation in the current study is supported by the distinct reflections for ettringite in all samples (Figure 4.9). The thermodynamic model predicts that ettringite is present and that it resists the levels of HCl addition tested (Figure 4.1).

Some AFm phases do however appear to be present as, indicated by the mass loss peaks in the derivative TGA-curves near 350 °C (Figure 4.7). There is a clear shift in the peaks upon acid addition, indicating changes in the AFm phases, but one cannot identify the specific phases with TGA alone.

SEM-EDS point analysis could help identifying low-crystalline AFm and AFt phases. In order to obtain elemental ratios of more or less pure phases, one tends to analyse phases crystallized in the porosity of the cement paste [20]. However, the AFm and AFt phases in the current samples appear to be so finely intermixed with the C-S-H so that no single-phase analyses could be performed. Most point scans that appear to indicate AFm or AFt in the Al/Si and Fe/Si ratio plots (Figure D.1 and Figure D.2 respectively) are most likely $C_4AF$, as can be seen in the (Fe+Al)/Si-ratio plots (Figure D.3).

## 5.4 Mechanism of altered chloride binding

Chlorides bound in cement paste are bound chemically in AFm phases such as Friedel's salt or are accumulated in the stern layer of C-S-H, as described in Section 2.3. The reason for the change in chloride binding observed upon HCl addition should therefore be found in changes in the AFm phases or the C-S-H.

The AFm phases in the investigated cement paste are not very crystalline and are finely intermixed with the C-S-H, preventing respectively XRD and SEM-EDS identification. The current study is therefore not able to conclude on whether the increased chloride binding upon HCl addition can be (partially) attributed to changes in the AFm phases. The thermodynamic model predicts that Friedel's salt is stable for the range of 0-28 ml acid added, however the model does overestimate the pH of the pore solution. Figure 4.4-A, where the chloride binding from GEMS is plotted as a function of the pH in the exposure solution, shows that Friedel's salt does dissolve when the pH drops to the levels that was measured in sample OPC-17. The model

overestimates the buffer capacity of the cement paste but should accurately predict at what pH Friedel's salt dissolves. When the pH drops to 11, Friedel's salt is no longer stable and therefore no longer contributes to chloride binding, which could partially explain why the paste in sample OPC-17 bound almost no chlorides. It can also be seen from the model that the amount of Friedel's salt should not increase as the pH of the solution is lowered from 13 to 12. The increase in chloride binding should therefore not be due to the formation of additional Friedel's salt, but the observed decrease could be explained by its decomposition. The experimental results are unfortunately unable to verify this.

The C-S-H and the exposure solution change in composition upon HCl addition. The increase in chloride binding could therefore be due to changes in accumulation of ions in the diffuse layer of C-S-H (Section 2.3.2). For small additions of acid and consequently small drops in pH (from 13 down to 12), the reduction of competing accumulation by hydroxyl ions, as well as a higher calcium concentration, can lead to increased accumulation of chloride ions in the double layer. Thus, the chloride binding increases. Below a certain pH the C-S-H starts to decalcify, potentially rendering the phase more negatively charged, and reducing the accumulation of chloride in the diffuse layer. The current study cannot conclude on the exact changes in the C-S-H composition and its relation to chloride binding, as the sample preparation for the SEM-EDS samples might have led to calcium precipitation.

In order to find a conclusive explanation for the change in chloride binding upon HCl addition, the current study needs to be repeated with cement paste samples with crystalline AFm (cement paste cured at 20 °C), and with improved sample preparation for SEM-EDS samples. The composition changes of the C-S-H could also be studied with Si-NMR [21].

## 5.5 Implications for service life prediction models

The fact that the chloride binding of hydrated cement is greatly reduced or totally removed by harsh leaching and large drops in pH is a very significant result. This could be an explanation for the shape of chloride profiles in chloride exposed concrete structures, confirming the hypothesis discussed in Section 2.5.4. Due to harsh leaching of the cement, the pH of the pore solution near the surface of the structure will be much lower than deeper inside. The chloride binding will then also be severely reduced in the same area. As mentioned in Section 2.3, most of the chloride in the concrete is either bound by C-S-H or in AFm, only a small portion is free in the pore solution. The reduced total chloride content that is observed at the surface is therefore likely to be the result of leaching reducing chloride binding.

Depending on the harshness of the leaching, the chloride binding can be either increased or decreased. Chloride binding is a significant factor in the chloride profiles that current service life models use to calculate chloride diffusion coefficients [7,12]. Since chloride profiles will change considerably as the cement is leached, integrating the effect of leaching into service life models can considerably improve their accuracy.

## 5.6 Further work

The current study was performed as a proof of concept for an experimental setup that can be used to study the impact of pore solution pH on the chloride binding of hydrated cement. In this section several recommendations for further improvements of the experimental setup are given. It is recommended that initial work is focused on improving the methods, before introducing more variables such as cement binder composition and curing temperature.

### 5.6.1 Repeating study with regular cement paste

The current study was limited by the availability of cement paste, and by the unusual curing of the paste. Preparing well-hydrated cement paste takes several months and could not have been prepared over the course of a master thesis, the current study was therefore only possible due to there being left-over paste from Alisa Machner's thesis work [50]. Because the paste was cured at 60 °C, the Friedel's salt in the paste was not crystalline and its contribution to the chloride binding could not be conclusively determined.

Despite these drawbacks the current study clearly lays out a proof of concept for further studies. With access to more cement paste cured at 20 °C with crystalline Friedel's salt, a follow up study using the methods developed here should be able to answer many of the questions the current study could not.

### 5.6.2 Improving determination of pH-development curve

As briefly mentioned in Section 5.1, some improvements can be made to the determination of the pH-development curve. The main purpose of the curve was to give an indication of what volume of acid addition corresponds to different levels of pH. Since no reliable chloride binding measurements are possible with the samples that are used to establish the curve, local dissolution of solids is less of an issue. The acidification programme used to establish the pH-development curve can therefore be harsher than the programme used for the chloride binding experiments.

Since the exposure solution reaches equilibrium within 10-15 minutes after acid addition (while there is still portlandite left in the cement paste), it is possible to add the acid in several steps of 0.25 ml per day or in larger steps of 1 ml. To reduce the required time to determine the pH-development curve (in the current study it took 5 weeks), it is suggested to add the acid in 1 ml steps for all the acidification steps rather than the 0.25 ml initially used in the current study. The dosage can also be increased to 2 ml after having 10 ml added, thereby also reducing the required time.

### 5.6.3 Sample preparation

Improvements should be made to the sample preparation for analysis of the solids. The current method of double solvent exchange and filtration appears to cause the precipitation and crystallization of NaCl. This makes the solids analyses by XRD, SEM and TGA less representative. Solving the problems caused by the currently used method should be the priority for further work, as it will enable reliable studies of the solid phases. A possible solution could be "washing" the solids with a known amount of deionized water over a specified amount of time, similarly to the method described by Plusquellec and De Weerdt [57] or He et al. [58]. This would help to remove precipitates like NaCl before solvent exchange.

Another challenge is the possible inhomogeneity of the extracted solids. This can easily be avoided by extracting the entire sample rather than just a few spatulas, as has been done in previous and the current studies. This is highly recommended for further studies. Since no other measurements of the liquid phase can be performed after parts of the solid have been extracted, there is no real downside to extracting all the solids.

When future samples for SEM-EDS are prepared, the inhomogeneity of the solids and different particle sizes should be considered. The solids are mixed with an epoxy. The solid particles have different sizes and densities and might accumulate at different heights in the cast epoxy. Hence a cross-section of the epoxy cast should be polished as that would ensure the inclusion of particles of all sizes and densities.

The exact issues with the ICP-MS results in the current study could not be verified. Reliable ICP-MS-measurements would help to better understand the phases changes caused by the artificial leaching. It is therefore recommended that future studies include ICP-MS, as long as the accuracy and reliability of the measurements are assured.

### 5.6.4 Chloride binding and pH

Once the methods developed in the current study have been improved, the relationship between the pH in pore solution and chloride binding in cement paste should be determined for a larger range of acid additions and thereby a larger pH range. Especially the transition from increasing to decreasing chloride binding as the pH must be better understood. This could be done by repeating the current study with several more data, e.g. for steps of 2 ml of acid in the range 0-25 ml acid. Initially adding acid in steps of 0.25 ml, eventually increasing to 0.5, 1 and 2 ml proved to not cause local dissolution of the solids. It is therefore recommended that a similar acidification programme as in the current study is used for chloride binding samples in further studies.

The exact mechanisms behind changes in chloride binding should be studied. The contribution of AFm-phases would be easier to determine for cement pastes cured at 20 °C, where AFm-phases are more likely to be crystalline. Studying the composition changes of C-S-H with Si-NMR could help to clarify how the changes in C-S-H affect the chloride binding.

Future studies should include chloride binding isotherms for NaCl made using the same methods as for the acidification. This would help to separate the contributions of free chloride concentration and pH on the chloride binding. Regular binding isotherms are made with exposure of the same amount of cement paste to the same volume of chloride solution, but at different chloride concentrations. A possible variation would be a binding isotherm where, after the initial NaCl-exposure, an NaCl-solution with the same concentration and volume as the HCl is added. This would allow for a direct comparison of the impact of pH.

Another possible way to confirm that pH is the determining factor in changed chloride binding would be performing the same study as previously suggested but with varying initial concentrations of NaCl. Figure 5.3 shows the expected results of such a study. If the chloride binding has the same response to lowered pH regardless of chloride concentration, the dominating effect of pH on chloride binding would be confirmed.

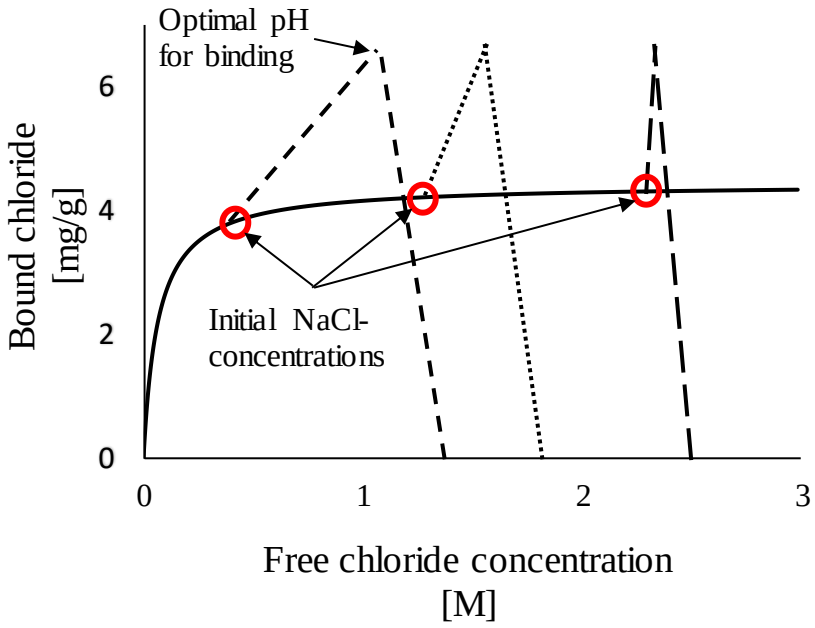


Figure 5.3: Hypothetical development of chloride binding for hydrated cement pastes exposed to NaCl-solutions of varying concentrations before being acidified with HCl. Here the concentration of HCl is larger than the NaCl-concentration, which means the chloride concentration also increases during acidification. The solid line is a hypothetical Langmuir chloride binding isotherm, while the three dashed lines indicate the development of three different pastes with varying starting chloride concentration. It is expected that the binding will increase until an optimal pH is reached before the binding will be reduced to near zero. Neither the maximum binding or the point at which binding is removed are dependent on the free chloride concentrations, as both are determined by the pH of the pore solution. The dashed lines are linear for simplicity, as the exact shape of the curves are unknown.

# 6 Conclusion

A method for lowering the pH of the pore solution in a hydrated cement paste in a closed system has been developed. The hydrated paste is exposed to a NaCl solution before HCl is added in steps of 0.25-2 ml, which proved to be sufficiently small to not cause local dissolution of the chloride binding phases. A pH-development curve was established, which proved to give an accurate relationship between the added volume of acid and the pH of the exposure solution, allowing for targeting of specific pH levels in the chloride binding experiments. The pH-development upon acid addition could not be accurately predicted with the thermodynamic model employed in the current study, due to an overestimation of the portlandite content.

Chloride binding of a hydrated cement paste is closely linked to the pH in the pore solution. As has been observed previously, lowering the pH slightly tends to increase chloride binding. This is likely due to changes in the main hydrate phase C-S-H. The current study shows that if the pH drops below 11, the chloride binding of the cement paste is greatly reduced. Thermodynamic modelling predicts the lowering of chloride binding is caused by the dissolution of Friedel's salt when the pH is below 11.

Leaching decreases the pH of the pore solution, thereby changing the chloride binding of the cement paste. In real concrete structures, harsh leaching at the surface will reduce the chloride binding, while slight leaching further into the structure leads to increased chloride binding and therefore a maximum in the chloride profile.

Current service life prediction models for concrete structures exposed to chlorides need to incorporate the effect of leaching on chloride binding, in order to obtain more accurate chloride ingress predictions.

# Bibliography


[1] S. Jacobsen (Ed.), TKT 4215 Concrete Technology 1, 2013.

[2] M.R. Geiker, TKT4235 Concrete Technology, advanced course: Service life prediction. Basic service life concepts, NTNU, Trondheim, 2017.

[3] K. Tuuti, Corrosion of steel in concrete. PhD, Stockholm, Sweden, 1982.

[4] M.R. Geiker, E.P. Nielsen, D. Herfort, Prediction of chloride ingress and binding in cement paste, Mater Struct 40 (2007) 405–417.

[5] E.P. Nielsen, M.R. Geiker, Chloride diffusion in partially saturated cementitious material, Cement and Concrete Research 33 (2003) 133–138.

[6] H. Justnes, M.O. Kim, S. Ng, X. Qian, Methodology of calculating required chloride diffusion coefficient for intended service life as function of concrete cover in reinforced marine structures, Cement and Concrete Composites 73 (2016) 316–323.

[7] P. Beverly, fib model code for concrete structures 2010: Paul Beverly, U.K, Ernst & Sohn, Berlin, Germany, 2013.

[8] J. Walraven, fib Model Code for Concrete Structures 2010: Mastering challenges and encountering new ones, Structural Concrete 14 (2013) 3–9.

[9] J. Tritthart, Chloride binding in cement II. The influence of the hydroxide concentration in the pore solution of hardened cement paste on chloride binding, Cement and Concrete Research 19 (1989) 683–691.

[10] C.M. Hansson, T. Frølund, J.B. Markussen, The effect of chloride cation type on the corrosion of steel in concrete by chloride salts, Cement and Concrete Research 15 (1985) 65–73.

[11] K. De Weerdt, A. Colombo, L. Coppola, H. Justnes, M.R. Geiker, Impact of the associated cation on chloride binding of Portland cement paste, Cement and Concrete Research 68 (2015) 196–202.

[12] I. Galan, F.P. Glasser, Chloride in cement, Advances in Cement Research 27 (2015) 63–97.

[13] A. Fick, V. On liquid diffusion, The London, Edinburgh, and Dublin Philosophical Magazine and Journal of Science 10 (1855) 30–39.

[14] M. Climent, G. de Vera, J.F. López, C. Garcia, C. Andrade, J. Kropp, Transport of chlorides through non-saturated concrete after an initial limited chloride supply, Proc. of the 2nd Int. Workshop on Testing and Modelling the Chloride Ingress Into Concrete (2000).

[15] L.O. Nilsson, E. Poulsen, P. Sandberg, H. Sørensen, O. Klinghoffer, HETEK, Chloride penetration into concrete, State-of-the-Art. Transport processes, corrosion initiation, test methods and prediction models, 1996.

[16] O.M. Jensen, Chloride ingress in cement paste and mortar measured by Electron Probe Micro Analysis, 1998.

[17] M.R. Geiker, Fly ash in concrete, Danish experience: State-of-the-art report, 2015.

[18] K. De Weerdt, H. Justnes, M.R. Geiker, Changes in the phase assemblage of concrete exposed to sea water, Cement and Concrete Composites 47 (2014) 53–63.

[19] H.F.W. Taylor, Cement chemistry, 1990.

[20] K.L. Scrivener, A. Bazzoni, B. Mota, J.E. Rossen, Electron microscopy, in: K.L. Scrivener, R. Snellings, B. Lothenbach (Eds.), A practical guide to microstructural analysis of cementitious materials, CRC Press, 2015.

[21] J. Hjorth, J. Skibsted, H.J. Jakobsen, 29Si MAS NMR studies of portland cement components and effects of microsilica on the hydration reaction, Cement and Concrete Research 18 (1988) 789–798.

[22] E. Bonaccorsi, S. Merlino, A.R. Kampf, The Crystal Structure of Tobermorite 14 A (Plombierite), a C-S-H Phase, J American Ceramic Society 88 (2005) 505–512.

[23] A. Nonat, X. Lecoq, The Structure, Stoichiometry and Properties of C-S-H Prepared by C3S Hydration Under Controlled Condition, in: P. Colombet, H. Zanni, A.R. Grimmer, P. Sozzani (Eds.), Nuclear Magnetic Resonance Spectroscopy of Cement-Based Materials, Springer Berlin Heidelberg, Berlin, Heidelberg, 1998, pp. 197–207.

[24] B. Lothenbach, A. Nonat, Calcium silicate hydrates: Solid and liquid phase composition, Cement and Concrete Research 78 (2015) 57–70.

[25] K. Momma, F. Izumi, VESTA 3 for three-dimensional visualization of crystal, volumetric and morphology data, J Appl Crystallogr 44 (2011) 1272–1276.

[26] D.M. Henderson, H.S. Gutowsky, A nuclear magnetic resonance determination of the hydrogen positions in Ca(OH)2 T = 25 C, American Mineralogist 47 (1962) 1231–1251.

[27] H.D. Megaw, The Thermal Expansions of Certain Crystals with Layer Lattices, Proceedings of the Royal Society A: Mathematical, Physical and Engineering Sciences 142 (1933) 198–214.

[28] T. Matschei, B. Lothenbach, F.P. Glasser, The AFm phase in Portland cement, Cement and Concrete Research 37 (2007) 118–130.

[29] B. Lothenbach, F. Winnefeld, C. Alder, E. Wieland, P. Lunk, Effect of temperature on the pore solution, microstructure and hydration products of Portland cement pastes, Cement and Concrete Research 37 (2007) 483–491.

[30] K.L. Scrivener, H.F.W. Taylor, Delayed ettringite formation: A microstructural and microanalytical study, Advances in Cement Research 5 (1993) 139–146.

[31] K. De Weerdt, S.G. Ytterdal, M.R. Geiker, On the impact of phase changes on chloride profiles in concrete, Iceland, 2014.

[32] J. Csizmadia, G. Balázs, F.D. Tamás, Chloride ion binding capacity of aluminoferrites, Cement and Concrete Research 31 (2001) 577–588.

[33] H. Zibara, Binding of external chlorides by cement pastes. Ph.D., Canada, 2001.

[34] F.P. Glasser, A. Kindness, S.A. Stronach, Stability and solubility relationships in AFm phases, Cement and Concrete Research 29 (1999) 861–866.

[35] M.H. Roberts, Effect of calcium chloride on the durability of pre-tensioned wire in prestressed concrete, Magazine of Concrete Research 14 (1962) 143–154.

[36] P.C. Hiemenz, R. Rajagopalan, Principles of Colloid and Surface Chemistry, 3rd ed., 1997.

[37] A.K. Suryavanshi, R.N. Swamy, Stability of Friedel's salt in carbonated concrete structural elements, Cement and Concrete Research 26 (1996) 729–741.

[38] H. Viallis-Terrisse, A. Nonat, J.C. Petit, Zeta-Potential Study of Calcium Silicate Hydrates Interacting with Alkaline Cations, Journal of colloid and interface science 244 (2001) 58–65.

[39] C. Labbez, A. Nonat, I. Pochard, B. Jönsson, Experimental and theoretical evidence of overcharging of calcium silicate hydrate, Journal of colloid and interface science 309 (2007) 303–307.

[40] G. Plusquellec, A. Nonat, Interactions between calcium silicate hydrate (C-S-H) and calcium chloride, bromide and nitrate, Cement and Concrete Research 90 (2016) 89–96.

[41] G. Plusquellec, In situ analysis of suspensions of calcium silicate hydrate: Application to the study of ionics interactions at the surface of the particules, 2014.

[42] K. De Weerdt, D. Orsáková, A.C.A. Müller, C.K. Larsen, B. Pedersen, M.R. Geiker, Towards the understanding of chloride profiles in marine exposed concrete, impact of leaching and moisture content, Construction and Building Materials 120 (2016) 418–431.

[43] K. De Weerdt, D. Orsáková, M.R. Geiker, The impact of sulphate and magnesium on chloride binding in Portland cement paste, Cement and Concrete Research 65 (2014) 30–40.

[44] K. Tuuti, Analysis of pore solution squeezed out of cement paste and mortar, Nordic Concrete Research 1 (1982) 25.1-25-16.

[45] L. Tang, L.O. Nilsson, Chloride Binding Capacity and Binding Isotherms of OPC Pastes and Mortars, Cement and Concrete Research 23 (1993) 247–253.

[46] A. Machner, M. Zajac, M.B. Haha, K.O. Kjellsen, M.R. Geiker, K. De Weerdt, Chloride-binding capacity of hydrotalcite in cement pastes containing dolomite and metakaolin, Revised version submitted to Cement and Concrete Research (January 2018).

[47] C. Arya, N.R. Buenfeld, J.B. Newman, Factors influencing chloride-binding in concrete, Cement and Concrete Research 20 (1990) 291–300.

[48] P. Henocq, E. Samson, J. Marchand, Portlandite content and ionic transport properties of hydrated C3S pastes, Cement and Concrete Research 42 (2012) 321–326.

[49] Z. Shi, M.R. Geiker, K. De Weerdt, T.A. Østnor, B. Lothenbach, F. Winnefeld, J. Skibsted, Role of calcium on chloride binding in hydrated Portland cement–metakaolin–limestone blends, Cement and Concrete Research 95 (2017) 205–216.

[50] A. Machner, Dolomite calcined clay composite cement - hydration and durability. Ph.D, Trondheim, Norway, 2018.

[51] M. Balonis, The Influence of Inorganic Chemical Accelerators and Corrosion Inhibitors on the Mineralogy of Hydrated Portland Cement Systems. PhD, Aberdeen, Scotland, 2012.

[52] B. Lothenbach, Durdzińskiski, K. De Weerdt, Thermogravimetric analysis, in: K.L. Scrivener, R. Snellings, B. Lothenbach (Eds.), A practical guide to microstructural analysis of cementitious materials, CRC Press, 2015.

[53] D.A. Kulik, T. Wagner, S.V. Dmytrieva, G. Kosakowski, F.F. Hingerl, K.V. Chudnenko, U.R. Berner, GEM-Selektor geochemical modeling package: Revised algorithm and GEMS3K numerical kernel for coupled simulation codes, Computational Geosciences 17 (2013) 1–24.

[54] T. Wagner, D.A. Kulik, F.F. Hingerl, S.V. Dmytrieva, GEM-Selektor geochemical modeling package: TSolMod library and data interface for multicomponent phase models, The Canadian Mineralogist 50 (2012) 1173–1195.

[55] A. Machner, M. Zajac, M.B. Haha, K.O. Kjellsen, M.R. Geiker, K. De Weerdt, Stability of the hydrate phase assemblage in Portland composite cements containing dolomite and metakaolin after leaching, carbonation, and chloride exposure, Revised version submitted to Cement and Concrete Composites (January 2018).

[56] R.H. Bogue, Calculation of the Compounds in Portland Cement, Ind. Eng. Chem. Anal. Ed. 1 (1929) 192–197.

[57] G. Plusquellec, K. De Weerdt, Cold water extraction (CWE): Procedure for the determination of the alkali content and pore solution composition, Trondheim, Norway.

[58] F. He, R. Wang, C. Shi, R. Zhang, Z. Shi, D. Zhang, Effect of bound chloride on extraction of water soluble chloride in cement-based materials exposed to a chloride salt solution, Construction and Building Materials 160 (2018) 223–232.

[59] K. De Weerdt, H. Justnes, The effect of sea water on the phase assemblage of hydrated cement paste, Cement and Concrete Composites 55 (2015) 215–222.

# Appendices

# Appendix A GEMS

This appendix contains detailed information of how the thermodynamic model was set up in GEMS v3.3.

## A.I Input materials

This model uses only one input material, which is OPC clinker. As mentioned in Section 3.7.6, the reactivity of different clinker phases can be accounted for by changing the input composition. In this model, the input material was changed to better fit the experimental data. What follows is the calculations used to transform the experimental oxide composition (provided by the clinker manufacturer Norcem AS) to the reactivity-corrected composition.

First, the non-reactive oxides $TiO_2$, MnO, $P_2O_5$ and 70% of MgO was subtracted from the original oxide composition. The resulting "Subtracted oxides"-composition was then normalized to 100%. Using the normalized oxide composition, the amount of $C_4AF$ was calculated by the Bogue calculations [56]. The amount of unreacted Al2O3 and Fe2O3 was then calculated from the amount of C4AF. These values were then subtracted from the normalized cement composition. This new composition was again normalized to 100 % to give the final oxide composition.

$$C_4AF\ (wt\%) = 3.0432 \cdot F_2O_3\ (wt\%)$$

$$Al_2O_{3,unreacted} = \frac{Mm_{Al_2O_3}}{Mm_{C_4AF}} \cdot C_4AF\ (wt\%) = 0.596 \cdot Al_2O_3\ (wt\%)$$

$$Fe_2O_{3,unreacted} = \frac{Mm_{Fe_2O_3}}{Mm_{C_4AF}} \cdot C_4AF\ (wt\%) = \frac{C_4AF\ (wt\%)}{3.0432} = Fe_2O_3\ (wt\%)$$

The following table gives the original oxide composition and the compositions calculated for each step in the process.

| Oxide | Original composition [wt%] | Subtracted oxides [wt%] | Normalized to 100 % [wt%] | Subtracted $C_4AF$ [wt%] | Final composition [wt%] |
|---|---|---|---|---|---|
| $SiO_2$ | 19.91 | 19.91 | 20.60 | 20.60 | 21.87 |
| $Al_2O_3$ | 5.15 | 5.15 | 5.33 | 3.07 | 3.26 |
| TiO2 | 0.282 | - | - | - | |
| MnO | 0.062 | - | - | - | |
| $Fe_2O_3$ | 3.42 | 3.42 | 3.54 | - | - |
| CaO | 62.73 | 62.73 | 64.91 | 64.91 | 68.90 |
| MgO | 2.34 | 0.702 | 0.73 | 0.73 | 0.77 |
| $K_2O$ | 1.09 | 1.09 | 1.13 | 1.13 | 1.20 |
| $Na_2O$ | 0.48 | 0.48 | 0.50 | 0.50 | 0.53 |
| $SO_3$ | 3.16 | 3.16 | 3.27 | 3.27 | 3.47 |
| $P_2O_5$ | 0.109 | - | - | - | - |
| **Sum** | 99.803 | 96.642 | 100 | 94.20 | 100.00 |

The input data window in GEMS:

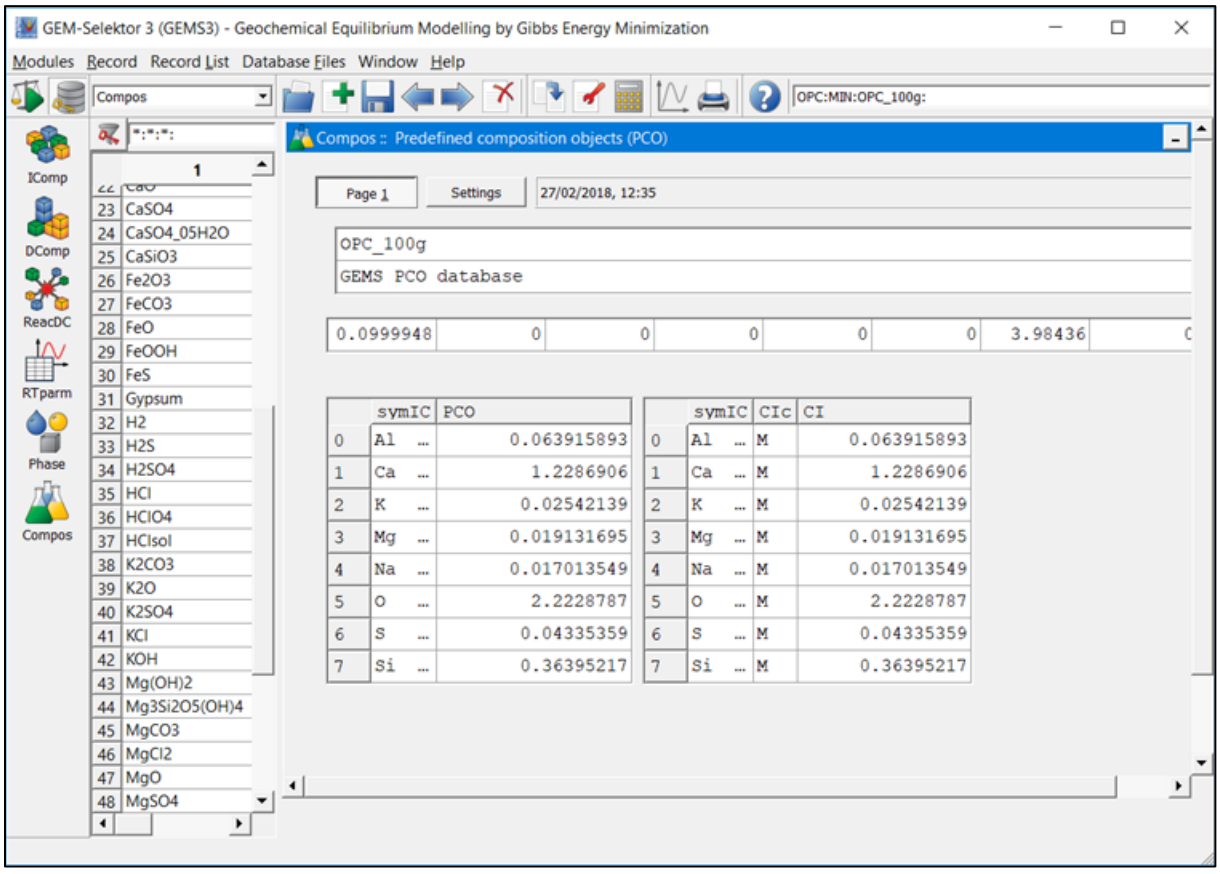


## A.II Assumptions

This method assumes 100 % reaction of the input OPC for simplicity. No unreacted OPC is therefore present at equilibrium.

## A.III Chloride exposure

### A.III.a Single equilibrium

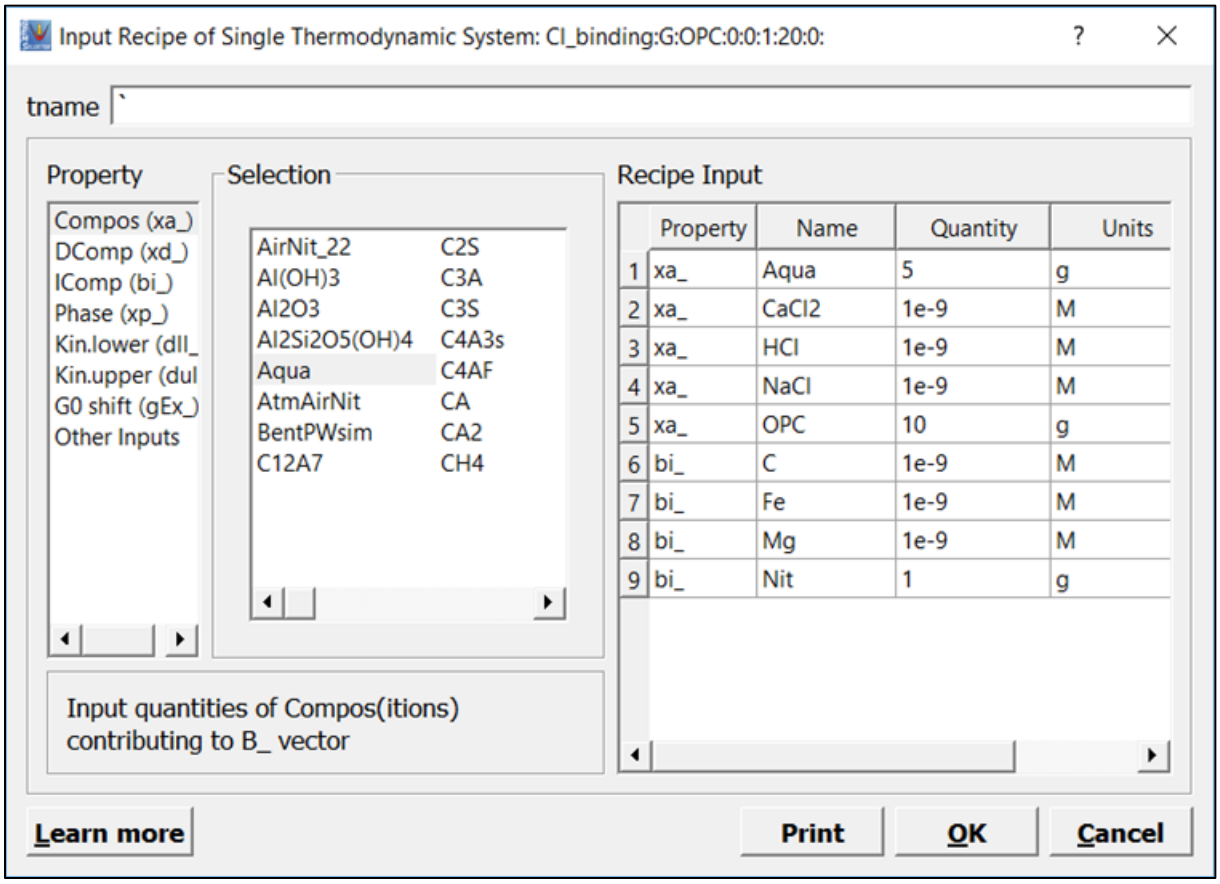

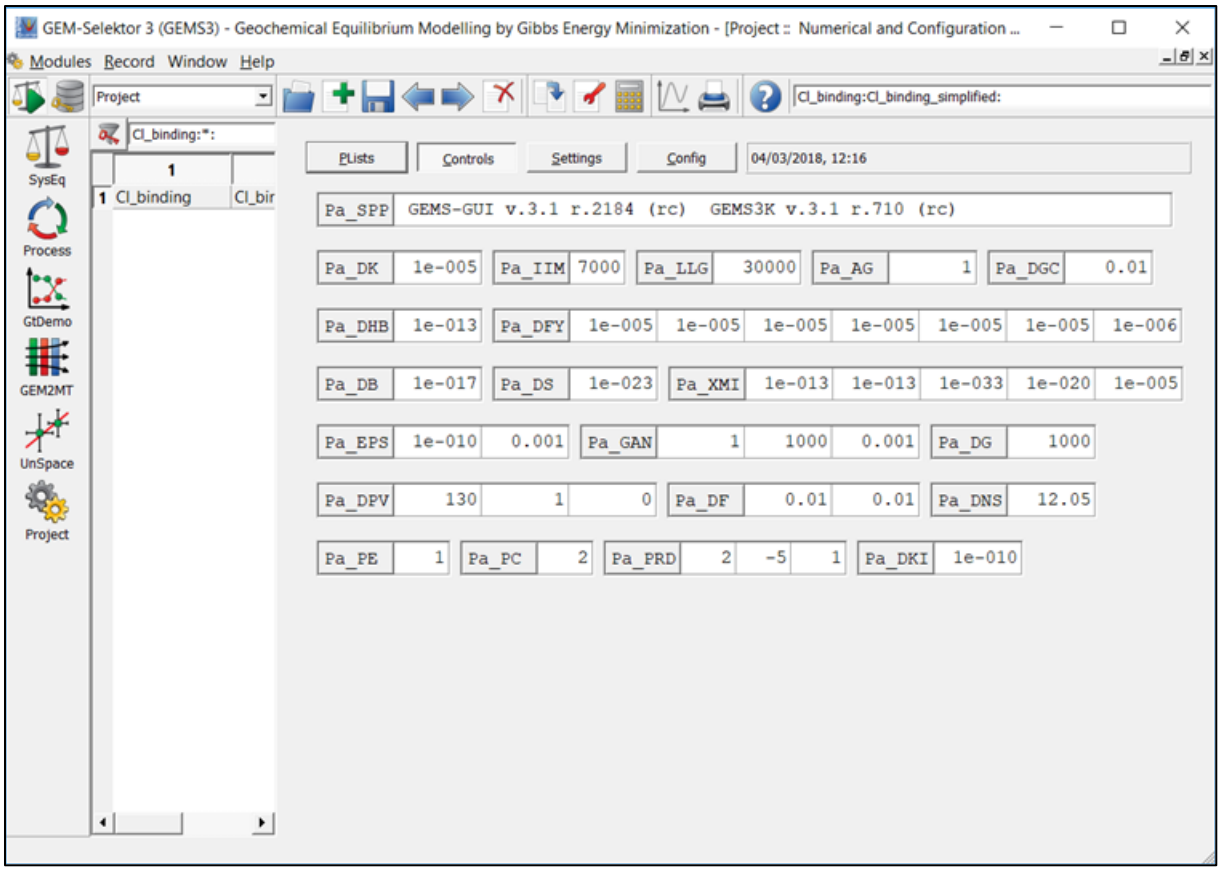
GEM-Selektor 3 (GEMS3) - Geochemical Equilibrium Modelling by Gibbs Energy Minimization - [Project :: Numerical and Configuration ...
Modules Record Window Help
Project
Cl_binding:Cl_binding_simplified:
Cl_binding:*:
SysEq
Process
GtDemo
GEM2MT
UnSpace
Project
1
1 Cl_binding
Cl_bir
PLists
Controls
Settings
Config
04/03/2018, 12:16
Pa_SPP GEMS-GUI v.3.1 r.2184 (rc) GEMS3K v.3.1 r.710 (rc)
Pa_DK 1e-005 Pa_IIM 7000 Pa_LLG 30000 Pa_AG 1 Pa_DGC 0.01
Pa_DHB 1e-013 Pa_DFY 1e-005 1e-005 1e-005 1e-005 1e-005 1e-005 1e-006
Pa_DB 1e-017 Pa_DS 1e-023 Pa_XMI 1e-013 1e-013 1e-033 1e-020 1e-005
Pa_EPS 1e-010 0.001 Pa_GAN 1 1000 0.001 Pa_DG 1000
Pa_DPV 130 1 0 Pa_DF 0.01 0.01 Pa_DNS 12.05
Pa_PE 1 Pa_PC 2 Pa_PRD 2 -5 1 Pa_DKI 1e-010

Phases enabled in the model:

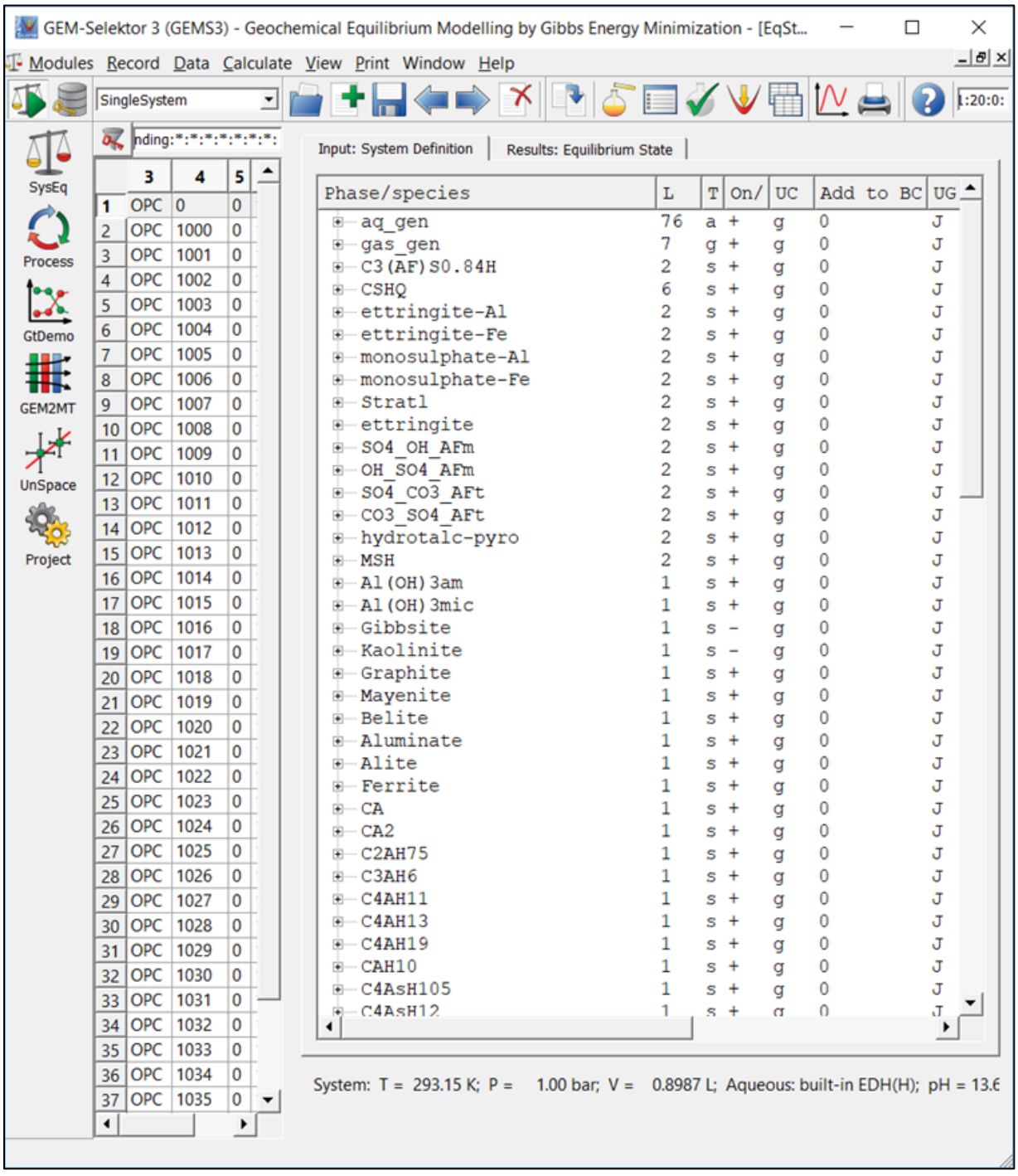

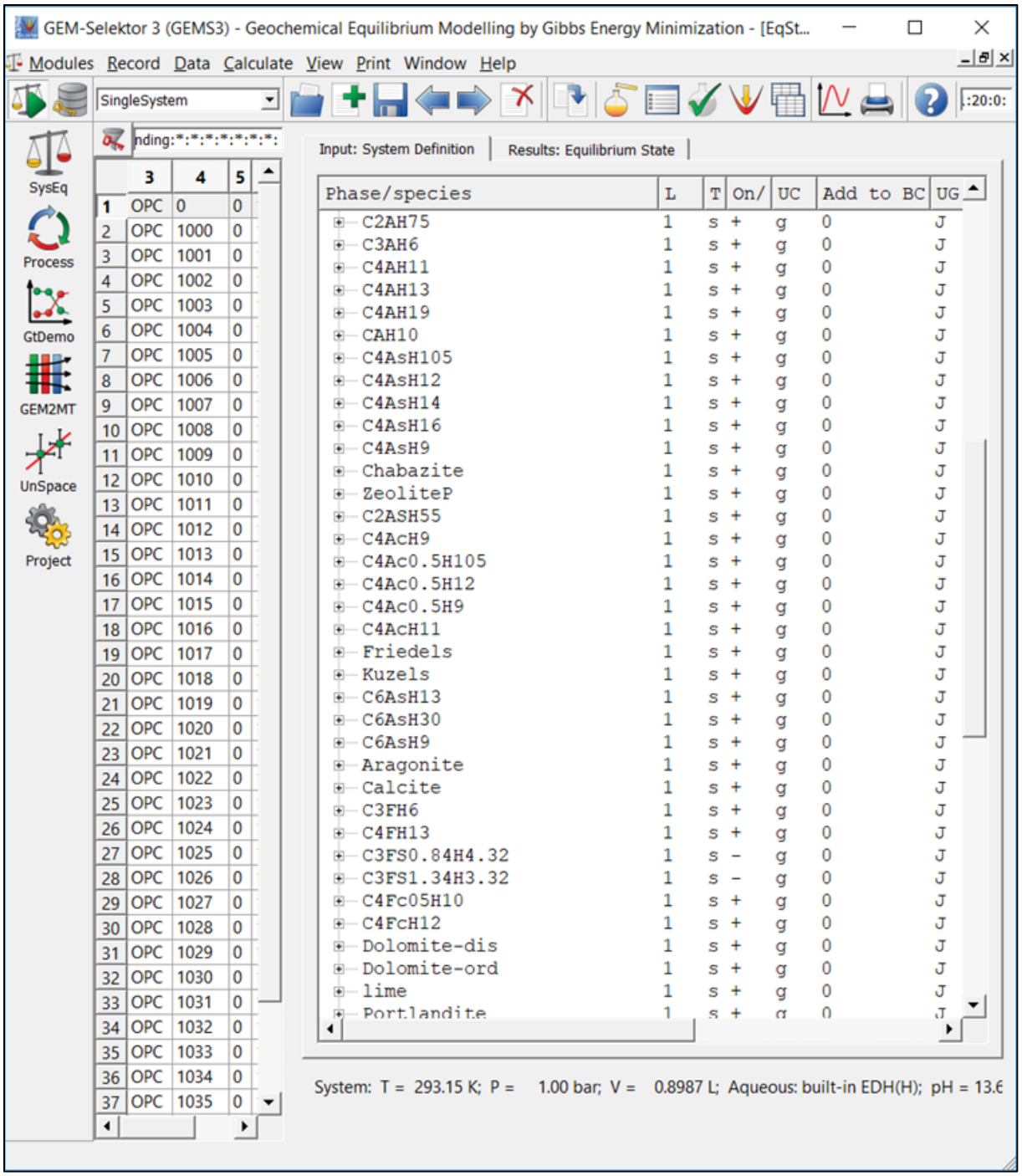
GEM-Selektor 3 (GEMS3) - Geochemical Equilibrium Modelling by Gibbs Energy Minimization - [EqSt...
Modules Record Data Calculate View Print Window Help
SingleSystem
SysEq
Process
GtDemo
GEM2MT
UnSpace
Project
Input: System Definition
Results: Equilibrium State
Phase/species L T On/ UC Add to BC UG
C2AH75 1 s + g 0 J
C3AH6 1 s + g 0 J
C4AH11 1 s + g 0 J
C4AH13 1 s + g 0 J
C4AH19 1 s + g 0 J
CAH10 1 s + g 0 J
C4AsH105 1 s + g 0 J
C4AsH12 1 s + g 0 J
C4AsH14 1 s + g 0 J
C4AsH16 1 s + g 0 J
C4AsH9 1 s + g 0 J
Chabazite 1 s + g 0 J
ZeoliteP 1 s + g 0 J
C2ASH55 1 s + g 0 J
C4AcH9 1 s + g 0 J
C4Ac0.5H105 1 s + g 0 J
C4Ac0.5H12 1 s + g 0 J
C4Ac0.5H9 1 s + g 0 J
C4AcH11 1 s + g 0 J
Friedels 1 s + g 0 J
Kuzels 1 s + g 0 J
C6AsH13 1 s + g 0 J
C6AsH30 1 s + g 0 J
C6AsH9 1 s + g 0 J
Aragonite 1 s + g 0 J
Calcite 1 s + g 0 J
C3FH6 1 s + g 0 J
C4FH13 1 s + g 0 J
C3FS0.84H4.32 1 s - g 0 J
C3FS1.34H3.32 1 s - g 0 J
C4Fc05H10 1 s + g 0 J
C4FcH12 1 s + g 0 J
Dolomite-dis 1 s + g 0 J
Dolomite-ord 1 s + g 0 J
lime 1 s + g 0 J
Portlandite 1 s + g 0 J
System: T = 293.15 K; P = 1.00 bar; V = 0.8987 L; Aqueous: built-in EDH(H); pH = 13.6

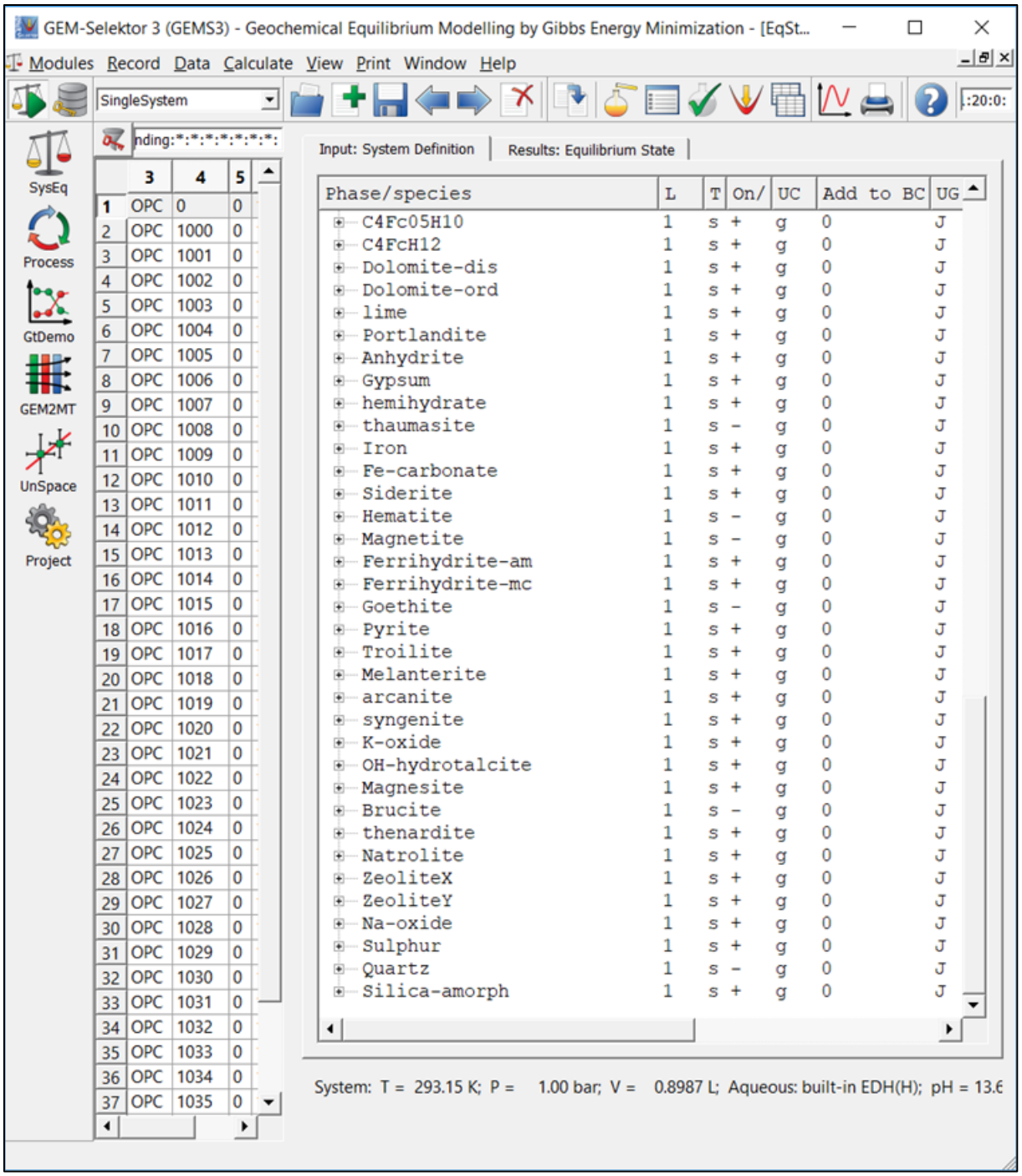


## A.IV Process

There are two processes, one for calculating solid/liquid volume (OPC_solids) and one for calculating concentrations in the liquid phase (OPC_liquid_Cl-sol).

## A.IV.a Input

The input is the same for both liquid and solid calculations:

```
$ linear counter
modC[J] =: cNu;

$Adding 15 g cement with w/c = 0.5 -> 5 ml H2O and 10 g OPC

$amount of water added in g (w/c ratio of 0.5; 20 ml NaCl added;
$HCl added in litre, mult. by 1000 to get grams of water)
$Cement paste contains 30 %wt free water
xa_[{Aqua}] =: 15-15*(2/3)*(1/1.3)+20+1000*cNu;

$amount reactive Portland cement in g:
$15 g hydrated paste, w/c ratio 0.5 => 2/3 of original paste is
cement
$Original paste added 30% water, final amount is 100% of 130%
xa_[{OPC}] =: 15*(2/3)*(1/1.3);

$NaCl addition in mol (M) (concentration 1.5M addition of 20 ml)
xa_[{NaCl}] =: 0.020*1.5;


$addition of HCl in mol (M) (conc * volume)
xa_[{HCl}] =: 4*cNu;
```

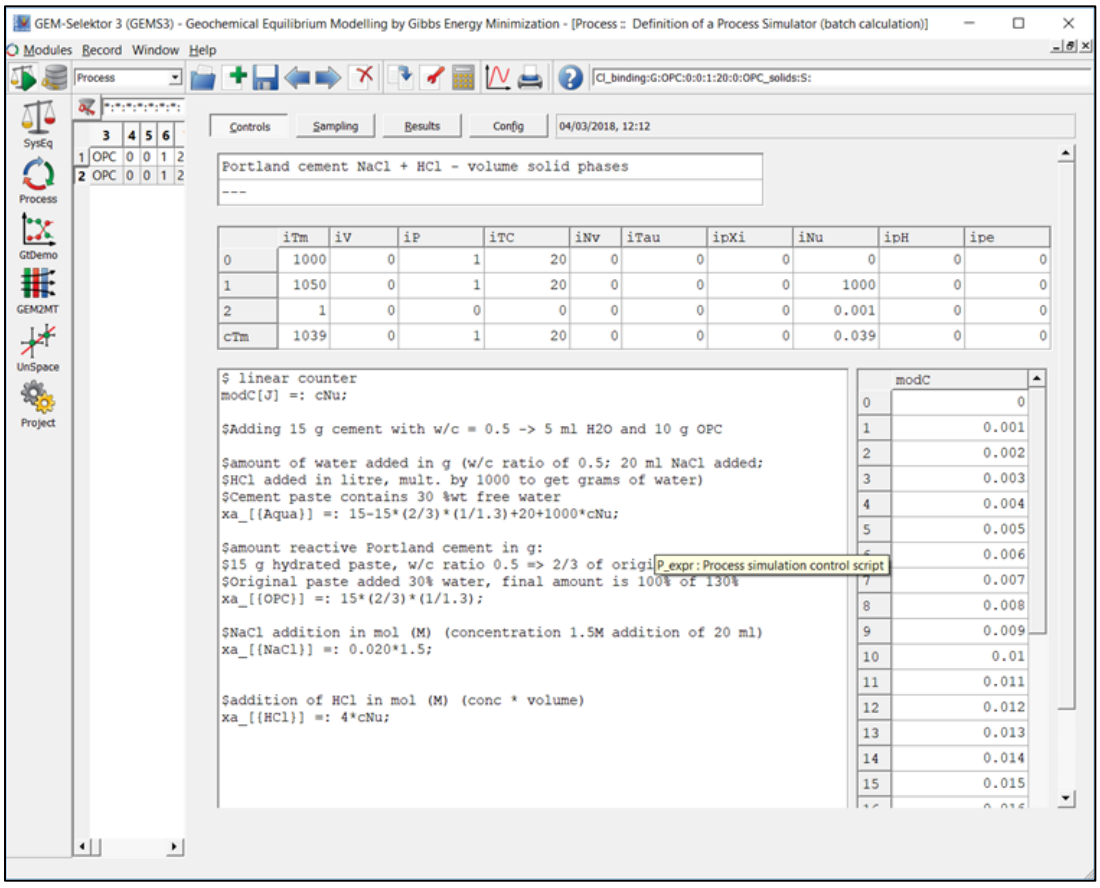

## A.IV.b Output

Output for liquid phase:

```
$Counter for calculation steps
xp[J] =: J;


$Outputs elemental concentrations in molality [mol/kg solvent]
yp[J][0] =: m_t[{Al}];
yp[J][1] =: m_t[{Ca}];
yp[J][2] =: m_t[{Cl}];
yp[J][3] =: m_t[{Mg}];
yp[J][4] =: m_t[{K}];
yp[J][5] =: m_t[{Na}];
yp[J][6] =: m_t[{S}];
yp[J][7] =: m_t[{Si}];
yp[J][8] =: my[{OH-}];

$pH of liquid phase
yp[J][9] =: pH;
```

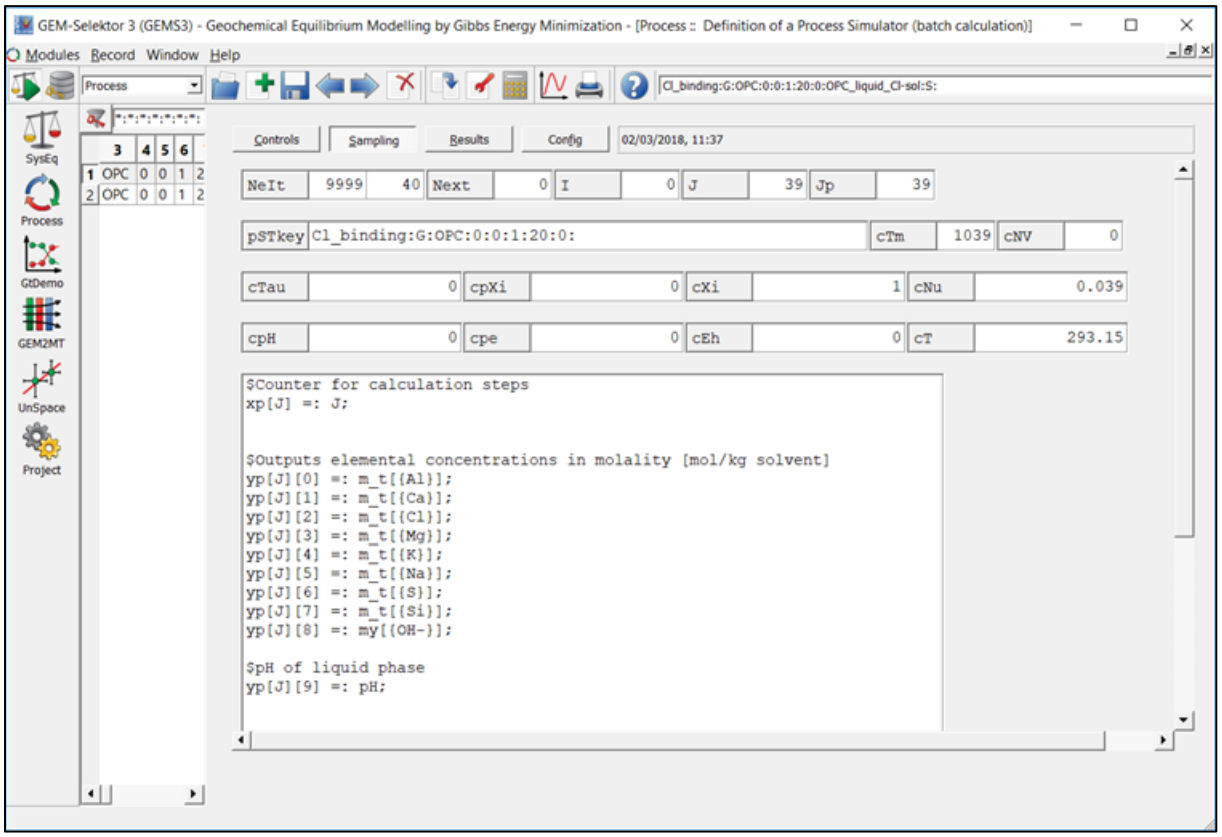

Output for solid phases:

```
$counter for calculation steps
xp[J] =: J;

$ phVol = volume of phase in cm^3

$ Unreacted OPC, if desired
yp[J][0] =: 0;

$outputs, volumes in cm^3
$CSH
yp[J][1] =: phVol[{CSHQ}]+phVol[{C3(AF)S0.84H}];
$Portlandite
yp[J][2] =: phVol[{Portlandite}];
$AFt, sum of AFt-phases
yp[J][3] =: phVol[{ettringite-Al}]+phVol[{ettringite-
Fe}]+phVol[{ettringite}]+phVol[{SO4_CO3_AFt}]+phVol[{CO3_SO4_AFt}];
$Friedel's salt
yp[J][4] =: phVol[{Friedels}];
$Ferrihydrate
yp[J][5] =: phVol[{Ferrihydrite-mc}];
$Natrolite
yp[J][6] =: phVol[{Natrolite}];
$Gypsum
yp[J][7] =: phVol[{Gypsum}];
$Silica-amorph
yp[J][8] =: phVol[{Silica-amorph}];
$MSH
yp[J][9] =: phVol[{MSH}];
$OH-hydrotalcite
yp[J][10] =: phVol[{OH-hydrotalcite}];
$Water
yp[J][11] =: phVol[{aq_gen}];

$CH mass
yp[J][12] =: phM[{Portlandite}];

$wt of all phases
yp[J][13] =: phM[{CSHQ}]+phM[{C3(AF)S0.84H}]+ phM[{Portlandite}] +
phM[{ettringite-Al}]+phM[{ettringite-
Fe}]+phM[{ettringite}]+phM[{SO4_CO3_AFt}]+phM[{CO3_SO4_AFt}] +
phM[{Friedels}] + phM[{Ferrihydrite-mc}] + phM[{Natrolite}] +
phM[{Gypsum}] + phM[{Silica-amorph}] +phM[{MSH}] + phM[{OH-
hydrotalcite}];

$wt% CH normalized to dry wt
yp[J][14] =: yp[J][12]/(15*(2/3)*(1/1.3));

$volume of paste
yp[J][15] =: phVol[{CSHQ}]+phVol[{C3(AF)S0.84H}]+
phVol[{Portlandite}] + phVol[{ettringite-Al}]+phVol[{ettringite-
Fe}]+phVol[{ettringite}]+phVol[{SO4_CO3_AFt}]+phVol[{CO3_SO4_AFt}] +
phVol[{Friedels}] + phVol[{Ferrihydrite-mc}] + phVol[{Natrolite}] +
```

```
phVol[{Gypsum}] + phVol[{Silica-amorph}] +phVol[{MSH}] + phVol[{OH-
hydrotalcite}];

$vol% CH
yp[J][16] =: yp[J][2]/yp[J][15];
```

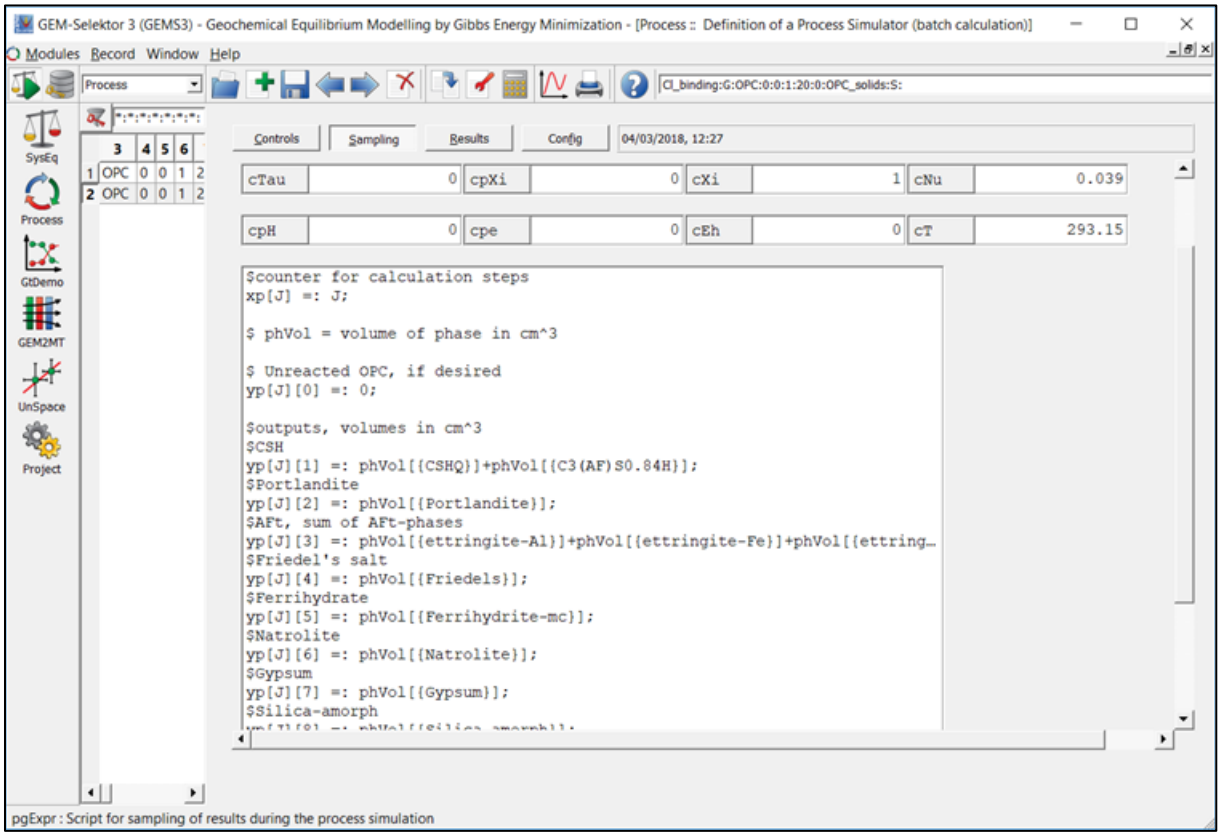

## A.IV.c Results

Liquid phase:

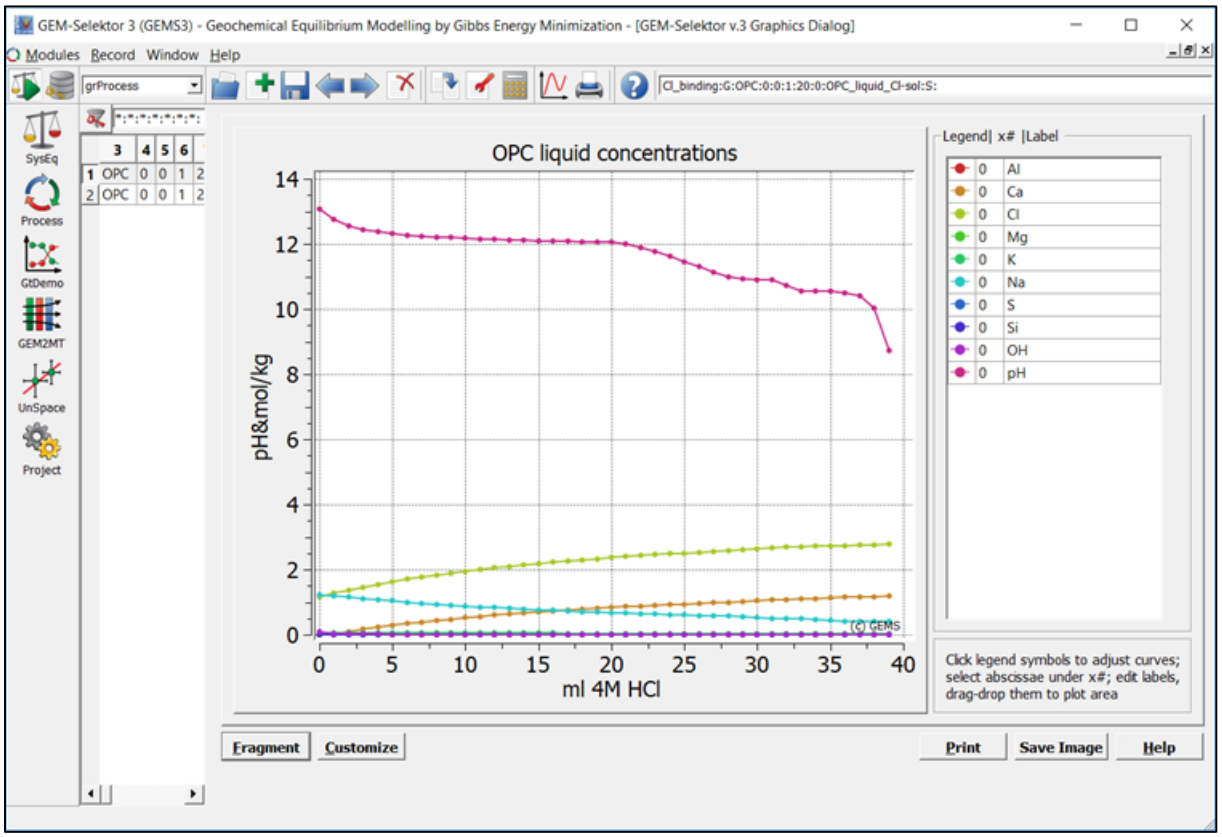


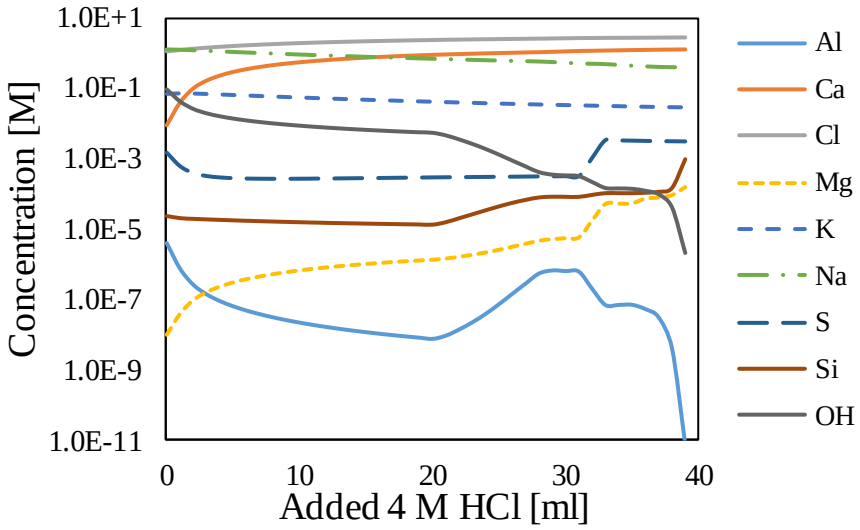

Solid phases:

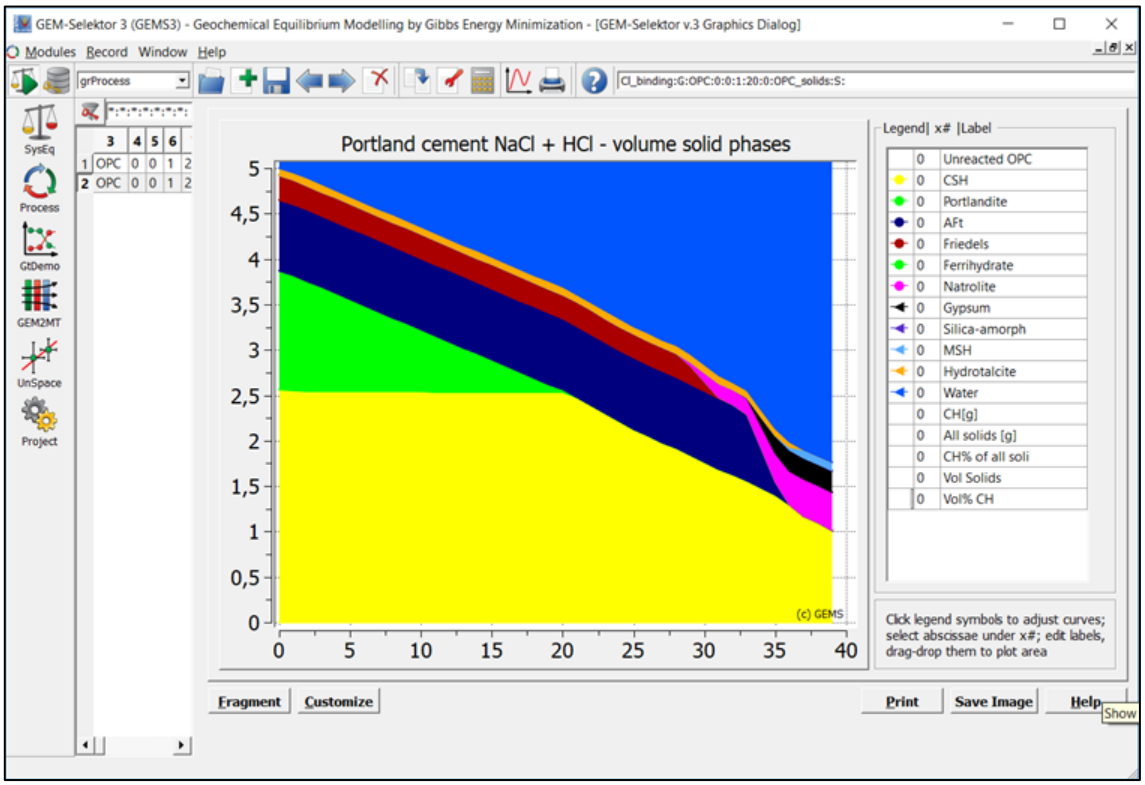


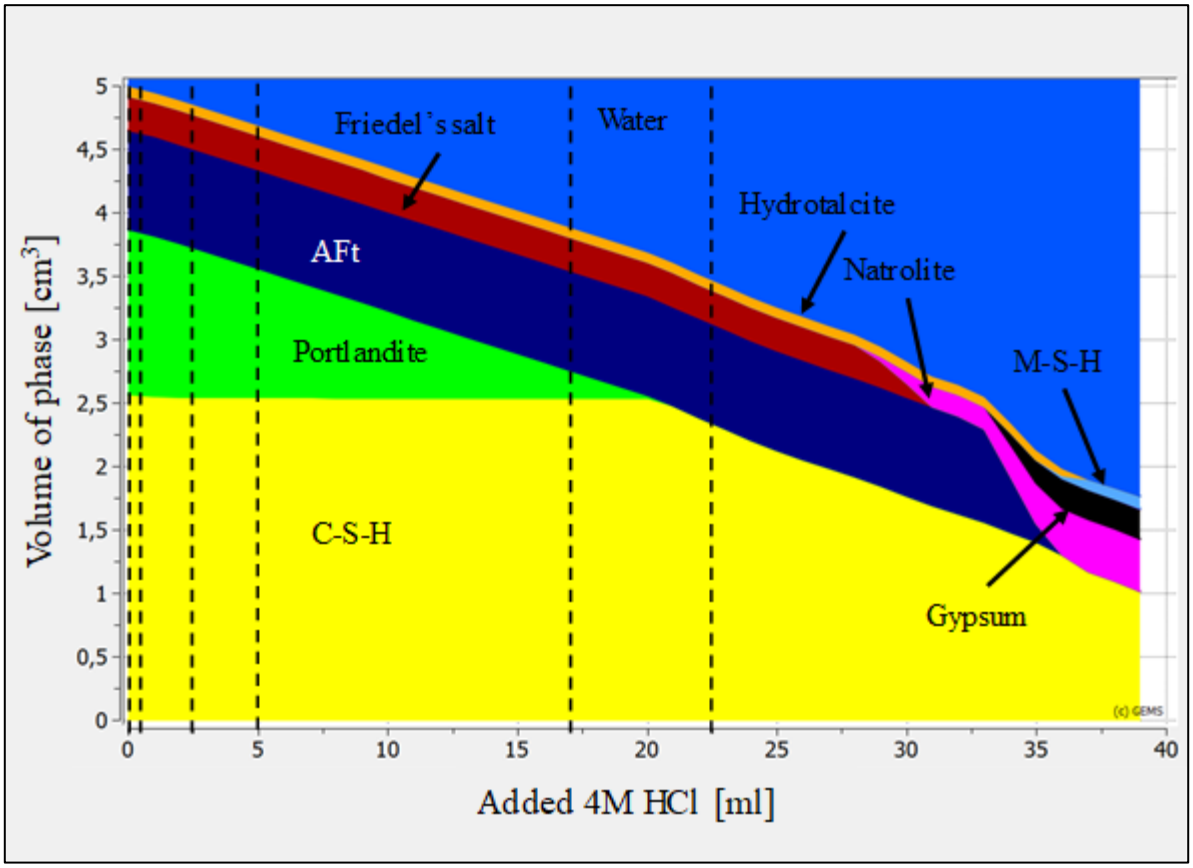

# Appendix B Error calculations

Standard Gaussian error propagation was used to calculate the standard deviations of the chloride binding values. All measured values were assumed to be normally distributed and not correlated (covariance = 0). The following table gives the symbols for values used in error calculations and their uncertainties. For a given value $N$, the uncertainty is denoted $\sigma_N$.

| **Symbol** | **Value** | **Error determination method** |
|---|---|---|
| $C_{Cl^-}$ | Chloride concentration measured by titration [M] | Gaussian |
| $V_{Cl^-}$ | Volume of sample liquid extracted for titration [l] | Pipette accuracy |
| $C_{AgNO3}$ | Concentration of titrant [M] | Assumed |
| $V_{AgNO3}$ | Volume of titrant [l] | Pipette accuracy |
| $C_{NaCl}$ | Concentration of NaCl solution [M] | |
| $V_{NaCl}$ | Volume of added NaCl solution [l] | Pipette accuracy |
| $n_{NaCl}$ | Amount of NaCl added to sample [mol] | |
| $C_{HCl}$ | Concentration of HCl [M] | Provided by manufacturer |
| $V^i_{HCl}$ | Volume 4 M HCl added in step *i* [l] | Gaussian |
| $V_{HCl}$ | Total colume HCl added to sample [l] | Gaussian |
| $n_{HCl}$ | Amount of HCl added to sample [mol] | Gaussian |
| $V_{H2O,\ paste}$ | Volume of free water in sample originating from the well-hydrated cement paste [l] | Gaussian |
| $\rho_{H2O}$ | Density of water, rounded to 1 [g/ml] | Assumed to be 0 |
| $m_{Paste}$ | Mass of cement paste without free water in a sample [g] | Gaussian |
| $m_{w.h.paste}$ | Mass of well-hydrated cement paste in each sample [g] | Balance accuracy |
| $\%H_2O$ | Mass percentage of free water in cement paste [%] | Assumed to be ± 5% of value |
| $V_{H2O}$ | Volume of free water in a sample [l] | Gaussian |
| $n_{Cl^-}$ | Amount of chloride in solution in sample [mol] | Gaussian |
| $n_{Bound}$ | Amount of bound chlorides [mol] | Gaussian |
| $C_b$ | Bound chlorides in mg chloride per g cement paste without free water [mg/g] | Gaussian |

The titrator uses the concentration and volume of AgNO3 and volume of the sample to calculate chloride concentrations by Equation B-1. Equation B-2 gives the calculation for error in chloride concentration.

$$C_{Cl^-} = \frac{C_{AgNO_3} V_{AgNO_3}}{V_{Cl^-}} \quad \text{B-1}$$

$$\sigma_{C_{Cl^-}} = |C_{Cl^-}| \sqrt{\left(\frac{\sigma_{C_{AgNO_3}}}{C_{AgNO_3}}\right)^2 + \left(\frac{\sigma_{V_{AgNO_3}}}{V_{AgNO_3}}\right)^2 + \left(\frac{\sigma_{V_{Cl^-}}}{V_{Cl^-}}\right)^2} \quad \text{B-2}$$

The same method was used to determine the concentration of the prepared NaCl exposure solution. Equation B-3 gives the calculation of the concentration while Equation B-4 gives the calculation of the error.

$$C_{NaCl} = \frac{C_{AgNO_3} V_{AgNO_3}}{V_{NaCl}} \quad \text{B-3}$$

$$\sigma_{C_{NaCl}} = |C_{NaCl}| \sqrt{\left(\frac{\sigma_{C_{AgNO_3}}}{C_{AgNO_3}}\right)^2 + \left(\frac{\sigma_{V_{AgNO_3}}}{V_{AgNO_3}}\right)^2 + \left(\frac{\sigma_{V_{NaCl}}}{V_{NaCl}}\right)^2} \quad \text{B-4}$$

With the concentration of NaCl and the weight difference of the samples before and after adding the solution, the amount of NaCl added to the sample was calculated. Equation B-5 gives the number of moles of NaCl added to a sample, while Equation B-6 gives the calculated error.

$$n_{NaCl} = C_{NaCl} V_{NaCl} \quad \text{B-5}$$

$$\sigma_{n_{NaCl}} = |n_{NaCl}| \sqrt{\left(\frac{\sigma_{C_{NaCl}}}{C_{NaCl}}\right)^2 + \left(\frac{\sigma_{V_{NaCl}}}{V_{NaCl}}\right)^2} \quad \text{B-6}$$

HCl was added in steps, and the samples were weighed after each addition. With the measured weight change and the known density of the HCl, the volume added in each step was calculated. The sum of each addition was multiplied by the concentration of HCl to find the moles of $Cl^-$ ions added to the sample, as in Equation B-7. Equation B-8 shows the calculation of error in moles HCl added to the sample.

$$n_{HCl} = C_{HCl}\, V_{HCl} = C_{HCl} \sum_{i=1}^{N} V_{HCl}^{i} \quad \text{B-7}$$

$$\sigma_{n_{HCl}} = |\, n_{HCl}| \sqrt{\left(\frac{\sigma_{C_{HCl}}}{C_{HCl}}\right)^2 + \sum_{i=1}^{N} \sigma_{V_{HCl}^{i}} \Big/ \left(\sum_{i=1}^{N} V_{HCl}^{i}\right)^2} \quad \text{B-8}$$

The amount of free water in the paste was determined by TGA. The weight percentage of free water from cement paste in each sample was calculated by multiplying the percentage of free water with the weight of the cement paste and using $\rho_{H2O}$ = 1 g/ml (Equation B-9). The error is calculated using Equation B-10

$$V_{H_2O,paste} = \frac{1}{\rho_{H_2O}} m_{paste} \cdot \%H_2O \quad \text{B-9}$$

$$\sigma_{V_{H_2O,paste}} = \left|\frac{1}{\rho_{H_2O}}\right| |\, V_{H_2O,paste}| \sqrt{\left(\frac{\sigma_{m_{paste}}}{m_{paste}}\right)^2 + \left(\frac{\sigma_{\%H_2O}}{\%H_2O}\right)^2} \quad \text{B-10}$$

Equation B-11 was used to calculated he total amount of water in each sample, which was the sum of water from the paste, from the NaCl-solution and from HCl, subtracted the amount of water removed during measurements. Equation B-12 was used to calculate the error.

$$V_{H_2O} = V_{H_2O,paste} + V_{NaCl} + V_{HCl} - V_{meas} \quad \text{B-11}$$

$$\sigma_{V_{H_2O}} = \sqrt{\left(\sigma_{V_{H_2O,paste}}\right)^2 + \left(\sigma_{V_{NaCl}}\right)^2 + \left(\sigma_{V_{HCl}}\right)^2 - \left(\sigma_{V_{meas}}\right)^2} \quad \text{B-12}$$

To find the amount of bound chlorides, the amount of chlorides in solution must be calculated. This is done by multiplying the chloride concentration by the volume of water in the sample, as shown in EquationB-13. The chloride concentration was measured by chloride titration, where it is calculated from how much $AgNO_3$ is required to precipitate all chlorides in a volume of pore solution as AgCl. Error of the chloride amount was calculated using Equation B-14.

$$n_{Cl^-} = V_{H_2O}\, C_{Cl^-} = V_{H_2O}\, \frac{C_{AgNO_3}\, V_{AgNO_3}}{V_{Cl^-}} \quad \text{B-13}$$

$$\sigma_{n_{Cl^-}} = |n_{Cl^-}| \sqrt{\left(\frac{\sigma_{V_{H_2O}}}{V_{H_2O}}\right)^2 + \left(\frac{\sigma_{C_{AgNO_3}}}{C_{AgNO_3}}\right)^2 + \left(\frac{\sigma_{V_{AgNO_3}}}{V_{AgNO_3}}\right)^2 + \left(\frac{\sigma_{V_{Cl^-}}}{V_{Cl^-}}\right)^2}^2 \quad \text{B-14}$$

The amount of bound chlorides is the total amount of chlorides added to a sample minus the amount of chlorides in solution (Equation B-15, error in Equation B-16).

$$n_{Bound} = n_{NaCl} + n_{HCl} - n_{Cl^-} \quad \text{B-15}$$

$$\sigma_{n_{Bound}} = \sqrt{\left(\sigma_{n_{NaCl}}\right)^2 + \left(\sigma_{n_{HCl}}\right)^2 + \left(\sigma_{n_{Cl^-}}\right)^2} \quad \text{B-16}$$

The amount of cement paste without free water is found by subtracting the amount of free water from the amount of well-hydrated cement paste, shown in Equation B-17 (error calculated with Equation B-18).

$$m_{Paste} = m_{w.h.paste} - \rho_{H_2O} \cdot V_{H_2O,paste} \quad \text{B-17}$$

$$\sigma_{m_{Paste}} = \sqrt{\left(\sigma_{m_{w.h.paste}}\right)^2 + \left(\rho_{H_2O} \cdot \sigma_{V_{H_2O,paste}}\right)^2} \quad \text{B-18}$$

To find the chloride binding in terms of mg chlorides per gram cement paste without free water, the amount of bound chlorides is multiplied by the molar mass of chloride, multiplied by 1000 mg/g and divided by the weight of cement paste (Equation B-19, error in Equation B-20).

$$C_b = 1000 \frac{mg}{g} \frac{n_{Bound}\, Mm_{Cl^-}}{m_{Paste}} \quad \text{B-19}$$

$$\sigma_{C_b} = \left| 1000 \frac{mg}{g} \right| |Mm_{Cl^-}|\, |C_b| \sqrt{\left(\frac{\sigma_{n_{Bound}}}{n_{Bound}}\right)^2 + \left(\frac{\sigma_{m_{Paste}}}{m_{Paste}}\right)^2} \quad \text{B-20}$$

# Appendix C BSE and EDS-images

## C.I OPC-No chloride exposure

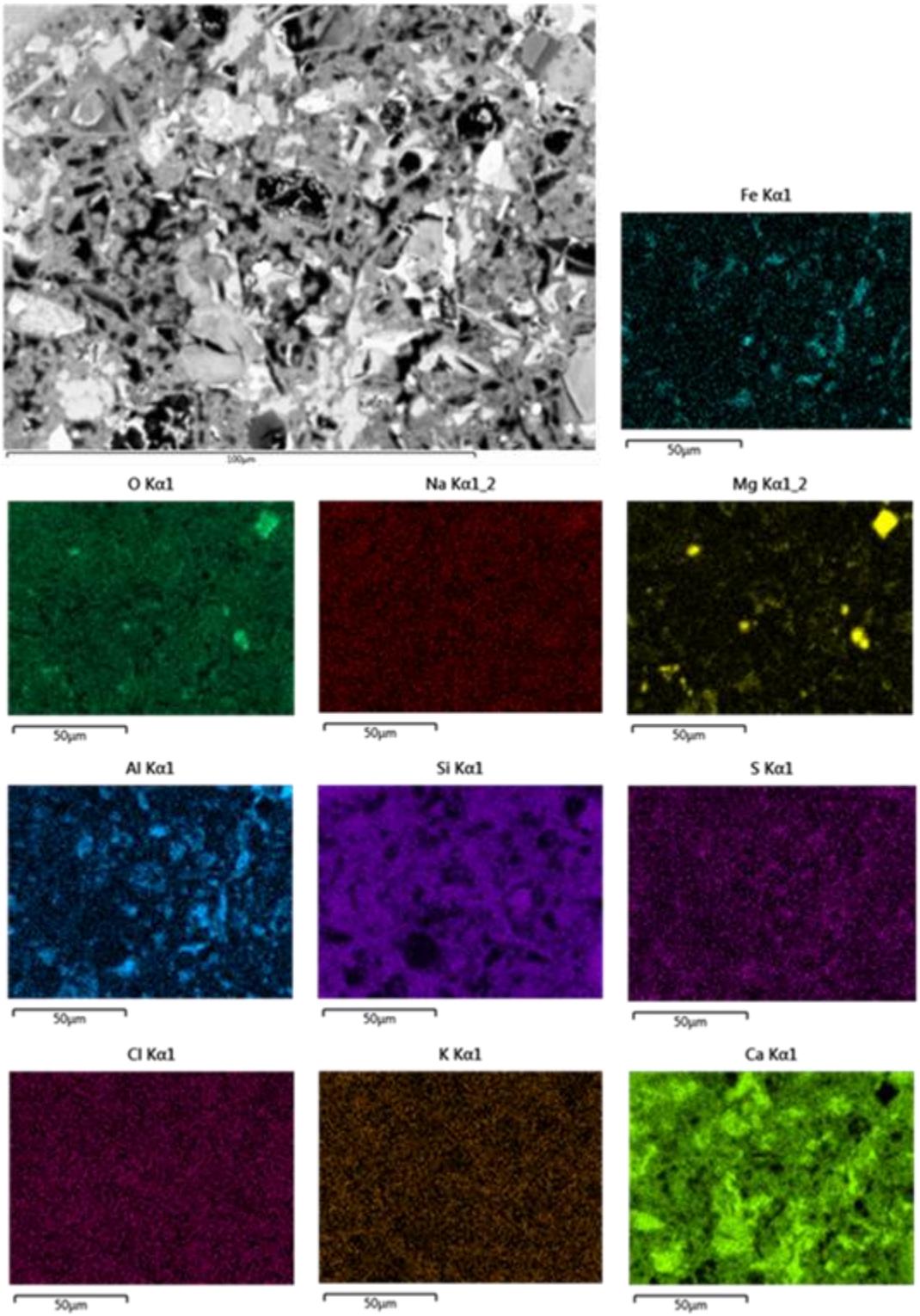

## C.II OPC-0, only NaCl

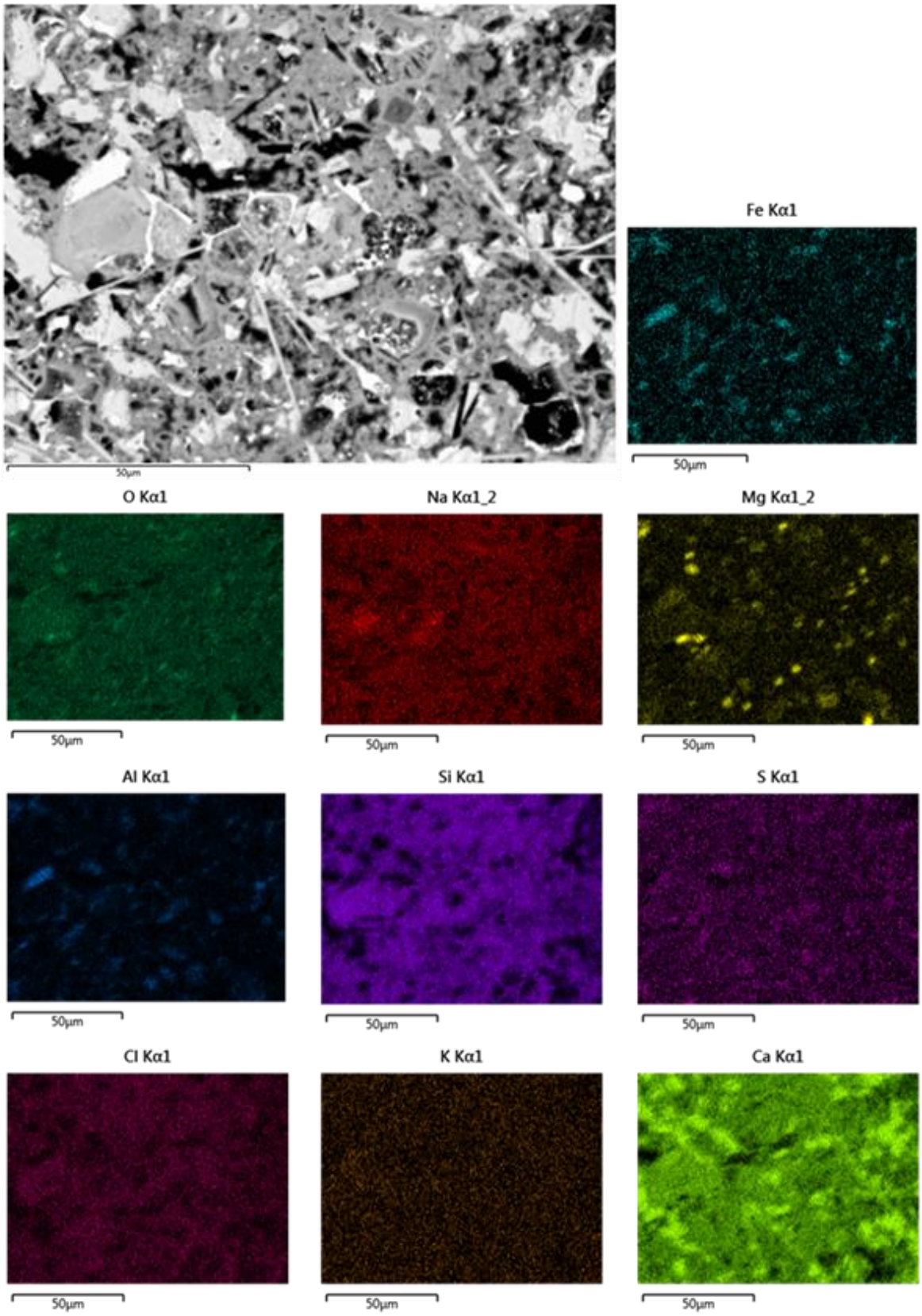

## C.III OPC-0.5 ml HCl

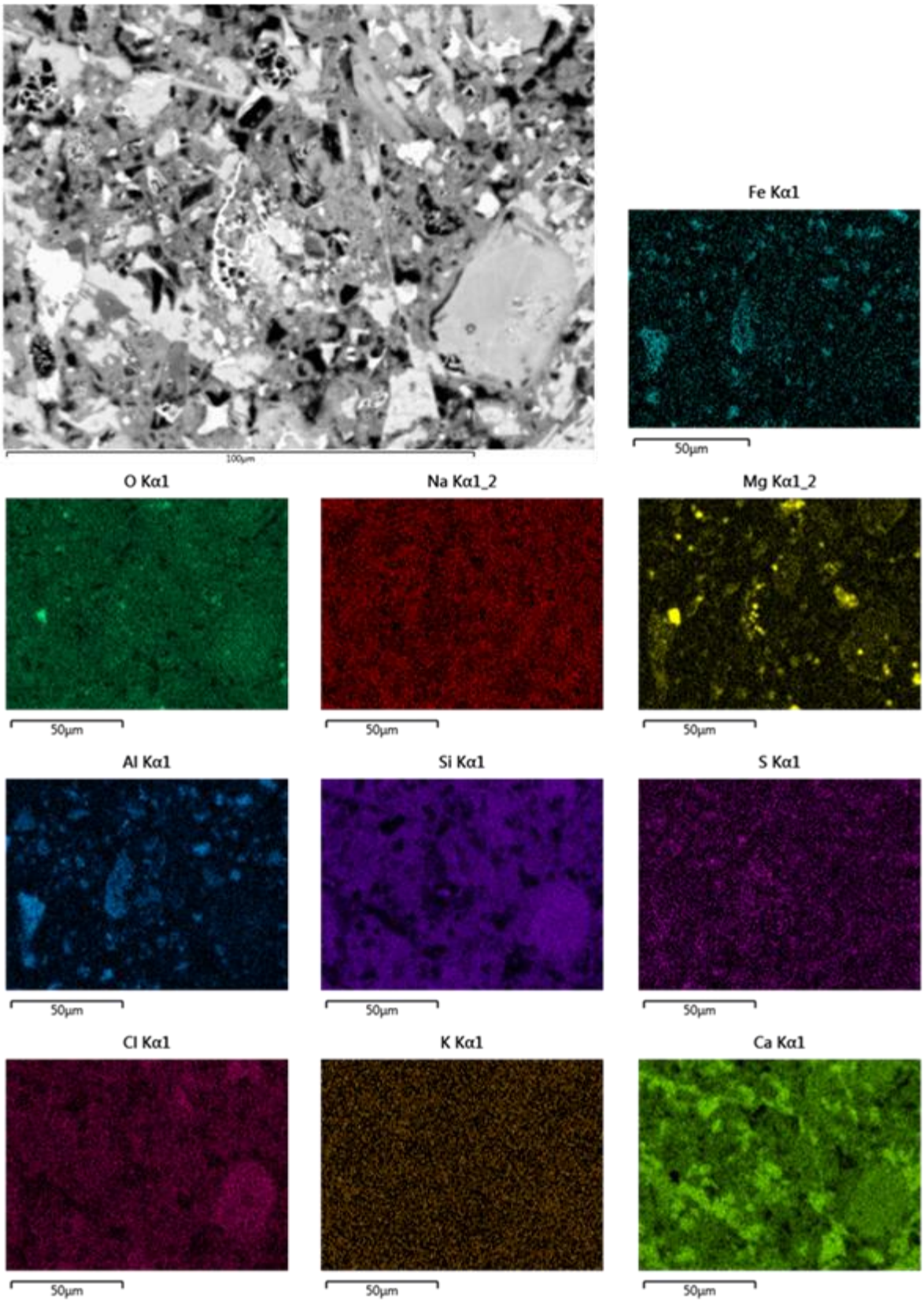

## C.IV OPC-2.5 ml HCl

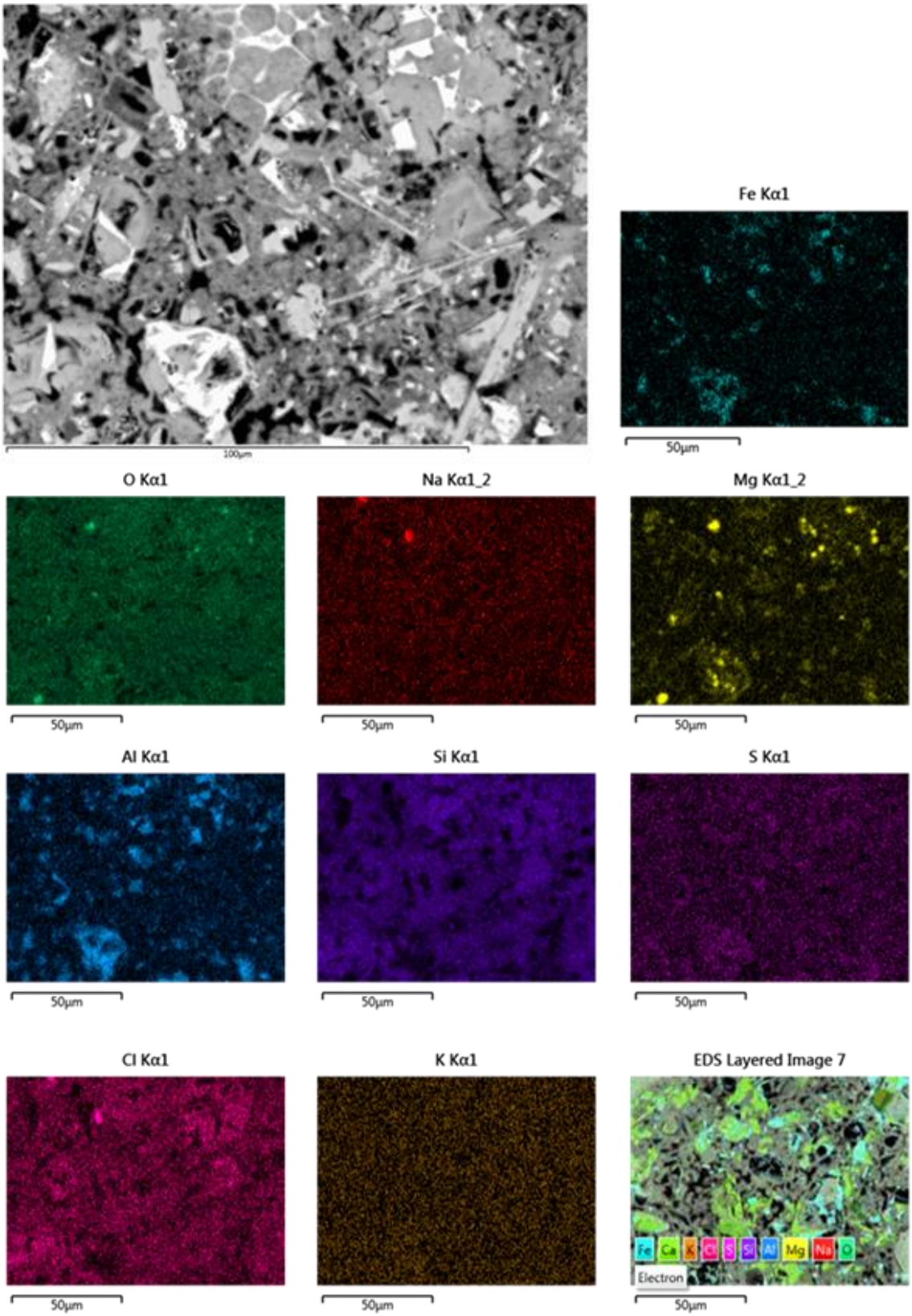

C.V OPC-5 ml HCl

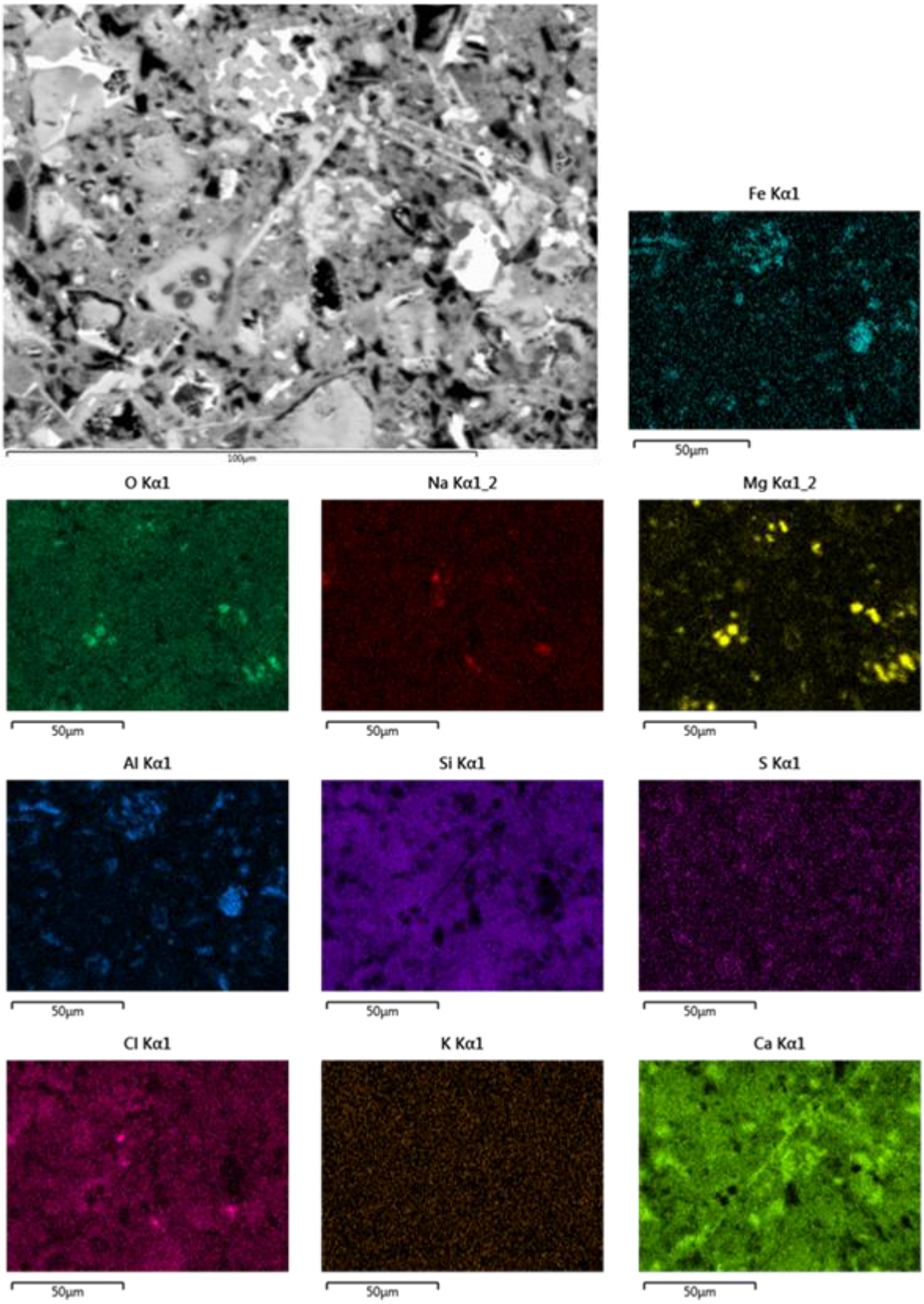

C.VI OPC-17 ml HCl

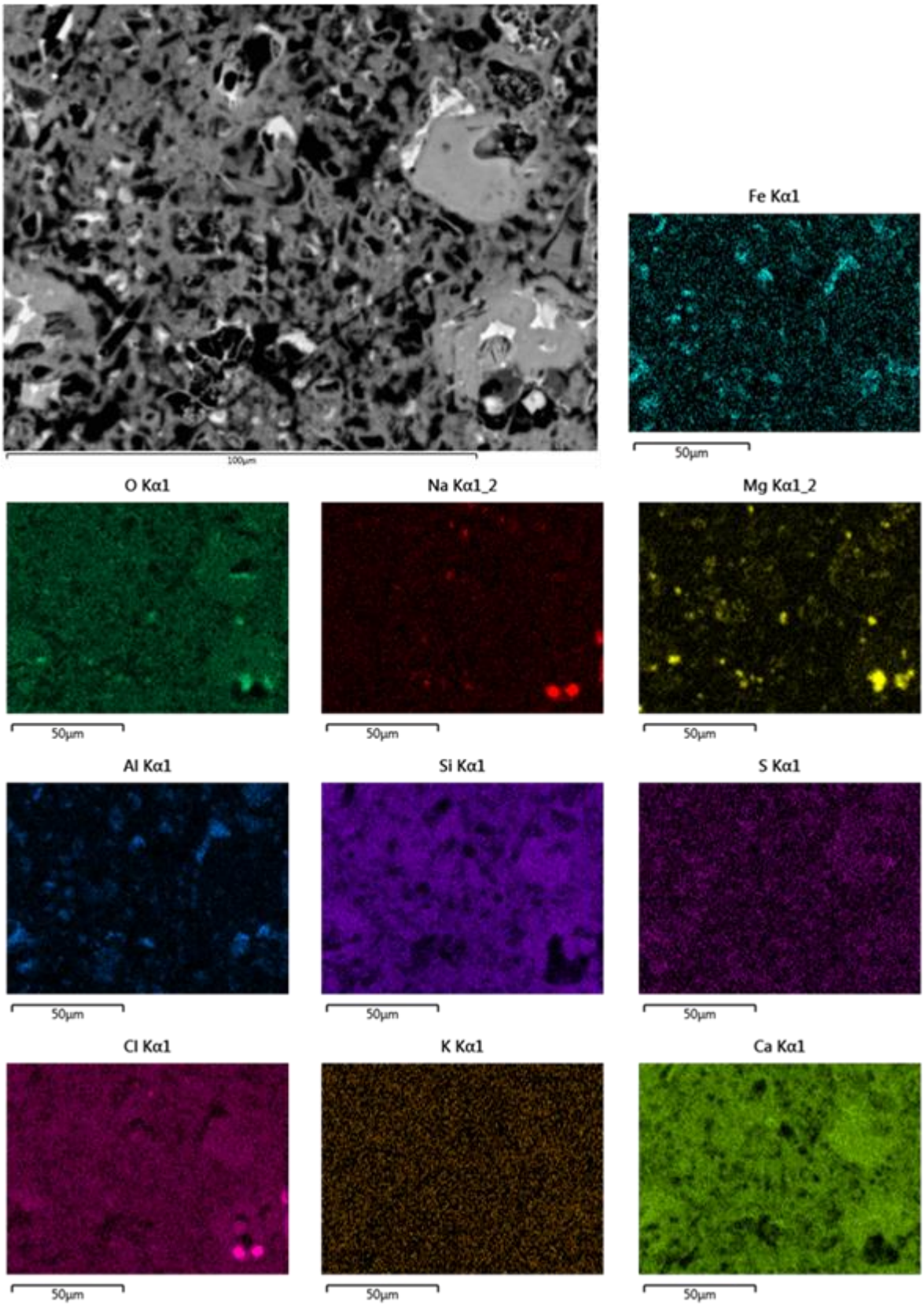

C.VII OPC-22.5 ml HCl

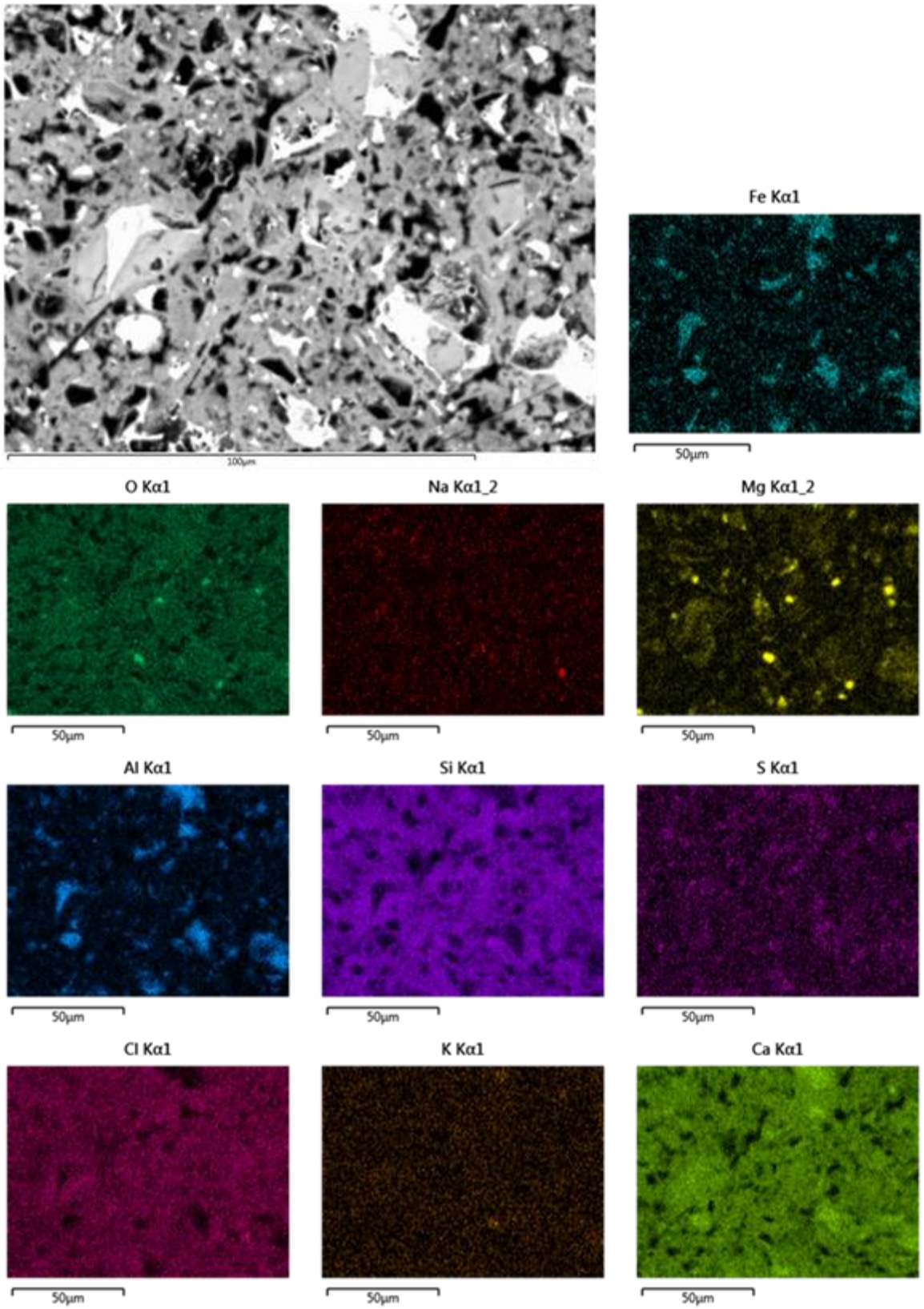

C.VIII OPC-0, only NaCl, small particles in epoxy

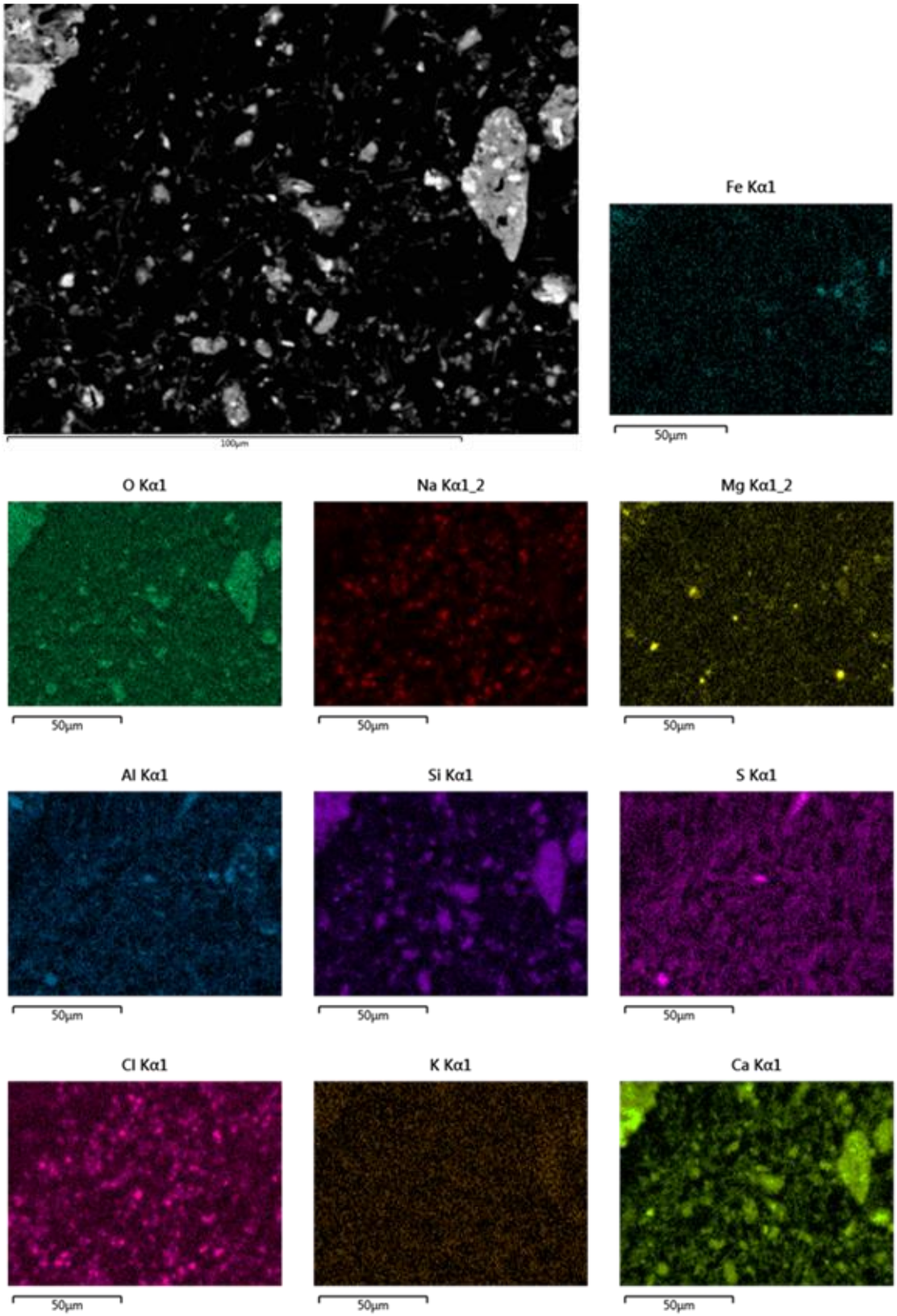

# Appendix D EDS point scans

## D.I Al/Si-ratios

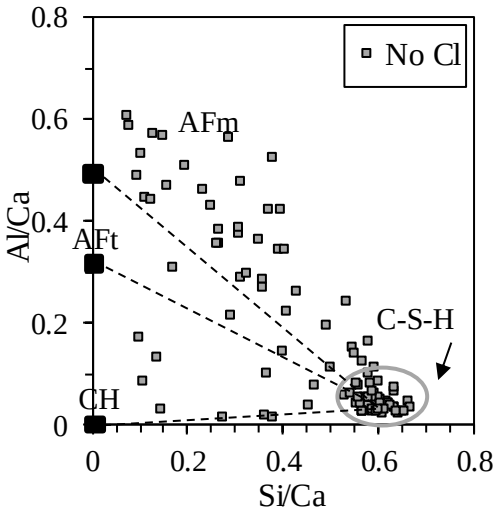


A

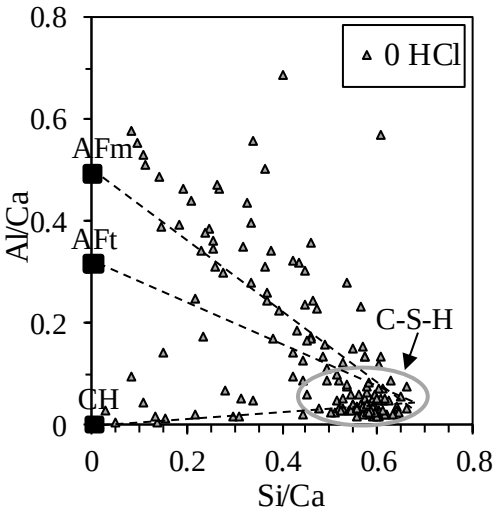


B

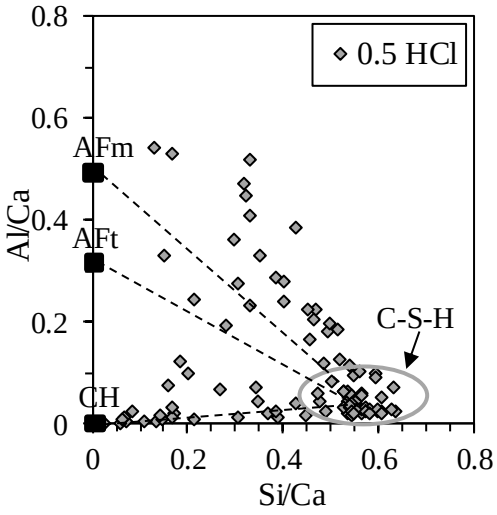


C

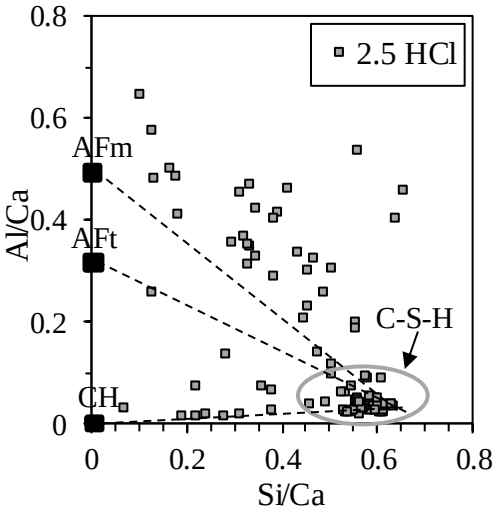


D

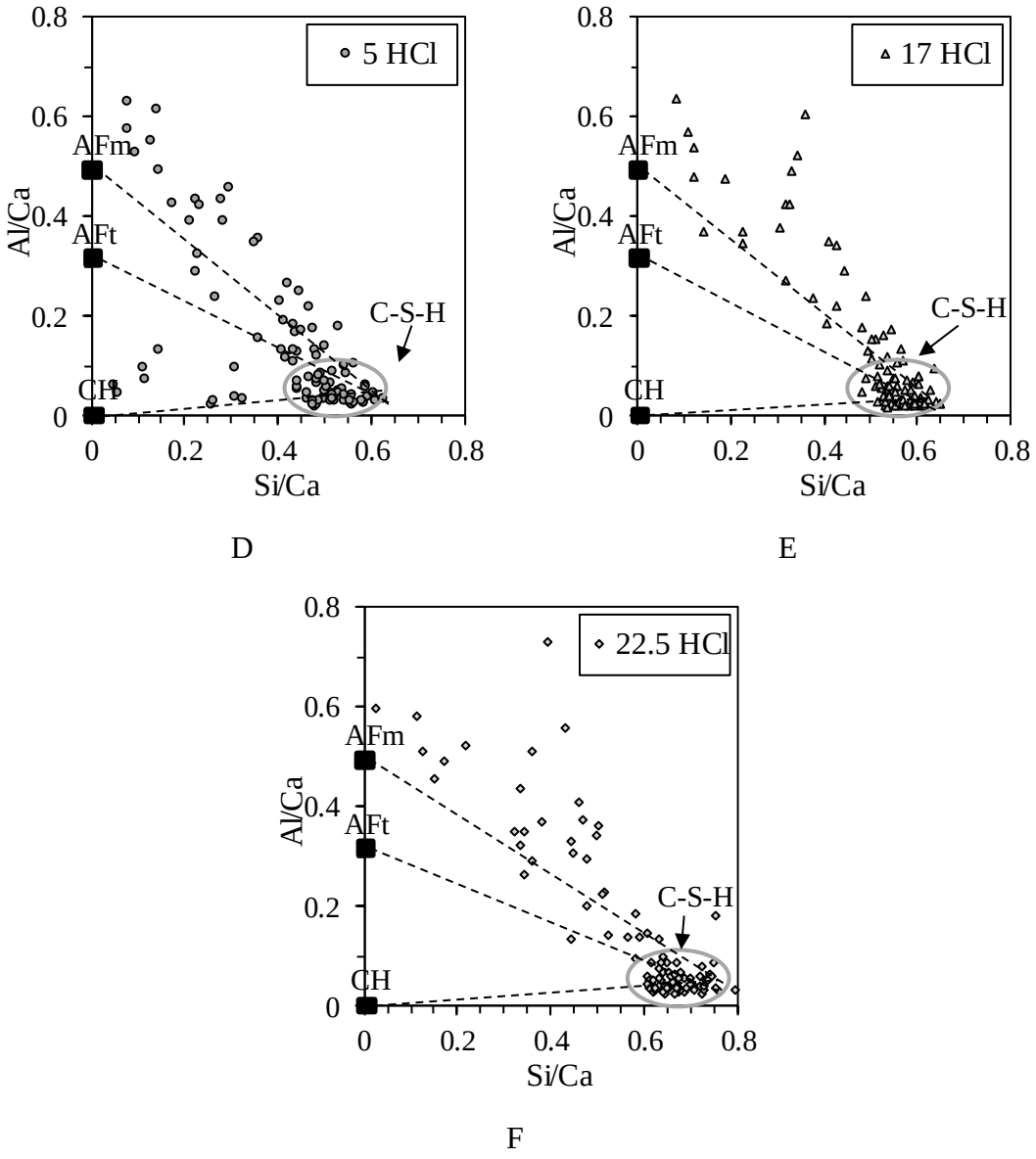


Figure D.1: EDS point scan data showing the atomic ratios of Al/Si normalized to the calcium content for all samples in the current study. The label indicates the amount of HCl added to the cement paste, except for subfigure A which is from the cement paste not exposed to chlorides. Black squares indicate pure phases that are common in cement pastes. Points lying on the lines between C-S-H and a pure phase indicate that the scan detected a mix of the phase and C-S-H. The dissolution of portlandite can be seen from the lack of points on the line between C-S-H and CH for subfigure E and F. The plots also indicate that AFm-phases are favoured rather than AFt, in contrast with the results from XRD which showed clear reflections of ettringite (AFt).

## D.II Fe/Si-ratios

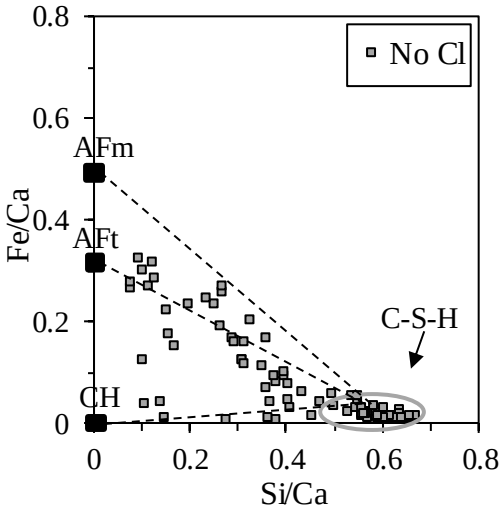


A

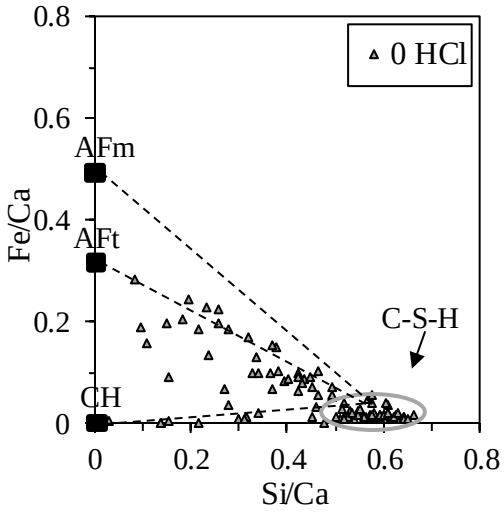


B

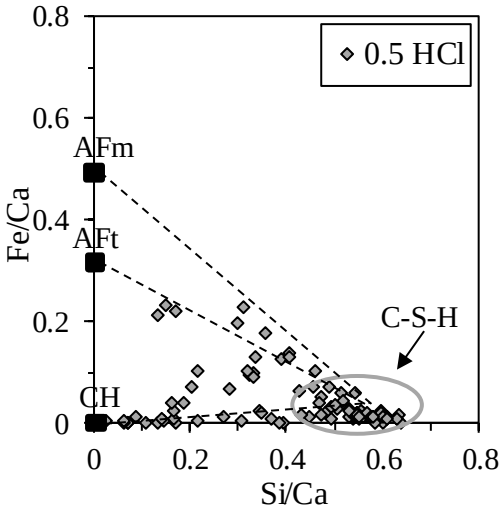


C

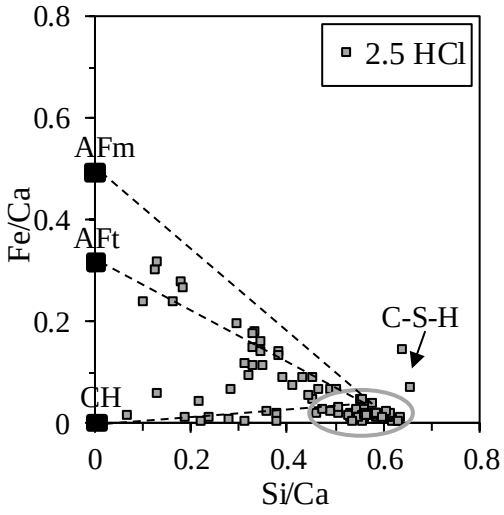


B

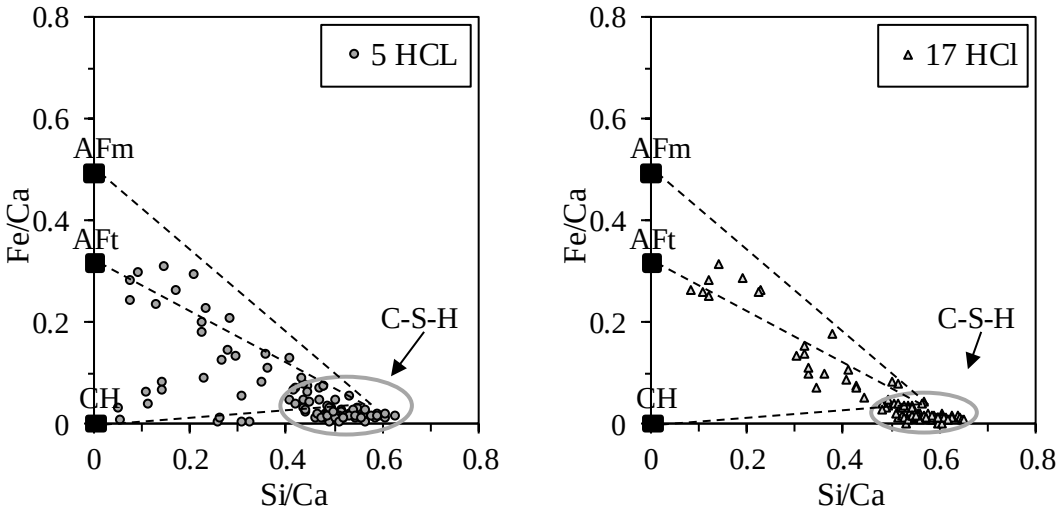


D




E

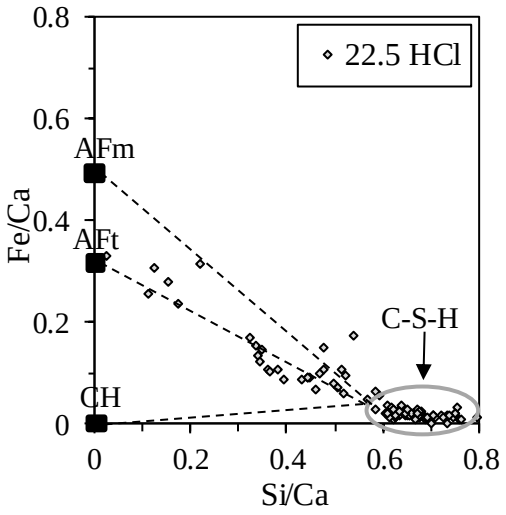


F

Figure D.2: EDS point scan data showing the atomic ratios of Al/Si normalized to the calcium content for all samples in the current study. The label indicates the amount of HCl added to the cement paste, except for subfigure A which is from the cement paste not exposed to chlorides. Black squares indicate pure phases that are common in cement pastes. Points lying on the lines between C-S-H and a pure phase indicate that the scan detected a mix of the phase and C-S-H. The dissolution of portlandite can be seen from the lack of points on the line between C-S-H and CH for subfigure E and F. The plots also indicate that AFm-phases are favoured rather than AFt, in contrast with the results from XRD which showed clear reflections of ettringite (AFt).

## D.III (Fe+Al)/Si-ratios

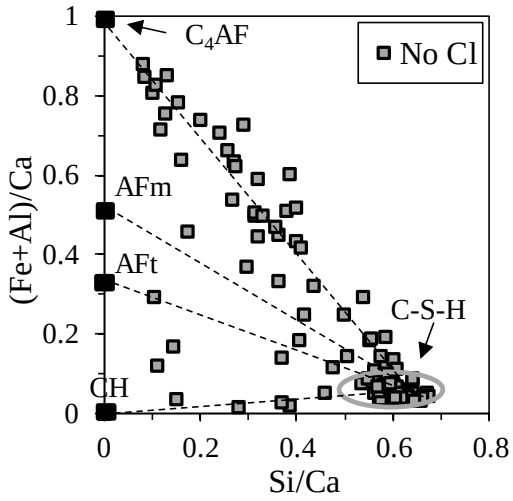


A

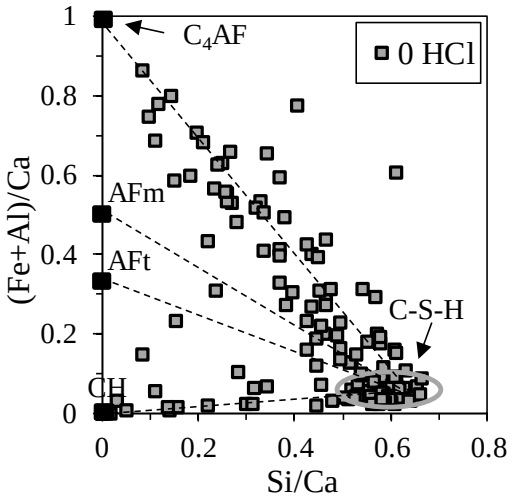


B

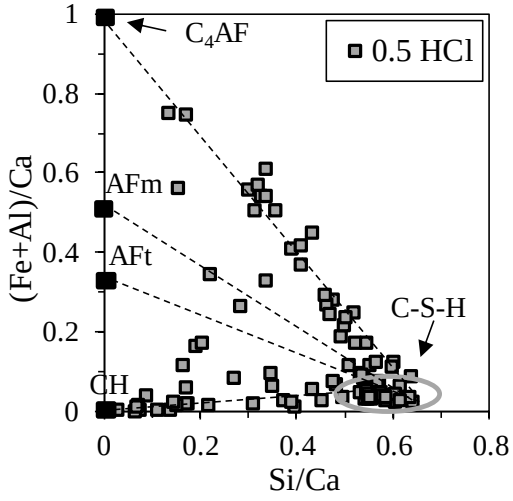


C

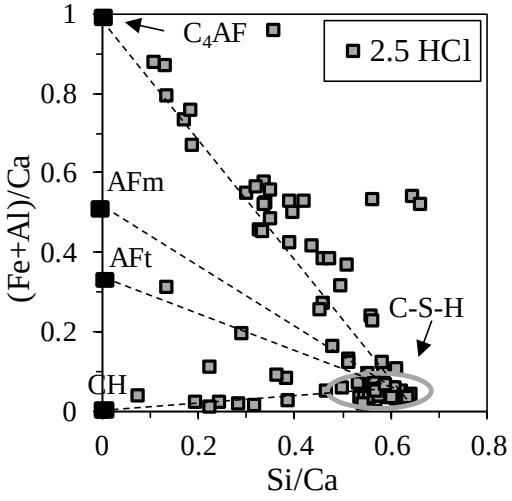


B

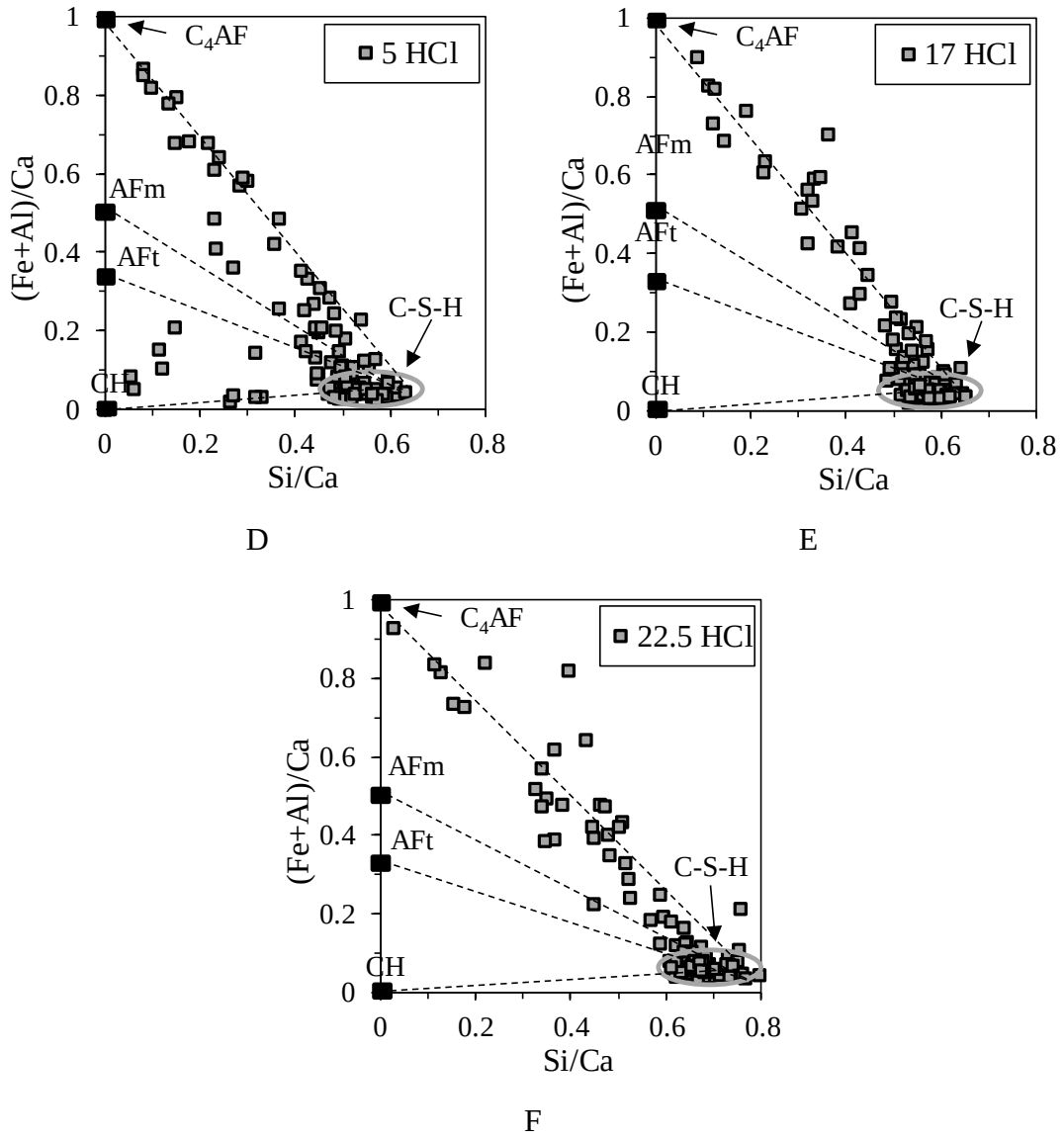


Figure D.3: EDS point scan data showing the atomic ratios of Al/Si normalized to the calcium content for all samples in the current study. The label indicates the amount of HCl added to the cement paste, except for subfigure A which is from the cement paste not exposed to chlorides. Black squares indicate pure phases that are common in cement pastes. Points lying on the lines between C-S-H and a pure phase indicate that the scan detected a mix of the phase and C-S-H. The dissolution of portlandite can be seen from the lack of points on the line between C-S-H and CH for subfigure E and F. The plots also indicate that AFm-phases are favoured rather than AFt, in contrast with the results from XRD which showed clear reflections of ettringite (AFt).

## D.IV S/Al-ratios

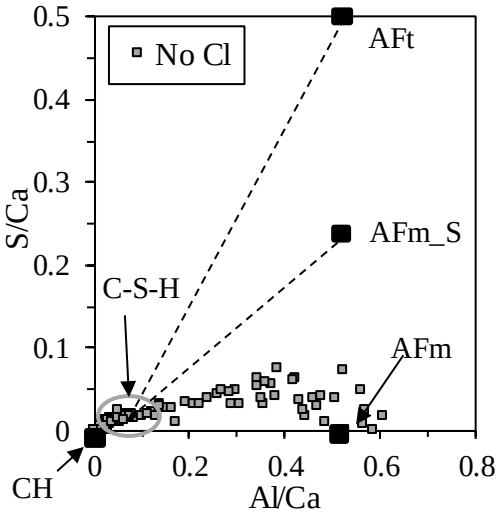


A

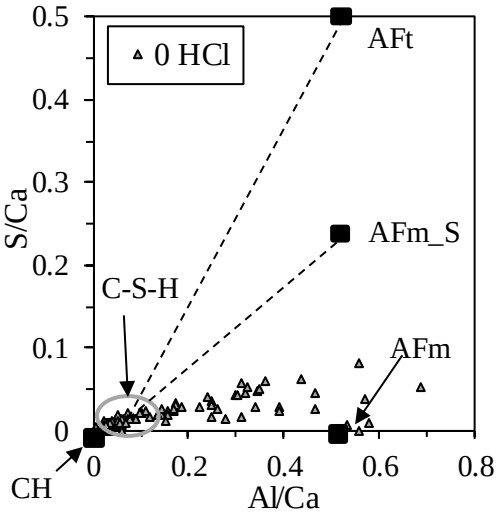


B

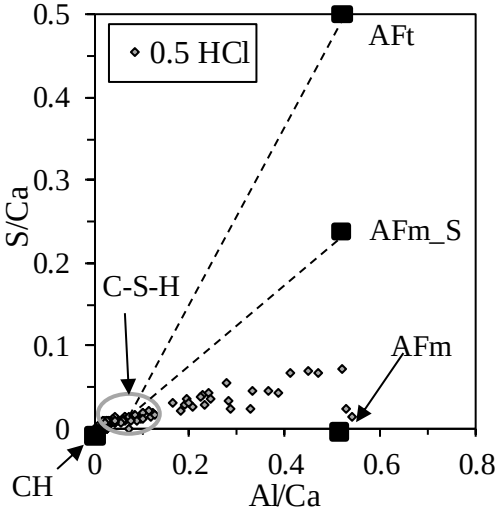


C

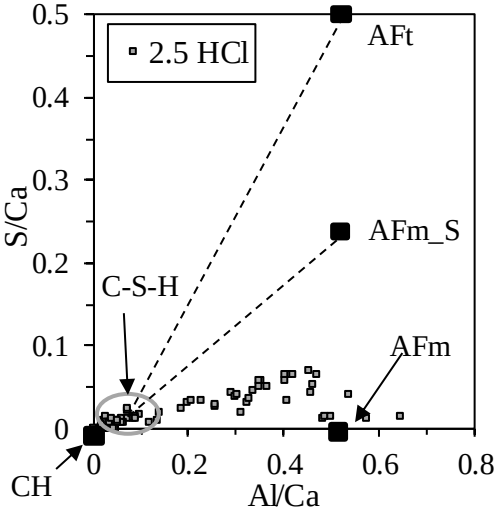


B

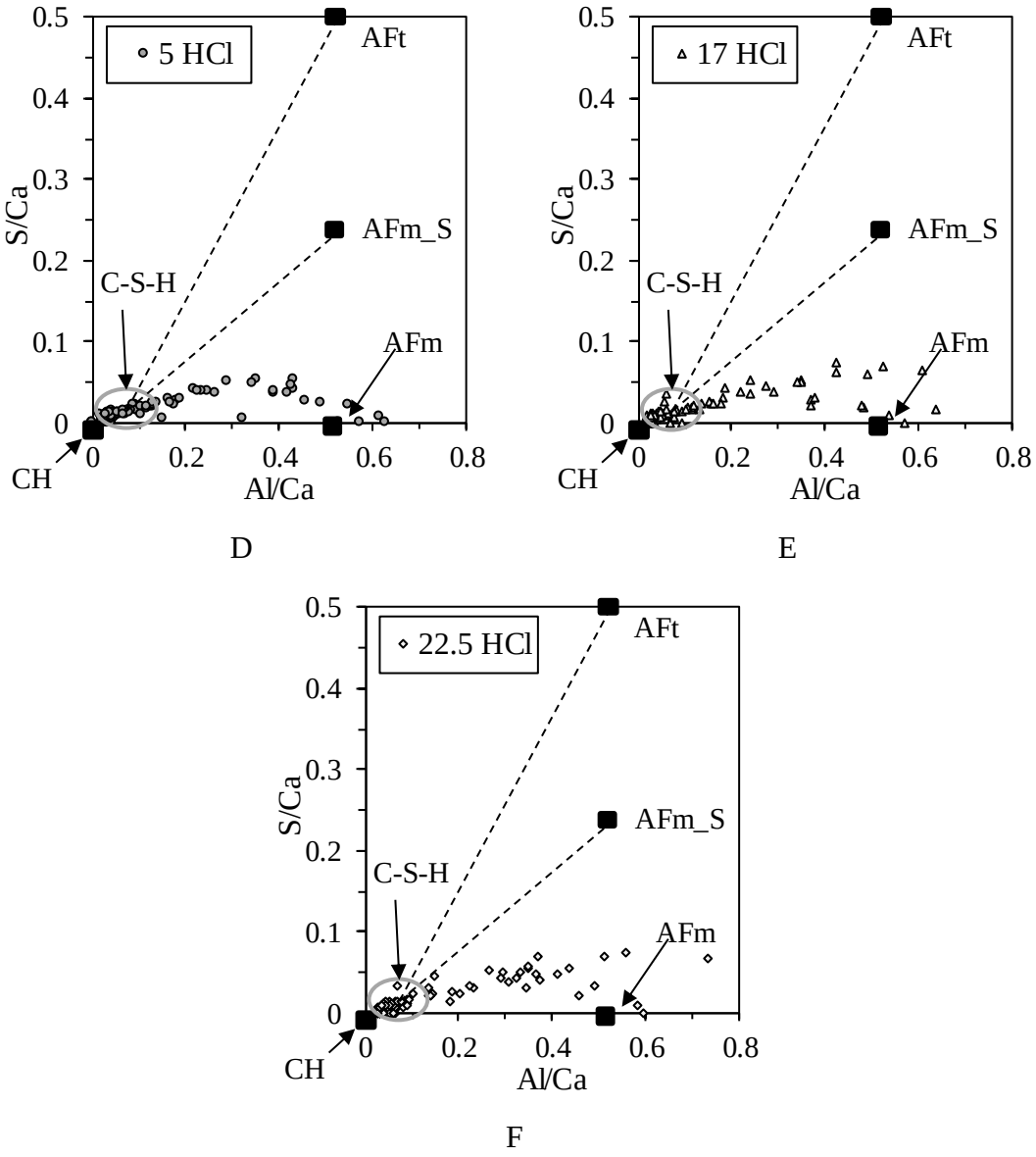


Figure D.4: EDS point scan data showing the atomic ratios of S/Al normalized to the calcium content for all samples in the current study. The label indicates the amount of HCl added to the cement paste, except for subfigure A which is from the cement paste not exposed to chlorides. Black squares indicate pure phases that are common in cement pastes. Here AFm_S is short for monosulphate. Points lying on the lines between C-S-H and a pure phase indicate that the scan detected a mix of the phase and C-S-H. The S/Al-ratios show that AFm-phases are favoured of AFt, in contrast with results from XRD which showed clear reflections from ettringite (AFt).

## D.V Cl/Al-ratios

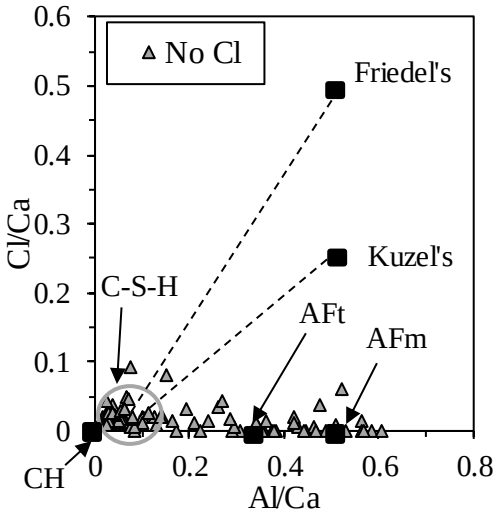


A

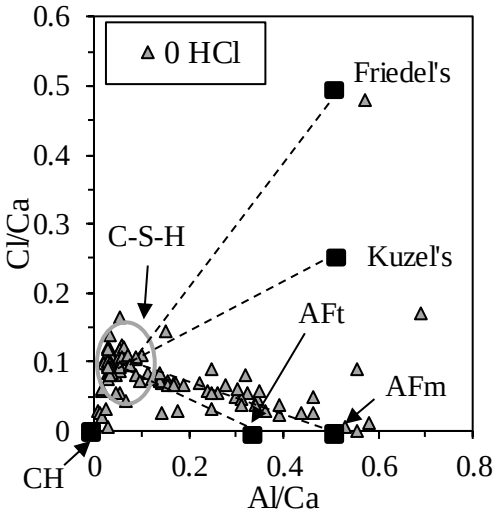


B

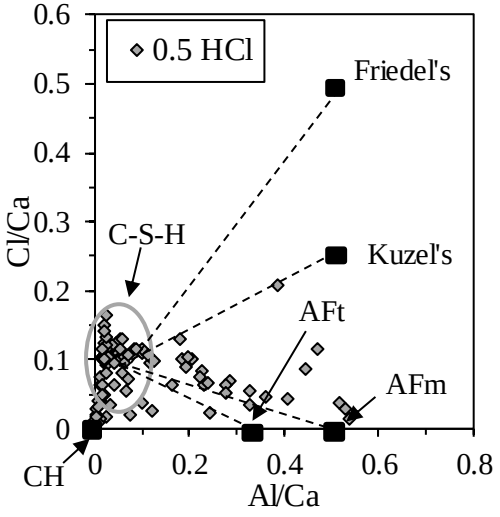


C

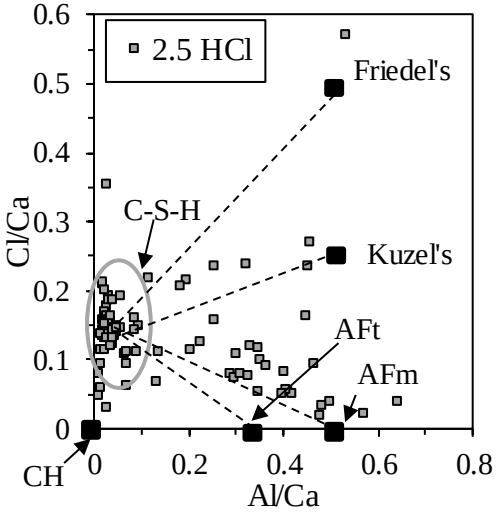


B

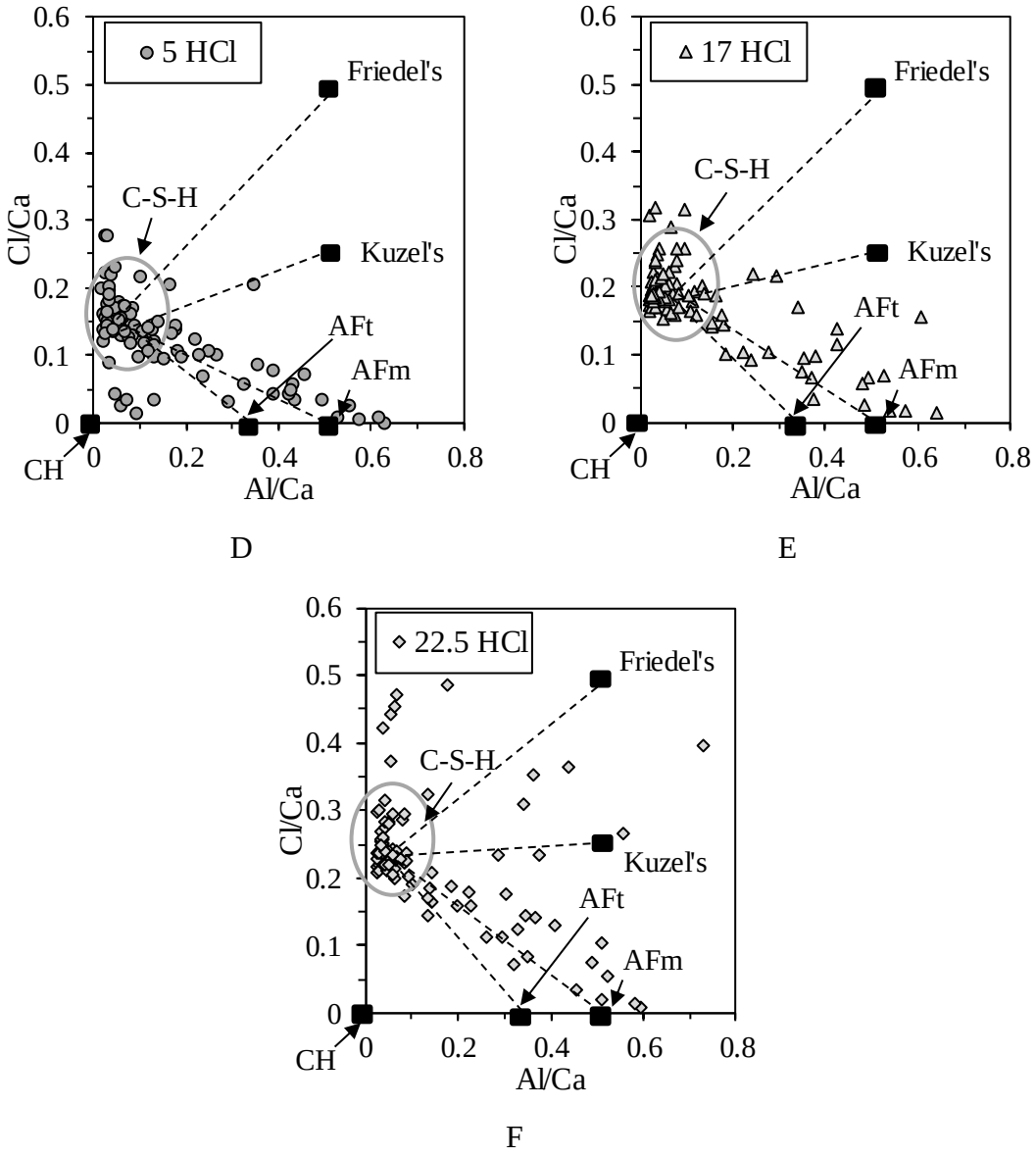


Figure D.5: EDS point scan data showing the atomic ratios of Cl/Al normalized to the calcium content for all samples in the current study. The label indicates the amount of HCl added to the cement paste, except for subfigure A which is from the cement paste not exposed to chlorides. Black squares indicate pure phases that are common in cement pastes. Points lying on the lines between C-S-H and a pure phase indicate that the scan detected a mix of the phase and C-S-H.

# Appendix E Developing the artificial leaching method

The goal of this thesis was to develop a method of lowering the pH of the pore solution in cement and measuring chloride binding as a function of the pH. The method of exposing hydrated paste to a chloride solution was chosen as a starting point. It has the advantage of being able to alter the pore solution by changing the liquid phase surrounding the cement paste and enables easy analysis of the pore solution without having to press it out of the cement paste. NaCl was chosen as the chloride source to avoid any effects on the pH caused by adding $Ca^{2+}$ or $Mg^{2+}$ to the system. Considering the chloride binding isotherms from previous studies [11,46,49], a NaCl-concentration of 1.5 M was chosen for the exposure solution. It was enough to make sure the samples would be at the plateau in the chloride binding isotherm, so that any changes in chloride binding would be due to changes in pH. Figure E.1 shows a hypothetical Langmuir (Equation 2-5) chloride binding isotherm for the system, with an indication of the expected effect of lowering the pH.

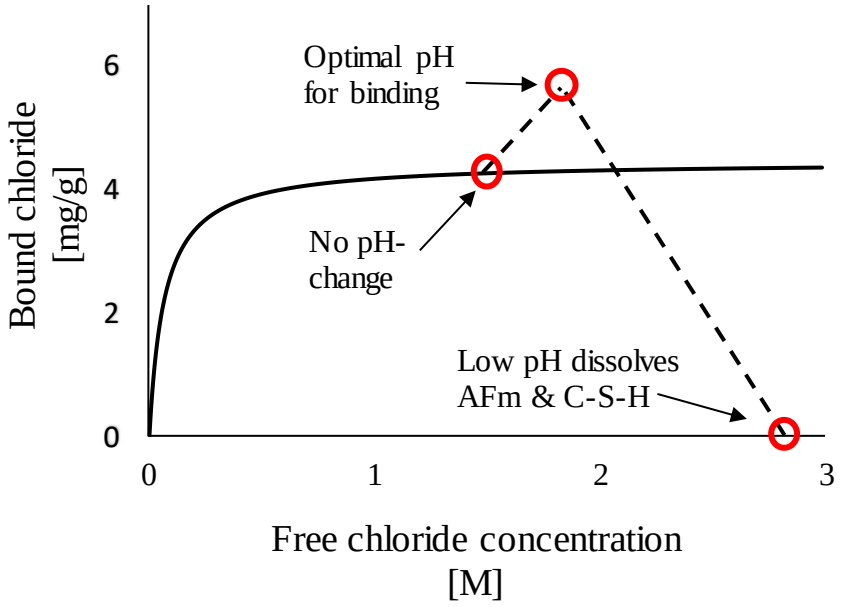


Figure E.1: Hypothetical Langmuir isotherm for chloride binding in cement paste exposed to NaCl. The solid line is the isotherm, while the dashed line indicates how the binding is expected to change as the pH is lowered by adding acid. Red circles indicate important points in the chloride binding vs. pH-curve. The acid has a larger chloride concentration than the exposure solution, but the increase in chloride binding is expected to be larger than the isotherm would predict.

The pH of the liquid had to be lowered by dilution with water or addition of acid. Dilution was not chosen due to its effect on the concentration of other ions and low accuracy. Due to error propagation a large liquid/solid-ratio would make accurate calculations of chloride binding nearly impossible.

Adding acid also leads to an increased volume, but acid lowers the pH more efficiently. Hydrochloric acid was chosen as it does not introduce new ions to the system. Two factors had to be balanced when choosing acid concentration. First, the acid had to be sufficiently concentrated so that a wide range of pH-values could be reached. The large amount of portlandite in cement paste gives it a large buffer capacity. Changing the pH from 13 to 10 by adding HCl could require a large volume of less concentrated acid. Large liquid volume would then result in the same low accuracy as with dilution.

Secondly, the acid had to be diluted enough as to not cause large instantaneous changes in pH. If the instant pH in the sample deviated greatly from the pH at equilibrium, there was a risk of locally dissolving AFm-phases or C-S-H. To determine chloride binding for the paste it was important that the solids remained homogeneous. A calculation of how the pH in the liquid phase would change directly after adding acid was made. Figure E.2 shows how the pH of a NaOH solution would change upon adding acid. To compensate for having to use highly concentrated acid it was added in small steps rather than all at once.

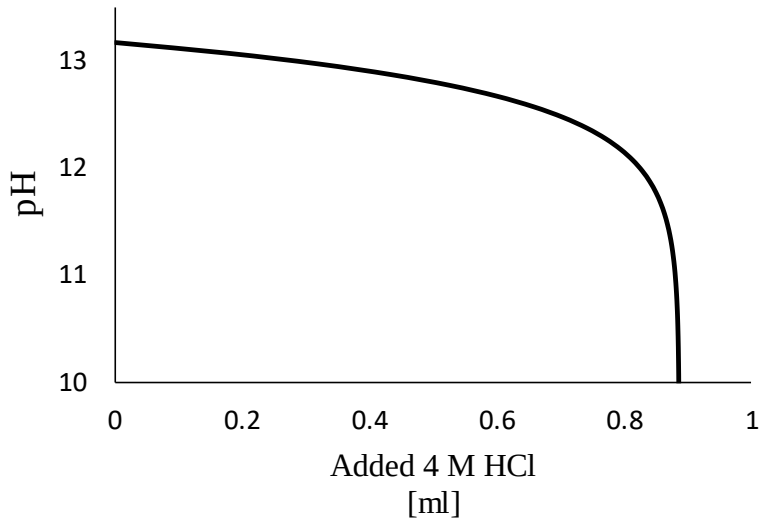


Figure E.2: Calculated pH of a NaOH-solution directly after addition of HCl. Calculated for an initial pH of 13.17, 20 ml exposure solution, 4 ml free water in cement paste and HCl-concentration of 4 M.

# Appendix F Weight measurements during acidification

In this appendix the weight measurements of the chloride binding samples during acidification are presented. Errors are not included, but the calculation of error is described in Appendix B.

| Sample weight [g] | Sample + acid [g] | Added acid [g] | Added HCl [ml] | Total volume HCl [ml] |
|---|---|---|---|---|
| **OPC-0.5** | | | | |
| 50.536 | 50.803 | 0.267 | 0.252 | 0.252 |
| 50.802 | 51.064 | 0.262 | 0.247 | 0.499 |
| **OPC-2.5** | | | | |
| 50.553 | 50.816 | 0.263 | 0.248 | 0.248 |
| 50.815 | 51.079 | 0.264 | 0.249 | 0.497 |
| 51.081 | 51.339 | 0.258 | 0.243 | 0.741 |
| 51.340 | 51.602 | 0.262 | 0.247 | 0.988 |
| 51.602 | 51.865 | 0.263 | 0.248 | 1.236 |
| 51.865 | 52.129 | 0.264 | 0.249 | 1.485 |
| 52.129 | 52.388 | 0.259 | 0.244 | 1.729 |
| 52.386 | 52.647 | 0.261 | 0.246 | 1.975 |
| 52.651 | 52.912 | 0.261 | 0.246 | 2.222 |
| 52.906 | 53.197 | 0.291 | 0.275 | 2.496 |
| **OPC-5** | | | | |
| 50.621 | 50.891 | 0.270 | 0.255 | 0.255 |
| 50.891 | 51.154 | 0.263 | 0.248 | 0.503 |
| 51.156 | 51.272 | 0.116 | 0.109 | 0.612 |
| 51.272 | 51.533 | 0.261 | 0.246 | 0.858 |
| 51.533 | 51.673 | 0.140 | 0.132 | 0.991 |
| 51.673 | 51.903 | 0.230 | 0.217 | 1.208 |
| 51.903 | 52.157 | 0.254 | 0.240 | 1.447 |
| 52.158 | 52.406 | 0.248 | 0.234 | 1.681 |
| 52.408 | 52.670 | 0.262 | 0.247 | 1.928 |
| 52.670 | 52.930 | 0.260 | 0.245 | 2.173 |
| 52.930 | 53.193 | 0.263 | 0.248 | 2.422 |
| 53.191 | 53.454 | 0.263 | 0.248 | 2.670 |
| 53.455 | 54.253 | 0.798 | 0.753 | 3.422 |
| 54.256 | 54.784 | 0.528 | 0.498 | 3.921 |
| 54.783 | 55.855 | 1.072 | 1.011 | 4.932 |
| **OPC-17** | | | | |
| 50.670 | 50.910 | 0.240 | 0.226 | 0.226 |
| 50.910 | 51.173 | 0.263 | 0.248 | 0.475 |
| 51.174 | 51.434 | 0.260 | 0.245 | 0.720 |

| | | | | |
|---|---|---|---|---|
| 51.434 | 51.687 | 0.253 | 0.239 | 0.958 |
| 51.689 | 51.946 | 0.257 | 0.242 | 1.201 |
| 51.947 | 52.206 | 0.259 | 0.244 | 1.445 |
| 52.205 | 52.461 | 0.256 | 0.242 | 1.687 |
| 52.462 | 52.664 | 0.202 | 0.191 | 1.877 |
| 52.663 | 52.977 | 0.314 | 0.296 | 2.174 |
| 52.978 | 53.235 | 0.257 | 0.242 | 2.416 |
| 53.273 | 53.499 | 0.226 | 0.213 | 2.629 |
| 53.498 | 53.760 | 0.262 | 0.247 | 2.876 |
| 53.760 | 54.391 | 0.631 | 0.595 | 3.472 |
| 54.393 | 54.918 | 0.525 | 0.495 | 3.967 |
| 54.918 | 55.983 | 1.065 | 1.005 | 4.972 |
| 55.983 | 58.067 | 2.084 | 1.966 | 6.938 |
| 58.067 | 60.198 | 2.131 | 2.010 | 8.948 |
| 60.198 | 62.317 | 2.119 | 1.999 | 10.947 |
| 62.314 | 64.436 | 2.122 | 2.002 | 12.949 |
| 64.117 | 66.189 | 2.072 | 1.955 | 14.904 |
| 66.126 | 68.360 | 2.234 | 2.108 | 17.011 |